4. ZERO-VOLTAGE SWITCHING TWO-INDUCTOR BOOST CONVERTER

Parts of this chapter have been published in the Proceedings of AUPEC 2003, PESC 2002 and 2005. A full list of publications arising from this thesis can be found on pages xxxiv to xxxvii.

The hard-switched two-inductor boost converter has been thoroughly studied as a dc-dc conversion stage in the MIC implementations [3]. However, under high switching frequency operation, the hard-switched converter is unlikely to maintain a reasonable efficiency due to the worsening switching losses. This chapter will concentrate on the analysis of the ZVS two-inductor boost converter and establish the critical circuit parameters and the variable power loss components under different operating conditions.

4.1 Introduction

Figure 4.1 shows the ZVS two-inductor boost converter, which has been previously developed by the author during his Master of Engineering study by introducing a resonant tank including one resonant inductor and two resonant capacitors to the hard-switched converter proposed in [112]. The resonant two-inductor boost converter is able to actively utilise the transformer leakage inductance and the MOSFET output capacitance as part of the resonant components. In this respect,

the ZVS is a better soft-switching solution than the ZCS as the MOSFET output capacitance in the latter cannot be absorbed into the resonant tank [146]. The resonant arrangement allows the switches to turn on at zero voltage and theoretically the turn-on switching losses are completely removed.

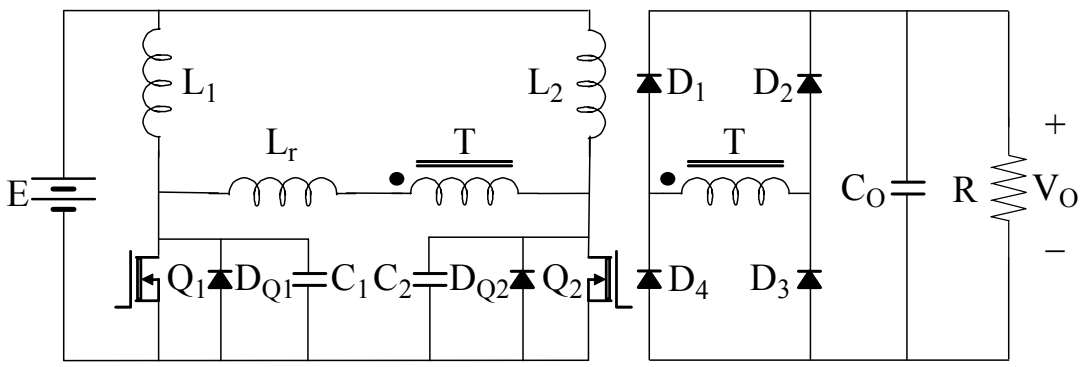

Figure 4.1 ZVS Two-Inductor Boost Converter

4.1.1 Three Circuit Parameters

Before the design and the control of the ZVS two-inductor boost converter are discussed in detail, the resonant waveforms in one discontinuous mode are given to introduce the three important circuit parameters.

The resonance of the converter can be analysed using the equivalent circuit shown in Figure 4.2. L_r is the effective resonant inductor and $C_1 = C_2 = C_r$ are the effective resonant capacitors. D_{Q1} and D_{Q2} are the embedded reverse body diodes of the MOSFETs. The current source I_0 models the input inductor L_1 or L_2. The voltage source V_d is the output capacitor C_O voltage reflected to the transformer primary

winding and the diode D corresponds to the diodes in the output full bridge rectifier. The arrangement for V_d and D assumes a positive resonant inductor current i_{Lr} as illustrated and their polarities reverse when the resonant inductor current becomes negative.

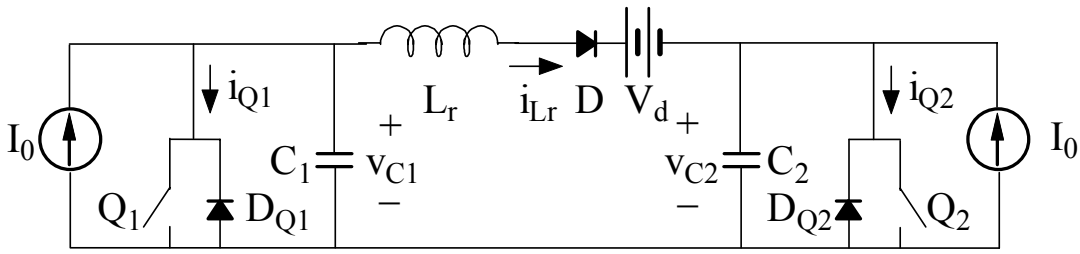

Figure 4.2 Equivalent Resonant Circuit

The analysis of the resonant circuit in Figure 4.2 will establish the equations of the resonant voltage and current in the converter. The resonant waveforms of a discontinuous current mode, in which the MOSFET turns off with a non-zero time delay after the resonant inductor current reaches zero, are shown in Figure 4.3.

In the analysis of the converter operation, there are three important circuit parameters and they are listed below:

- The load factor k, defined by the equation $I_0 Z_0 = kV_d$, where $Z_0 = \sqrt{\frac{L_r}{C_r}}$ is the characteristic impedance of the resonant tank made up of the resonant inductor and capacitors. It is normally required that k be greater than or equal to one in order to maintain the ZVS condition.

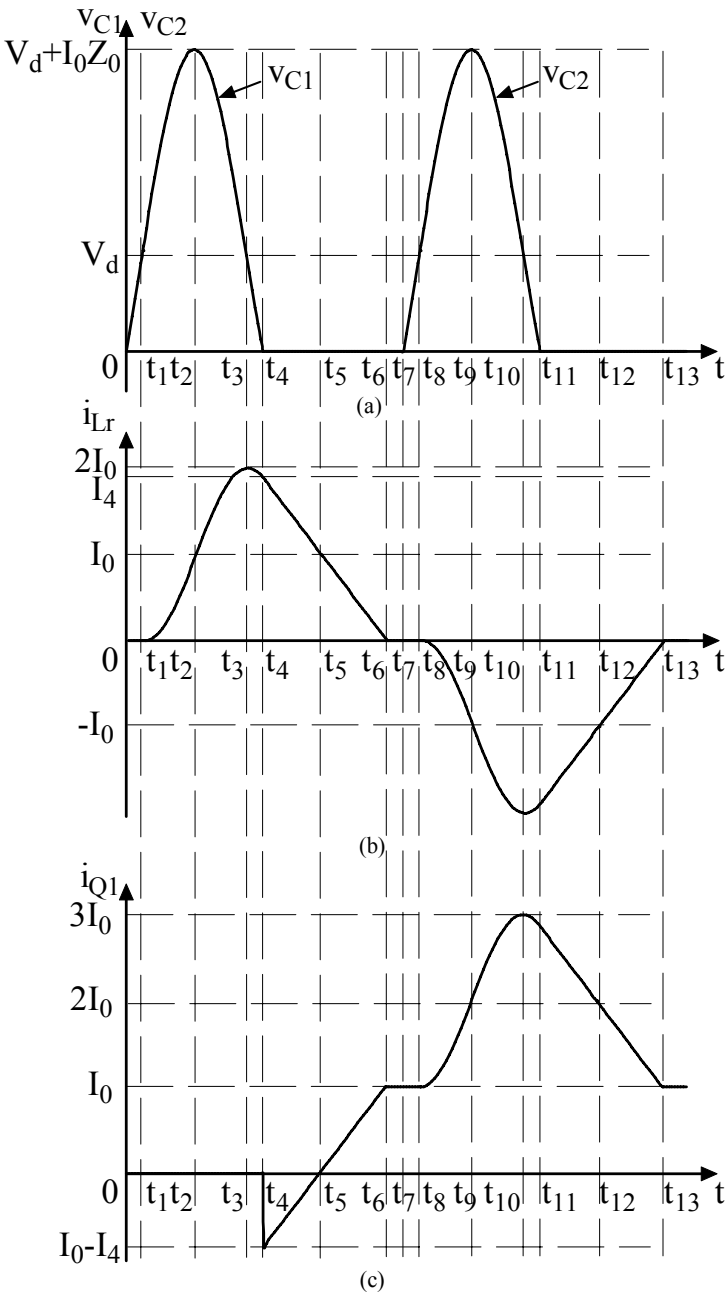

Figure 4.3 Resonant Waveforms of One Discontinuous Mode

(a) Capacitor Voltage (b) Inductor Current (c) MOSFET Current

- The timing factor Δ_1, which determines the initial resonant inductor current $i_{Lr}(0) = -\Delta_1 I_0$ when Q_1 turns off or $i_{Lr}(t_7) = \Delta_1 I_0$ when Q_2 turns off. It can

be observed that $\Delta_1 = 0$ in the operation mode shown in Figure 4.3.

- The delay angle α_d, defined as the angle between the instant when the inductor current falls to zero and the instant when the corresponding MOSFET turns off. It can be observed that $\alpha_d = \omega_0(t_7 - t_6)$ in the waveforms shown in Figure 4.3, where $\omega_0 = \frac{1}{\sqrt{L_r C_r}}$ is the angular resonance frequency of the resonant tank.

4.1.2 Wide Load Range Operation

The three circuit parameters including the load factor k, the timing factor Δ_1 and the delay angle α_d determine the resonant operation of the ZVS two-inductor boost converter. Variations of these circuit parameters may result in either the continuous or the discontinuous operation modes of the converter. Different operation modes lead to different average values of the absolute resonant inductor current, which controls the rectifier average current on the secondary side and determines the output power of the converter. Therefore, the wide load range operation of the resonant two-inductor boost converter can be realised by varying the three circuit parameters.

The resonant two-inductor boost converter discussed here has an input of 20 V, a maximum output of 340 V and 200 W. The analysis of the wide load range operation of this converter is based on varying the three circuit parameters. A

variation of the two-inductor boost converter with the voltage clamp is also studied. The theoretical and the simulation waveforms are provided for both converters and the experimental results are also provided for the ZVS two-inductor boost converter without the voltage clamp.

4.2 Design Method and Control Function

According to different values of the load factor k, the timing factor Δ_1 and the delay angle α_d, the operation of the ZVS two-inductor boost converter can be classified into three operating regions as shown in Table 4.1. It is obvious that the resonant waveforms shown in Figure 4.3 belong to the converter operating in Region 1.

Region	1	2	3
Load Factor k	≥ 1	≥ 1	< 1
Timing Factor Δ_1	$= 0$	> 0	> 0
Delay Angle α_d	> 0	$= 0$	$= 0$
Possible Operation Modes	Discontinuous	Continuous and Discontinuous	Continuous and Discontinuous

Table 4.1 Three Operating Regions

In Region 3, k is less than 1 but close to 1 and the converter still maintains the ZVS condition. However, in this operating region, the range of the values of k is very limited and the output voltage of the converter varies only slightly. In studying the wide load range operation of this converter, the operation in this region may be

safely neglected. The discussion of the design method and the control function is given below for the converter operations in Regions 1 and 2. The discussion can be started with the operation in Region 2 first.

4.2.1 Design Method

The converter design normally involves the determination of the component values and the selection of the components with the proper electrical ratings. This section discusses the circuit equations that determine the component values, which are considered as the key design parameters. The key design parameters of the resonant two-inductor boost converter are the resonant inductance L_r, the resonant capacitance C_r and the transformer turns ratio n. Once the key design parameters are known, the current and the voltage terms in the circuit can be explicitly established and they are used as the references in the component selection process.

In order to find the key design parameters in Region 2, the circuit parameters including the timing factor Δ_1 and the load factor k must be given initially. The design equations are:

- The balance of power at the input supply and the output load:

$$E \cdot 2I_0 = \frac{V_O^2}{R} \tag{4.1}$$

where E is the dc input source voltage, V_O is the output load voltage and R is the load resistance.

- The balance of power at the transformer primary and the output load:

$$V_d \hat{g}_\Delta(\Delta_1, k) I_0 = \frac{V_O^2}{R} \tag{4.2}$$

where the function $\hat{g}_\Delta(\Delta_1, k)$ is the ratio of the average of the absolute value of the transformer primary current, that is the resonant inductor current, to the average input inductor current, I_0. The function $\hat{g}_\Delta(\Delta_1, k)$ is determined by two independent variables, Δ_1 and k and can be obtained through the state analysis.

- The load condition:

$$I_0 Z_0 = k V_d \tag{4.3}$$

- The transformer turns ratio:

$$V_O = n V_d \tag{4.4}$$

From Equations (4.1) to (4.4), once E, V_O, R, Δ_1 and k are known, four unknown variables, I_0, V_d, Z_0 and n can be solved. In order to further find the resonant

inductance and capacitance, a circuit variable γ must be defined in Equation (4.5) and it is a direct result of the state analysis:

$$\gamma = \frac{\omega_0}{f_s} \tag{4.5}$$

where f_s is the switching frequency. If f_s is selected, the angular resonant frequency ω_0 can then be calculated from Equation (4.5). The resonant inductance L_r and capacitance C_r can be duly obtained from Equations (4.6) and (4.7):

$$L_r = \frac{Z_0}{\omega_0} \tag{4.6}$$

$$C_1 = C_2 = C_r = \frac{1}{\omega_0 Z_0} \tag{4.7}$$

4.2.2 Control Function

Once the key design parameters including the resonant inductance and capacitance and the transformer turns ratio are fixed, the load factor k is no longer an independent variable. The operation of the ZVS two-inductor boost converter is completely determined by the magnitude of the initial resonant inductor current, $\Delta_1 I_0$, when the MOSFET turns off. This means that the output voltage or power is solely dependent on the timing factor Δ_1. This section aims to establish the relationship between V_d, the output capacitor voltage reflected to the transformer

primary winding, and Δ_1, the timing factor. First, the dependent variable k must be removed from function $\hat{g}_\Delta(\Delta_1, k)$ in Equation (4.2). Equation (4.2) can be rewritten as:

$$V_d g_\Delta(\Delta_1) I_0 = \frac{V_O^2}{R} \tag{4.8}$$

Using Equation (4.1), Equation (4.8) can be written as:

$$V_d = \frac{2E}{g_\Delta(\Delta_1)} \tag{4.9}$$

Equation (4.9) is of the format of the control function however the function $g_\Delta(\Delta_1)$ cannot be solved directly. An indirect method is to add the dependant variable k and replace $g_\Delta(\Delta_1)$ with $\hat{g}_\Delta(\Delta_1, k)$ in Equation (4.9):

$$V_d = \frac{2E}{\hat{g}_\Delta(\Delta_1, k)} \tag{4.10}$$

From Equation (4.10), V_d can be solved indirectly by calculating the possible values of $\hat{g}_\Delta(\Delta_1, k)$ against a range of the values of Δ_1 and k first and then choosing the sets of the values of Δ_1 and k that fulfil the circuit constraints inherently imposed by Equations (4.1) to (4.4). As the analytical solution of the function $\hat{g}_\Delta(\Delta_1, k)$ contains inverse trigonometric functions and presents a significant level of

complexity, the understanding of the physical implication of the function is greatly hindered. Therefore, the function is solved numerically by MATLAB program in the analysis. The qualified sets of Δ_1 and k values that obey the circuit constraints are also obtained numerically and can be found through the following process.

Manipulations of Equations (4.1) to (4.4) yield:

$$k = \frac{n^2 Z_0}{R} \cdot \frac{1}{\hat{g}_\Delta(\Delta_1, k)} \tag{4.11}$$

This is the circuit constraint which is used to find the qualified sets of Δ_1 and k values and then the numerical relationship between Δ_1 and k. Two supplemental functions can be defined as:

$$h_{1,\Delta}(\Delta_1, k) = k \tag{4.12}$$

$$h_{2,\Delta}(\Delta_1, k) = \frac{n^2 Z_0}{R} \cdot \frac{1}{\hat{g}_\Delta(\Delta_1, k)} \tag{4.13}$$

Equations (4.12) and (4.13) respectively represents a surface in a three-dimensional space with Δ_1 and k as two axes. Then the circuit constraint given in Equation (4.11) simply means that the relationship between Δ_1 and k can be found numerically by solving the intersection curve of the surfaces $h_{1,\Delta}(\Delta_1, k)$ and $h_{2,\Delta}(\Delta_1, k)$. Once the relationship between Δ_1 and k is established, it can be

substituted to Equation (4.10) to remove the dependent variable k and the numerical relationship between V_d and Δ_1 can be found. Therefore the final control function in Region 2 can be derived by the polynomial fitting and expressed as:

$$V_d = M_\Delta(\Delta_1) \tag{4.14}$$

In Region 1, the timing factor is zero and the delay angle is greater than zero. The analysis of the design method and the control function in this region is similar to that in Region 2 and will not be repeated. The equations in Region 1 share the same format with those in Region 2 but the variable Δ_1 needs to be replaced with α_d and the subscript Δ with α to maintain the nomenclatural clarity and consistency. Table 4.2 lists the equations in Region 2 and their counterparts in Region 1. As Equations (4.1), (4.3) to (4.7) are the same in both operating regions, they are not listed here.

4.3 Wide Load Range Operation of the ZVS Two-Inductor Boost Converter

This section applies the theoretical analysis in Section 4.2 to the ZVS two-inductor boost converter which has an input voltage of 20 V, a maximum output of 340 V and 200 W and establishes the possible output voltage range.

4.3.1 State Analysis

This section provides the state analysis of the ZVS two-inductor boost converter.

Before Q_1 turns off, both Q_1 and Q_2 are on. At time $t = 0$, Q_1 turns off and the converter will move up to four possible states before Q_2 turns off as shown in Figure 4.4. The resonant capacitor voltage and inductor current waveforms are shown in Figure 4.5.

Equations in Region 2 Operation	Equations in Region 1 Operation
$V_d \hat{g}_\Delta(\Delta_1, k) I_0 = \frac{V_O^2}{R}$ (4.2)	$V_d \hat{g}_\alpha(\alpha_d, k) I_0 = \frac{V_O^2}{R}$ (4.15)
$V_d g_\Delta(\Delta_1) I_0 = \frac{V_O^2}{R}$ (4.8)	$V_d g_\alpha(\alpha_d) I_0 = \frac{V_O^2}{R}$ (4.16)
$V_d = \frac{2E}{g_\Delta(\Delta_1)}$ (4.9)	$V_d = \frac{2E}{g_\alpha(\alpha_d)}$ (4.17)
$V_d = \frac{2E}{\hat{g}_\Delta(\Delta_1, k)}$ (4.10)	$V_d = \frac{2E}{\hat{g}_\alpha(\alpha_d, k)}$ (4.18)
$k = \frac{n^2 Z_0}{R} \cdot \frac{1}{\hat{g}_\Delta(\Delta_1, k)}$ (4.11)	$k = \frac{n^2 Z_0}{R} \cdot \frac{1}{\hat{g}_\alpha(\alpha_d, k)}$ (4.19)
$h_{1,\Delta}(\Delta_1, k) = k$ (4.12)	$h_{1,\alpha}(\alpha_d, k) = k$ (4.20)
$h_{2,\Delta}(\Delta_1, k) = \frac{n^2 Z_0}{R} \cdot \frac{1}{\hat{g}_\Delta(\Delta_1, k)}$ (4.13)	$h_{2,\alpha}(\alpha_d, k) = \frac{n^2 Z_0}{R} \cdot \frac{1}{\hat{g}_\alpha(\alpha_d, k)}$ (4.21)
$V_d = M_\Delta(\Delta_1)$ (4.14)	$V_d = M_\alpha(\alpha_d)$ (4.22)

Table 4.2 Equations in Regions 1 and 2

The initial conditions in State (a) are $i_{Lr}(0) = -\Delta_1 I_0$ and $v_{C1}(0) = 0$. The analysis of each state is given below.

- State (a) ($0 \le t \le t_1$)

This state starts when Q_1 turns off. In this state, the current in the resonant inductor is still negative. This current and the current source I_0 charge the capacitor and the resonant inductor current decreases. The capacitor voltage v_{C1} and the inductor current i_{Lr} are respectively:

$$v_{C1}(t) = (1+\Delta_1)I_0 Z_0 \sin\omega_0 t + V_d \cos\omega_0 t - V_d \tag{4.23}$$

$$i_{Lr}(t) = \frac{V_d}{Z_0}\sin\omega_0 t - (1+\Delta_1)I_0 \cos\omega_0 t + I_0 \tag{4.24}$$

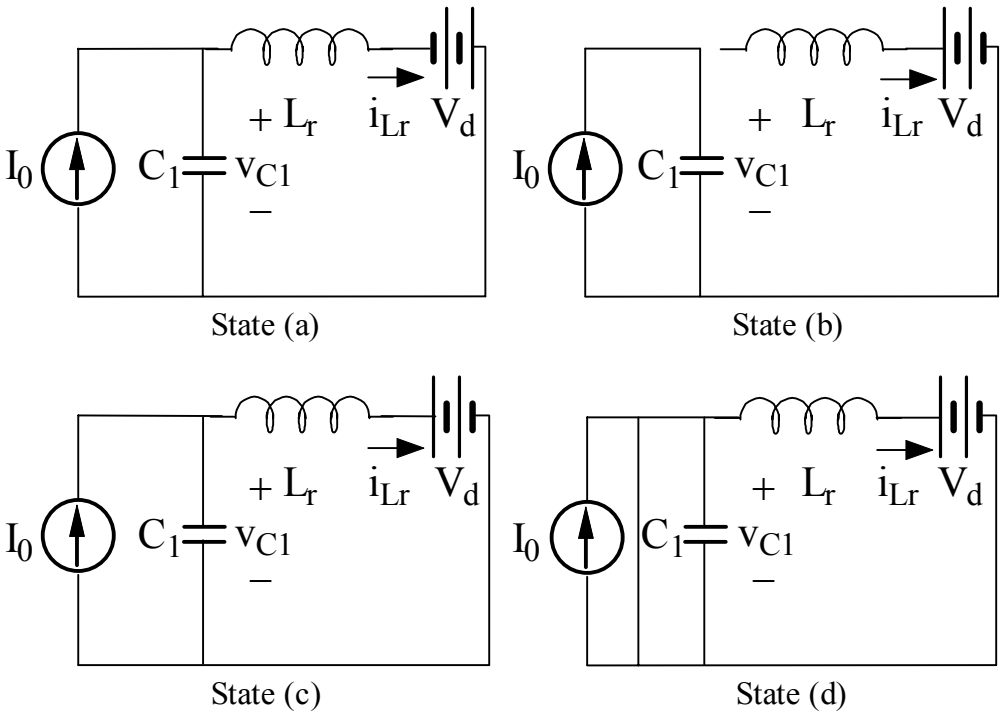

Figure 4.4 Four Possible States

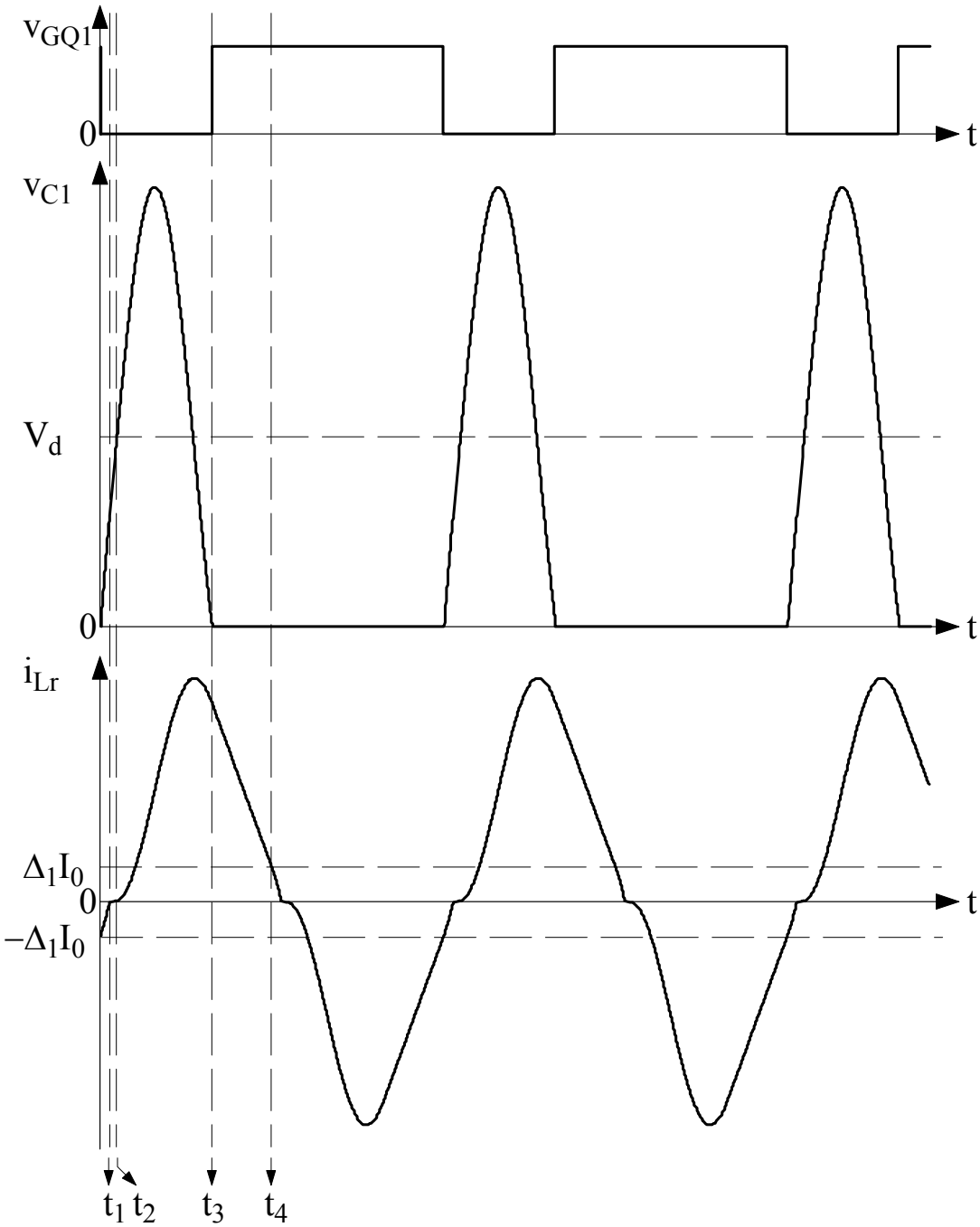

Figure 4.5 Resonant Capacitor Voltage and Inductor Current Waveforms

If $\Delta_1 = 0$, this state will be bypassed and $t_1 = 0$ under this condition.

- State (b) ($t_1 \le t \le t_2$)

This state starts when the current in the resonant inductor reaches zero and V_d reverses its polarity. If the capacitor voltage v_{C1} is still lower than V_d, the diode D is reverse biased and the current source I_0 linearly charges the capacitor. The capacitor voltage v_{C1} and the inductor current i_{Lr} are respectively:

$$v_{C1}(t) = \frac{I_0}{C_1}(t - t_1) + v_{C1}(t_1) \tag{4.25}$$

$$i_{Lr}(t) = 0 \tag{4.26}$$

Substituting Equation (4.7) to (4.25) yields:

$$v_{C1}(t) = I_0 Z_0 \omega_0 (t - t_1) + v_{C1}(t_1) \tag{4.27}$$

If the initial resonant inductor current in State (a) is sufficiently high to cause v_{C1} to exceed V_d at the end of State (a), this state will be bypassed and $t_2 = t_1$ under this condition.

- State (c) ($t_2 \le t \le t_3$)

This state starts when v_{C1} reaches V_d at the end of State (b) or i_{Lr} reaches zero if State (b) is bypassed. In this state, the capacitor resonates with the inductor. The capacitor voltage v_{C1} and the inductor current i_{Lr} are respectively:

$$v_{C1}(t) = I_0 Z_0 \sin\omega_0(t-t_2) + [v_{C1}(t_2) - V_d]\cos\omega_0(t-t_2) + V_d \tag{4.28}$$

$$i_{Lr}(t) = \frac{v_{C1}(t_2) - V_d}{Z_0}\sin\omega_0(t-t_2) - I_0\cos\omega_0(t-t_2) + I_0 \tag{4.29}$$

- State (d) ($t_3 \le t \le t_4$)

This state starts when v_{C1} reaches zero. In this state, the resonant inductor is linearly discharged by V_d. The capacitor voltage v_{C1} and the inductor current i_{Lr} are respectively:

$$v_{C1}(t) = 0 \tag{4.30}$$

$$i_{Lr}(t) = i_{Lr}(t_3) - \frac{V_d}{L_r}(t-t_3) \tag{4.31}$$

Substituting Equation (4.6) to (4.30) yields:

$$i_{Lr}(t) = i_{Lr}(t_3) - \frac{V_d}{Z_0}\omega_0(t-t_3) \tag{4.32}$$

After Q_2 turns off, the above states repeat.

4.3.2 Design Process

The output voltage of the resonant converter is higher when it operates in Region 1

while the output voltage of the converter is lower when it operates in Region 2. Therefore, the maximum output voltage, 340 V, must be designed in Region 1 with a non-zero delay angle α_d. The other parameters used in the converter design are $E = 20\ V$ and $R = 576\ \Omega$.

From Equation (4.18), the surface V_d can be drawn against α_d and k in Figure 4.6, where $0 \le \alpha_d \le 10$ and $1 \le k \le 10$. Table 4.3 shows the maximum and the minimum values of V_d on the surface and the relevant circuit parameters.

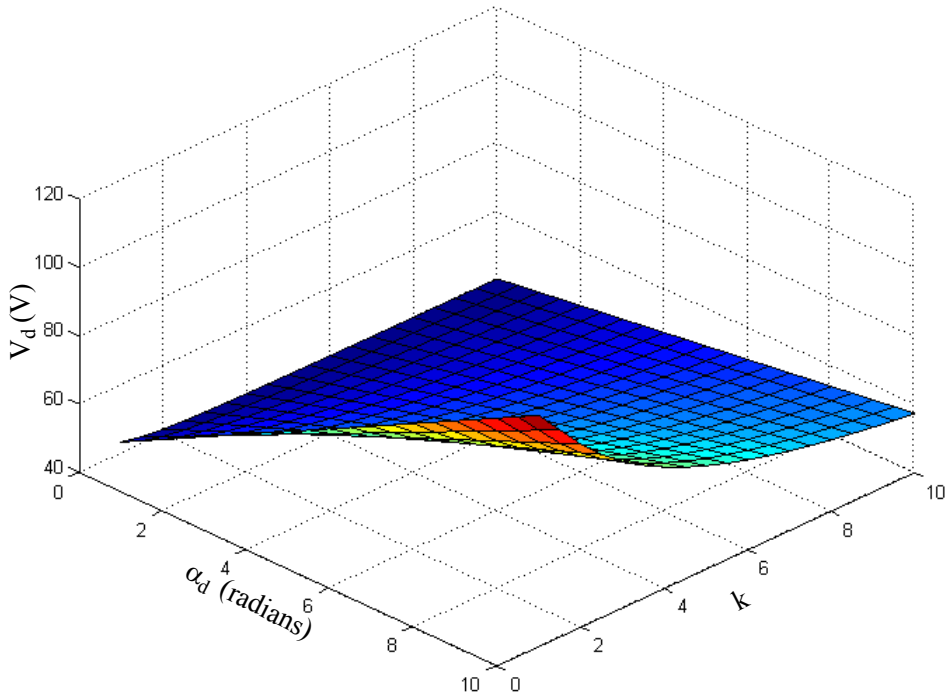

Figure 4.6 Surface V_d in Region 1

In the design of the ZVS two-inductor boost converter with a wide load range, special attention must be paid to the peak MOSFET voltage because the MOSFET

with a higher voltage rating normally has a higher drain source on resistance, which leads to a higher conduction loss. If a lower drain source on resistance is required under higher voltage ratings, the MOSFET input capacitance will increase considerably as the product of the input capacitance and drain source on resistance increases with the drain-source voltage rating [147]. This leads to a higher drive power and a lower converter overall efficiency. From Equations (4.3) and (4.28), the peak MOSFET voltage can be calculated as:

$$V_{Q,peak} = \left\{ 1 + \sqrt{k^2 + \left[\frac{v_{C1}(t_2)}{V_d} - 1 \right]^2} \right\} V_d \tag{4.33}$$

As $v_{C1}(t_2) = V_d$ when $\Delta_1 = 0$ in Region 1, Equation (4.33) can be simplified to:

$$V_{Q,peak} = (1+k)V_d \tag{4.34}$$

V_d (V)	α_d (radians)	k	$\hat{g}_\alpha(\alpha_d, k)$
107.5	10	1	0.372
40.1	0	10	0.998

Table 4.3 Maximum and Minimum Values of V_d in Region 1

Figure 4.7 shows the surface $V_{Q,peak}$ in Equation (4.34), where $0 \le \alpha_d \le 10$ and $1 \le k \le 10$. This surface shows that the peak switch voltage can be extremely high for certain sets of α_d and k values. A horizontal surface $V_{Q,rating} = 200\ V$ is also

drawn in Figure 4.7. In order for the peak MOSFET voltage to be less than 200 V, the values of α_d and k must be selected in the domains where surface $V_{Q,peak}$ is below surface $V_{Q,rating}$.

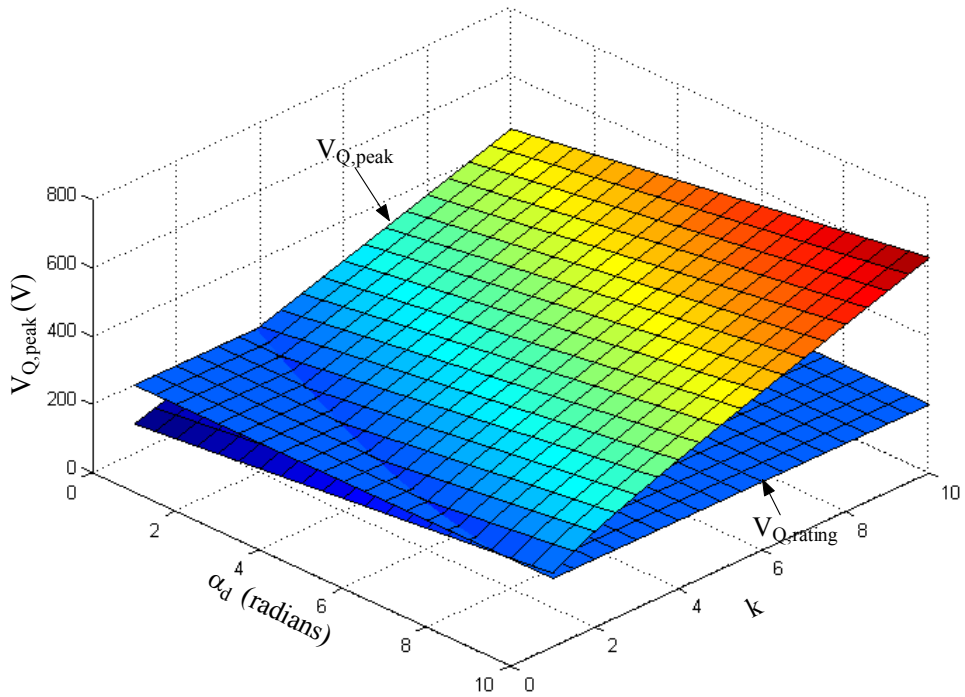

Figure 4.7 Surfaces $V_{Q,peak}$ and $V_{Q,rating}$ in Region 1

An initial set of the circuit parameters $\alpha_d = 4$ and $k = 2.31$ is selected. The justification of the selection will be provided in due course. The peak MOSFET voltage under this condition is 200 V. The calculation results from Equations (4.1), (4.3), (4.4) and (4.15) and the state analysis are given in Table 4.4.

The key design parameters including the resonant inductance and capacitance will be calculated from Equations (4.5) to (4.7) in the due course when the analyses in

both Regions 1 and 2 are conducted and the switching frequency is selected.

E (V)	I_0 (A)	$\hat{g}_\alpha(\alpha_d, k)$	V_d (V)	n	Z_0 (Ω)	γ (radians)
20	5	0.660	60.6	5.6	27.9	24.8

Table 4.4 Initial Calculation Results in Region 1

The surfaces of the functions described in Equations (4.20) and (4.21) are drawn in Figure 4.8. The intersection curve u_α can be found and the corresponding values of α_d and k of the points on the curve u_α are listed in Table 4.5. In this region, the converter operates in the discontinuous mode only.

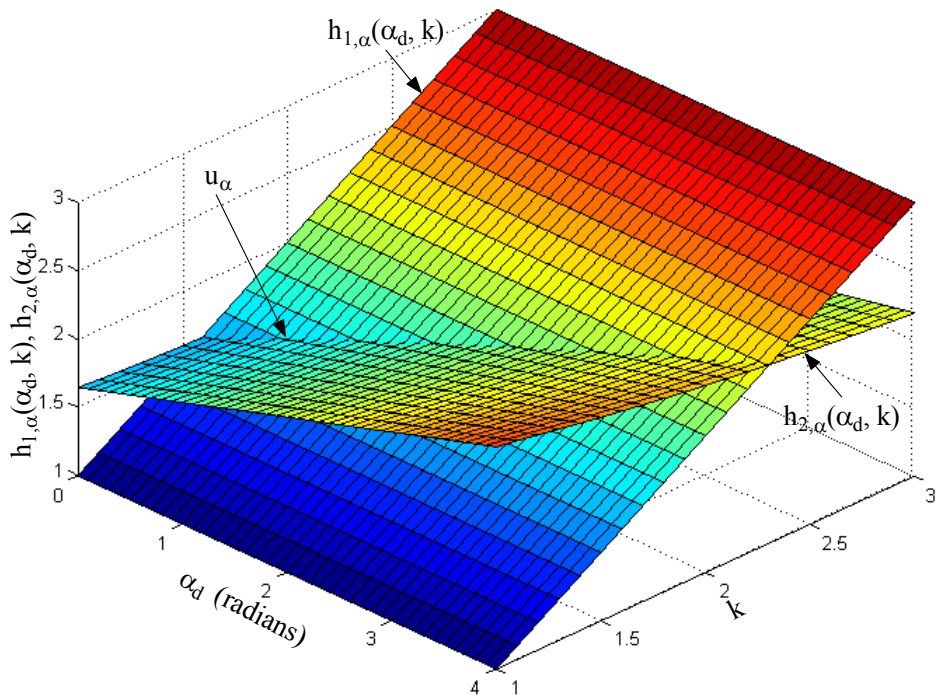

Figure 4.8 Surfaces $h_{1,\alpha}(\alpha_d, k)$ and $h_{2,\alpha}(\alpha_d, k)$

α_d (radians)	k	V_d (V)	α_d (radians)	k	V_d (V)	α_d (radians)	k	V_d (V)
0.0	1.59	41.8	1.4	1.87	49.0	2.8	2.11	55.5
0.1	1.61	42.3	1.5	1.88	49.5	2.9	2.13	55.9
0.2	1.63	42.9	1.6	1.90	50.0	3.0	2.15	56.3
0.3	1.65	43.4	1.7	1.92	50.4	3.1	2.16	56.8
0.4	1.67	43.9	1.8	1.94	50.9	3.2	2.18	57.2
0.5	1.69	44.5	1.9	1.96	51.4	3.3	2.20	57.6
0.6	1.71	45.0	2.0	1.97	51.8	3.4	2.21	58.1
0.7	1.73	45.5	2.1	1.99	52.3	3.5	2.23	58.5
0.8	1.75	46.0	2.2	2.01	52.8	3.6	2.24	58.9
0.9	1.77	46.5	2.3	2.03	53.2	3.7	2.26	59.3
1.0	1.79	47.0	2.4	2.04	53.7	3.8	2.28	59.7
1.1	1.81	47.5	2.5	2.06	54.1	3.9	2.29	60.2
1.2	1.83	48.0	2.6	2.08	54.6	4.0	2.31	60.5
1.3	1.85	48.5	2.7	2.10	55.0			

Table 4.5 Numerical Relationship of α_d and k

Through the polynomial fitting, the control function $M_\alpha(\alpha_d)$ can be found as:

$$V_d = M_\alpha(\alpha_d) = 0.0079\alpha_d^3 - 0.2124\alpha_d^2 + 5.4130\alpha_d + 41.7942 \qquad (4.35)$$

The control function $M_\alpha(\alpha_d)$ can be drawn in Figure 4.9.

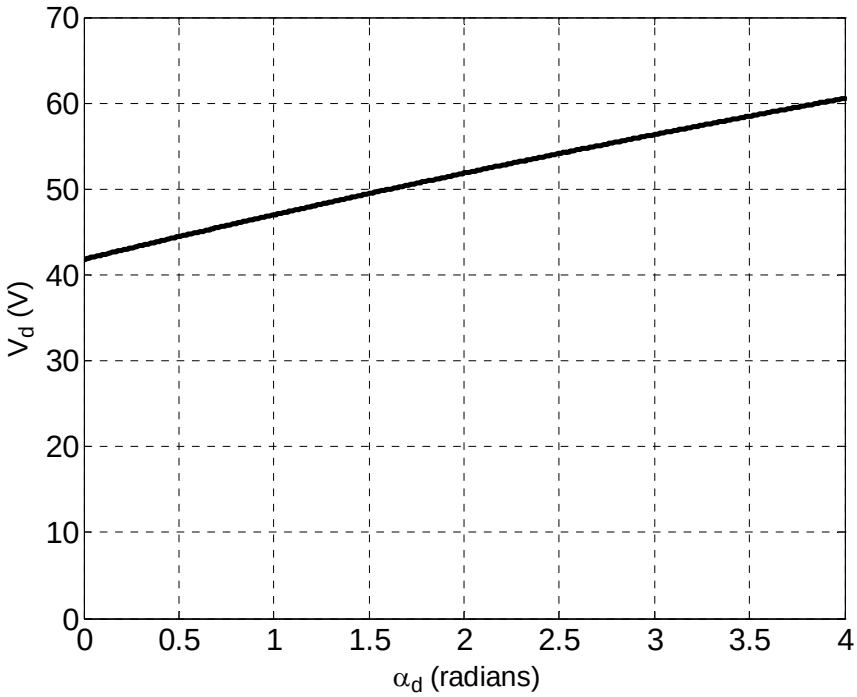

Figure 4.9 Control Function $M_{\alpha}(\alpha_d)$

When α_d reaches zero, Region 1 operation ends and Region 2 operation starts. At this point, $\alpha_d = 0$, $k = 1.59$ and $V_d = 41.8\ V$.

In Region 2, the load factor k continues to decrease from 1.59. From Equation (4.10), the surface V_d can be drawn against Δ_1 and k as shown in Figure 4.10, where $0 \le \Delta_1 \le 3$ and $1 \le k \le 10$.

In this region, the peak MOSFET voltage can be calculated by Equation (4.33). The surfaces $V_{Q,peak}$ and $V_{Q,rating} = 200\ V$ when $0 \le \Delta_1 \le 3$ and $1 \le k \le 10$ are drawn in Figure 4.11. It can be observed in Figure 4.11 that the peak MOSFET voltage is

well below 200 V when $k \leq 1.59$.

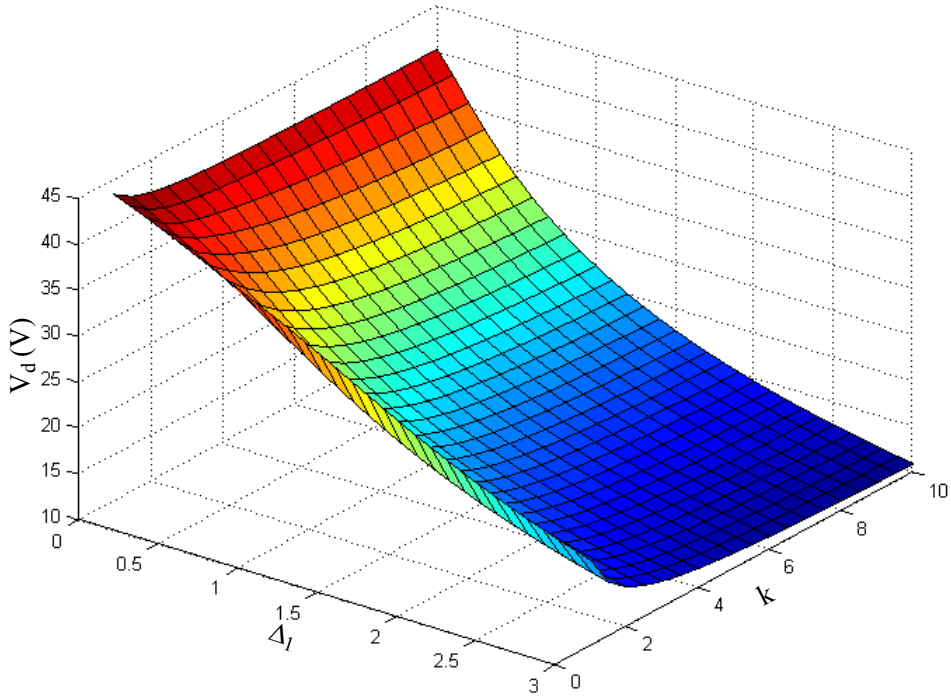

Figure 4.10 Surface V_d in Region 2

The surfaces of the functions described in Equations (4.12) and (4.13) are drawn in Figure 4.12. The intersection curve u_Δ can be found and the corresponding values of Δ_1 and k of the points on the curve u_Δ are listed in Table 4.6. Under each set of the circuit parameters in Table 4.6, the converter operates in the discontinuous mode when $k \geq 1.42$ and in the continuous mode when $k \leq 1.39$.

Through the polynomial fitting, the control function $M_\Delta(\Delta_1)$ can be found as:

$$V_d = M_\Delta(\Delta_1) = 0.3005\Delta_1^3 + 0.0221\Delta_1^2 - 9.0395\Delta_1 + 41.7931 \qquad (4.36)$$

The control function $M_{\Delta}(\Delta_1)$ can be drawn in Figure 4.13.

When Δ_1 reaches 2, k reaches 1 and Region 2 operation ends. At this point, $V_d = 26.2\ V$.

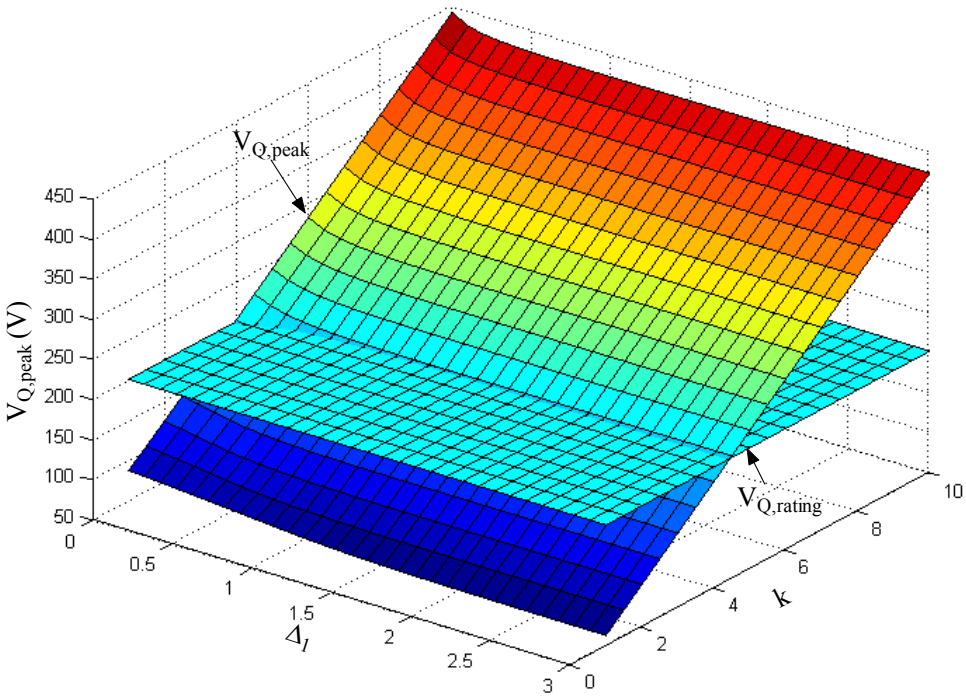

Figure 4.11 Surfaces $V_{Q,peak}$ and $V_{Q,rating}$ in Region 2

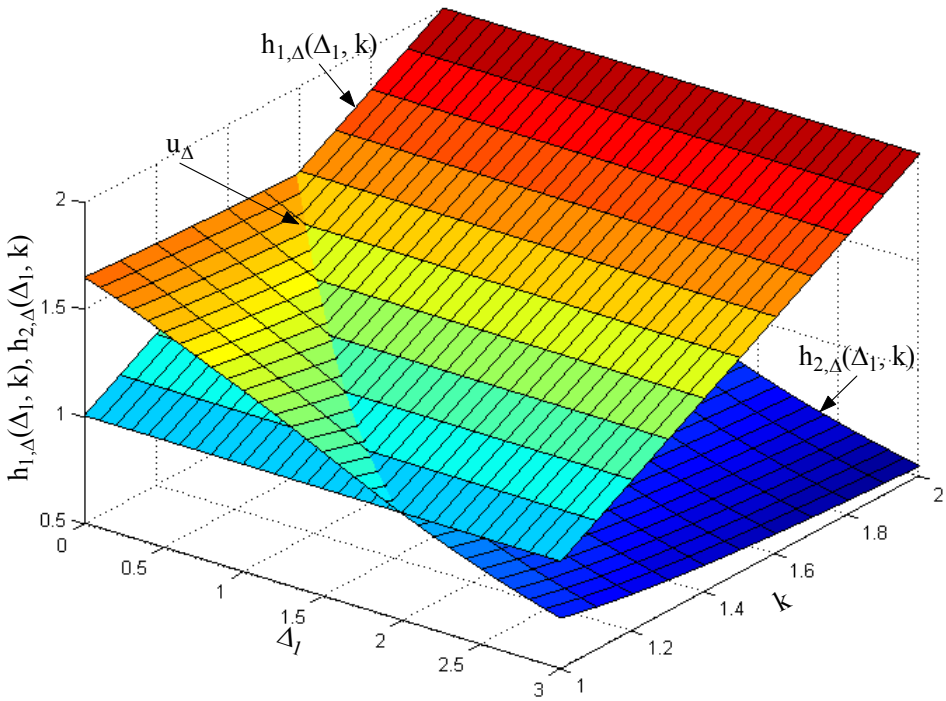

Figure 4.12 Surfaces $h_{1,\Delta}(\Delta_1, k)$ and $h_{2,\Delta}(\Delta_1, k)$ in Region 2

Δ_1	k	V_d (V)	Δ_1	k	V_d (V)	Δ_1	k	V_d (V)
0.0	1.59	41.8	0.7	1.36	35.6	1.4	1.14	30.0
0.1	1.56	40.9	0.8	1.32	34.8	1.5	1.12	29.3
0.2	1.52	40.0	0.9	1.29	33.9	1.6	1.09	28.6
0.3	1.49	39.1	1.0	1.26	33.1	1.7	1.07	27.9
0.4	1.45	38.2	1.1	1.23	32.3	1.8	1.04	27.4
0.5	1.42	37.3	1.2	1.20	31.5	1.9	1.02	26.8
0.6	1.39	36.4	1.3	1.17	30.7	2.0	1.00	26.2

Table 4.6 Numerical Relationship of Δ_1 and k

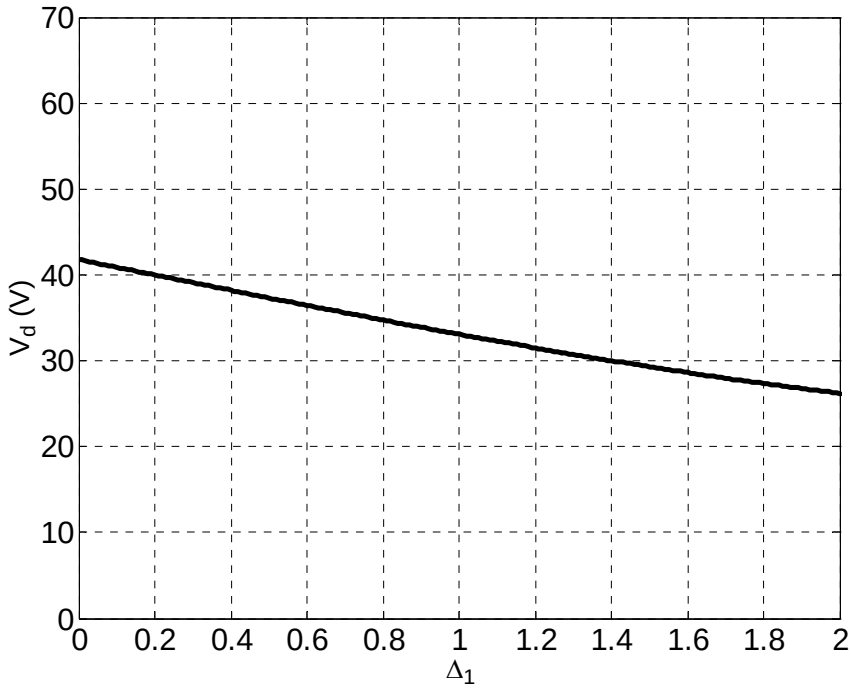

Figure 4.13 Control Function $M_{\Delta}(\Delta_1)$

From the above discussion, it can be summarised that the maximum and the minimum output voltages by operating the ZVS two-inductor boost converter in both Regions 1 and 2 are respectively 340 V and 146.7 V, which respectively correspond to 60.6 V and 26.2 V on the transformer primary winding. The ratio of the maximum to the minimum voltages is 2.3. This ratio depends on the selection of the initial set of the values of α_d and k. The mathematical manipulation through the same process shows that the selection of other initial sets of the values of α_d and k results in a similar or smaller ratio of the maximum to the minimum output voltages if the same restriction of a 200-V peak MOSFET voltage applies.

A switching frequency of 500 kHz is selected for the lowest output voltage when $\Delta_1 = 2.0$ and $k = 1.00$. Therefore the angular resonance frequency of the resonant tank and the switching frequency when $\alpha_d = 4.0$ and $k = 2.31$ can be calculated and the results are given in Table 4.7.

Δ_1	α_d (radians)	k	γ (radians)	f_s (kHz)	ω_0 (Mrad/s)
2.0	0	1.00	8.1	500	4.069
0	4.0	2.31	24.8	163.9	

Table 4.7 Final Calculation Results of the ZVS Two-Inductor Boost Converter

According to Equations (4.6) and (4.7), $L_r = 6.85\ \mu H$ and $C_r = 8.82\ nF$.

4.3.3 Theoretical and Simulation Waveforms

In this section, the theoretical and the simulation waveforms are provided for the selected operating points listed in Table 4.8. These operating points are selected from Tables 4.5 and 4.6. The theoretical waveforms are generated by plotting the device waveforms obtained from Equations (4.23) to (4.32) and the simulation waveforms are generated in SIMULINK. The converter operates in the discontinuous mode under points 1 to 3 and in the continuous mode under points 4 to 6.

Operating Points	Δ_1	α_d (radians)	k	V_d (V)	Theoretical Waveforms	Simulation Waveforms
1	0	4.0	2.31	60.6	Figure 4.14	Figure 4.15
2	0	2.0	1.97	51.8	Figure 4.16	Figure 4.17
3	0	0	1.59	41.8	Figure 4.18	Figure 4.19
4	1.0	0	1.26	33.1	Figure 4.20	Figure 4.21
5	1.6	0	1.09	28.6	Figure 4.22	Figure 4.23
6	2.0	0	1.00	26.2	Figure 4.24	Figure 4.25

Table 4.8 Selected Operating Points

Some important parameters used in the theoretical analysis and the simulation circuit are summarised below:

- $E = 20\ V$,
- $L_r = 6.85\ \mu H$,
- $C_1 = C_2 = 8.82\ nF$,
- $n = 5.6$,
- $R = 576\ \Omega$.

It can be observed that the simulation waveforms agree reasonably well with the theoretical waveforms except that the peak resonant capacitor voltage or the peak MOSFET drain source voltage in the simulation waveforms is slightly higher than that in the theoretical waveforms.

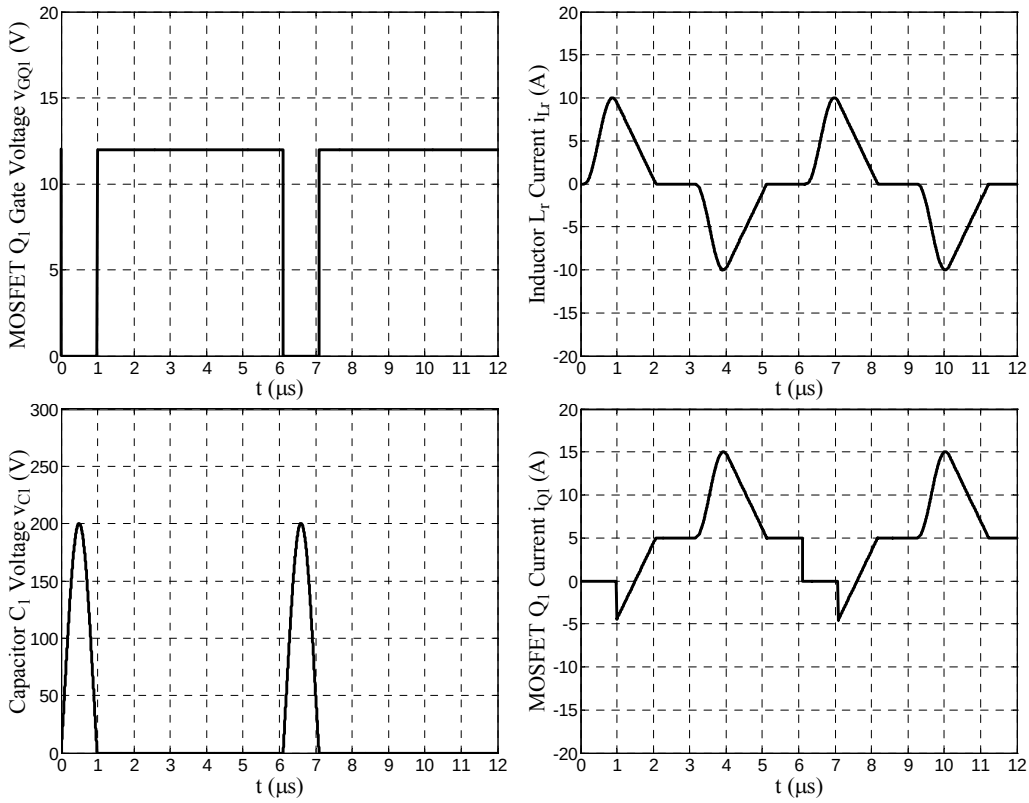

Figure 4.14 Theoretical Waveforms of Point 1

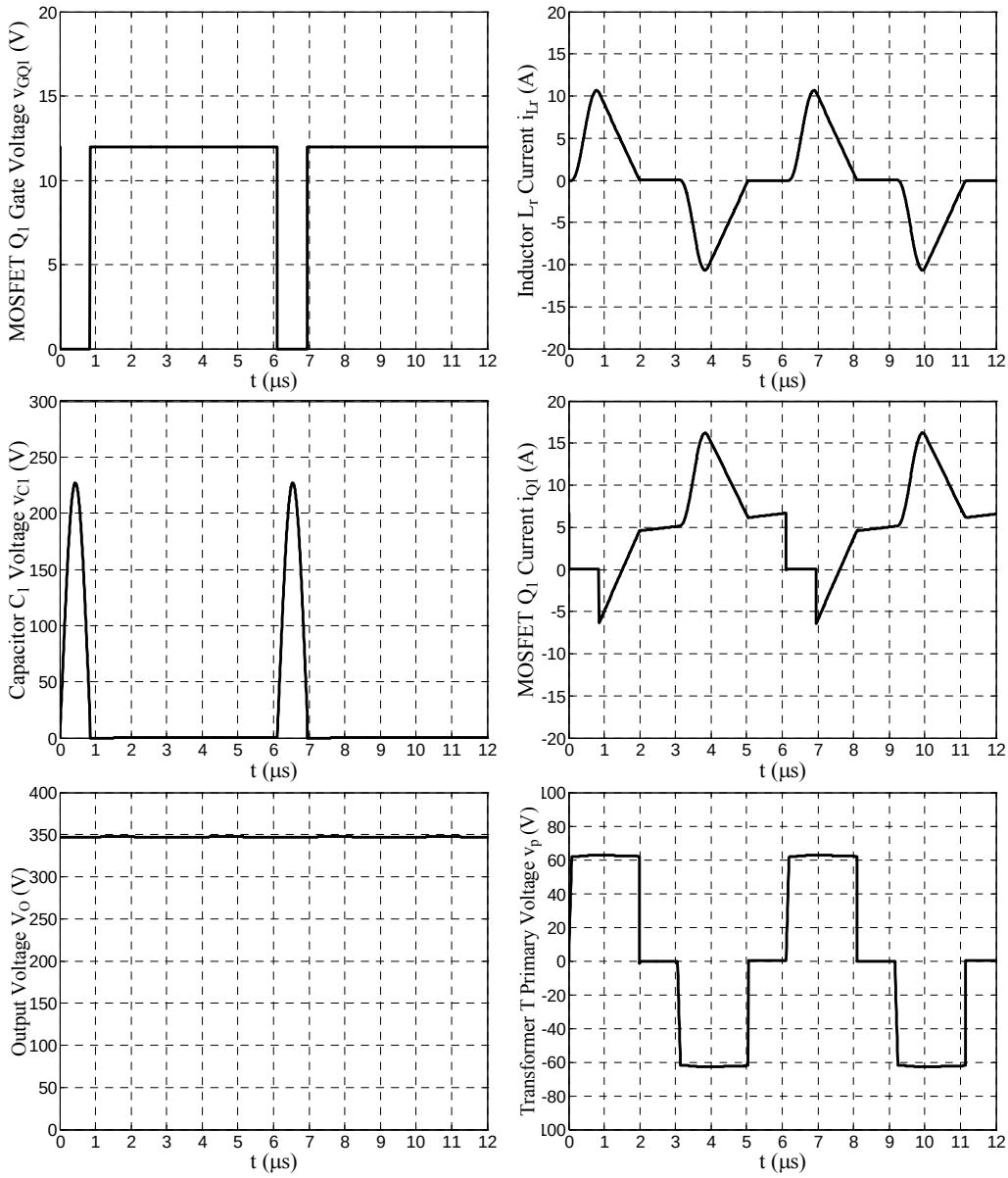

Figure 4.15 Simulation Waveforms of Point 1

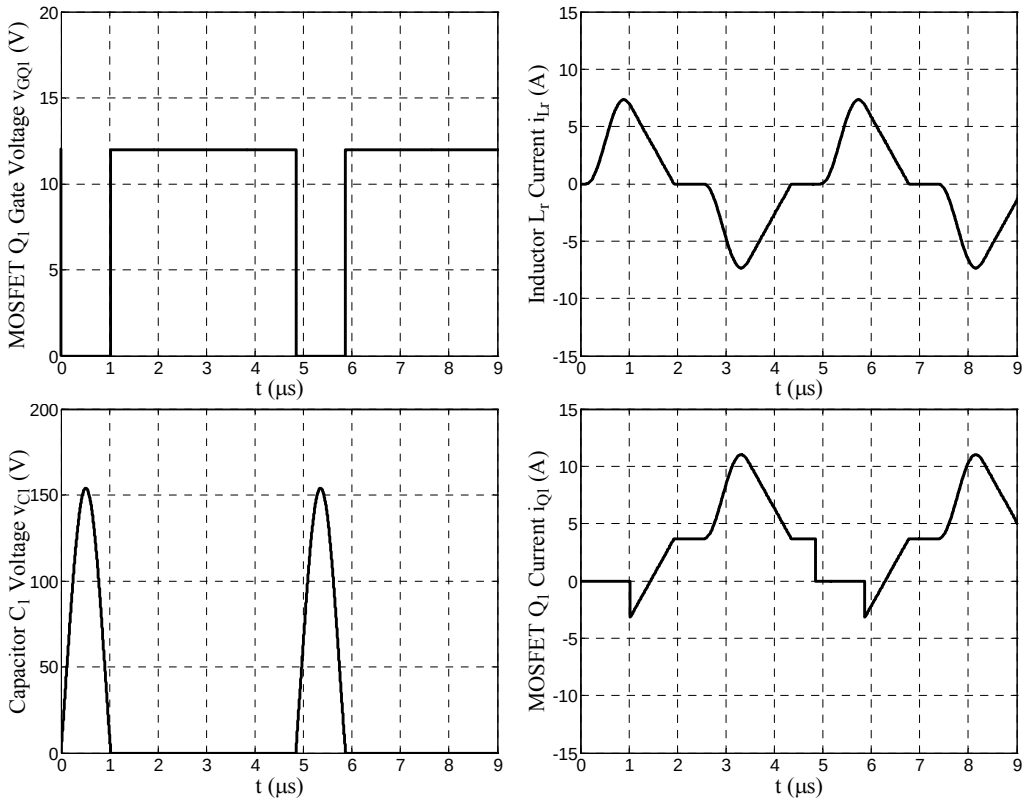

Figure 4.16 Theoretical Waveforms of Point 2

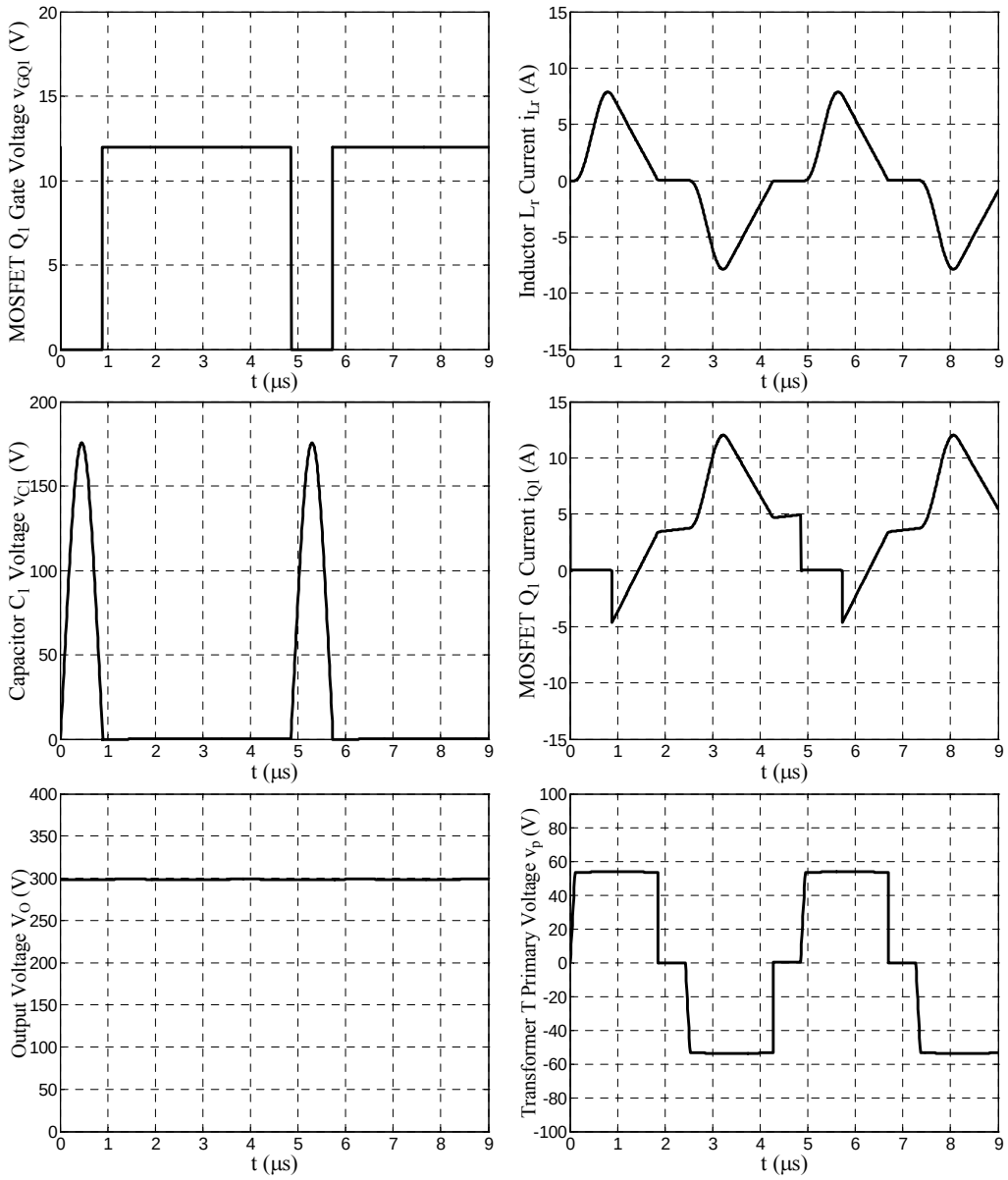

Figure 4.17 Simulation Waveforms of Point 2

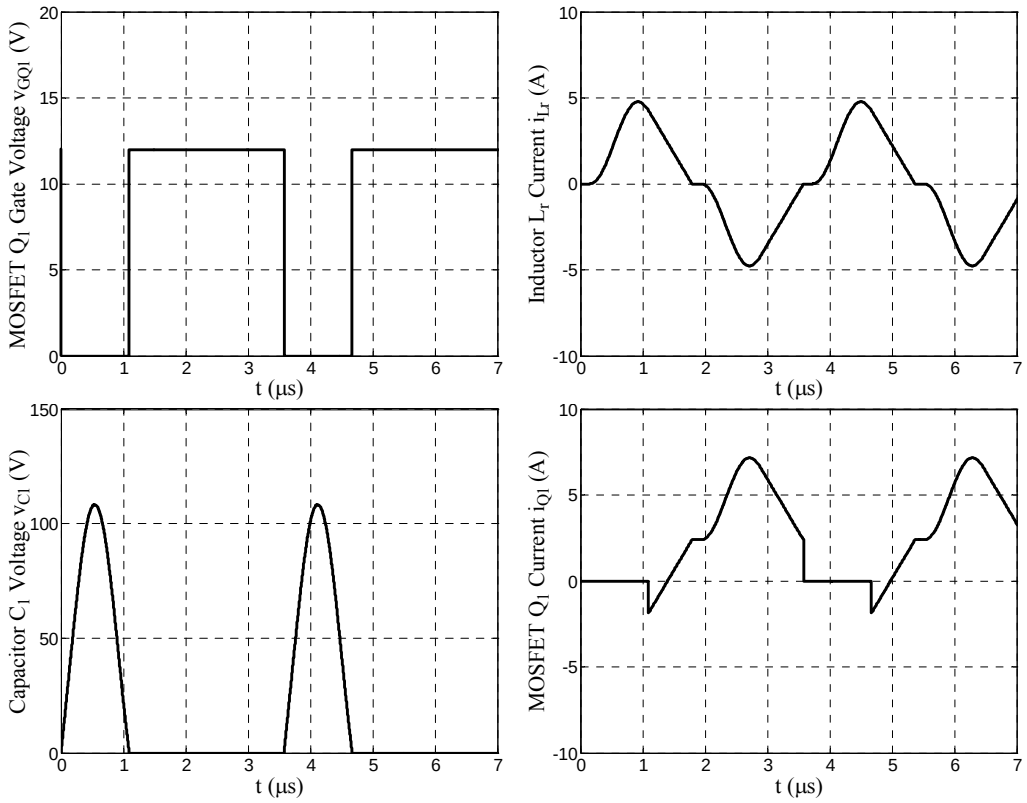

Figure 4.18 Theoretical Waveforms of Point 3

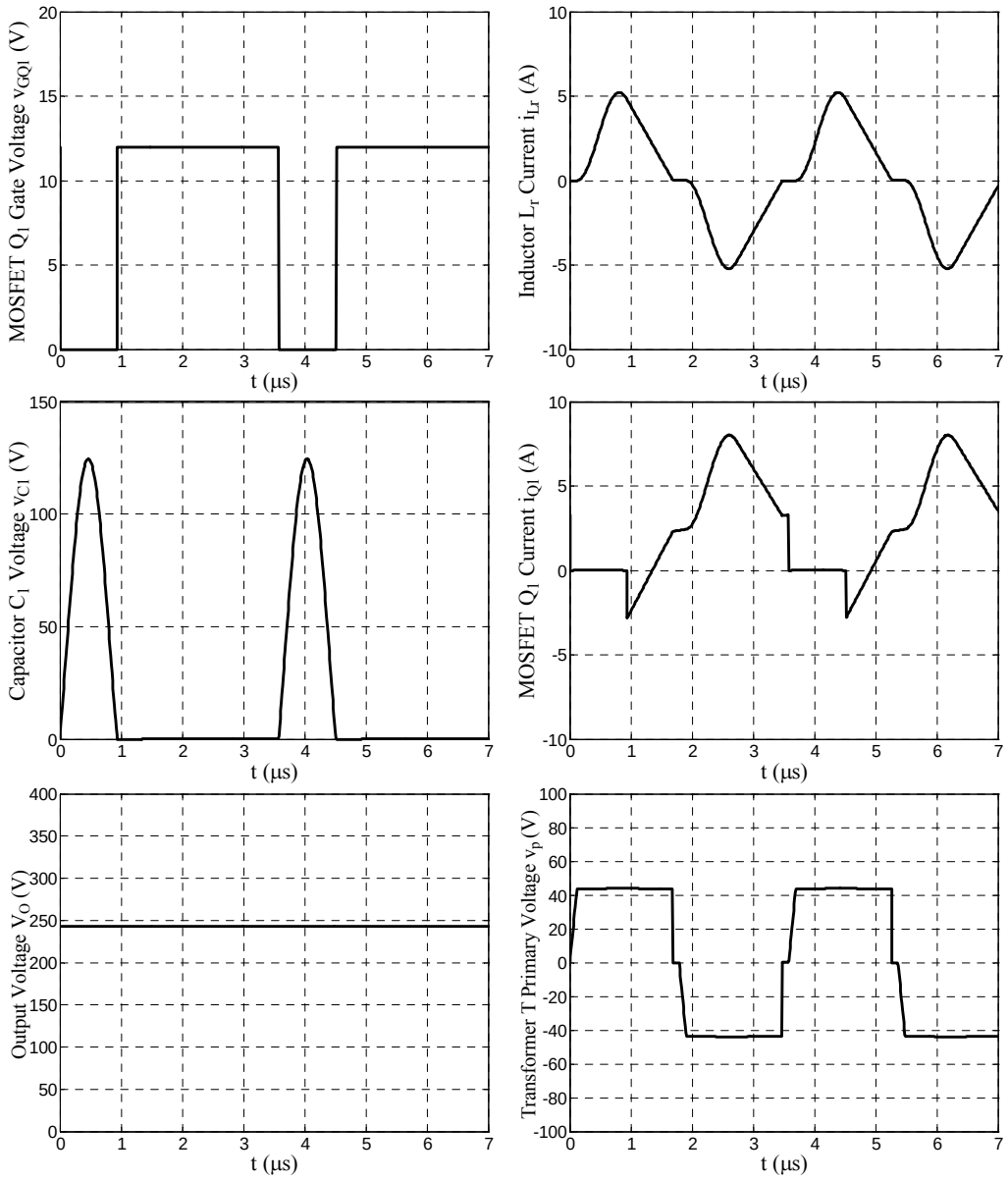

Figure 4.19 Simulation Waveforms of Point 3

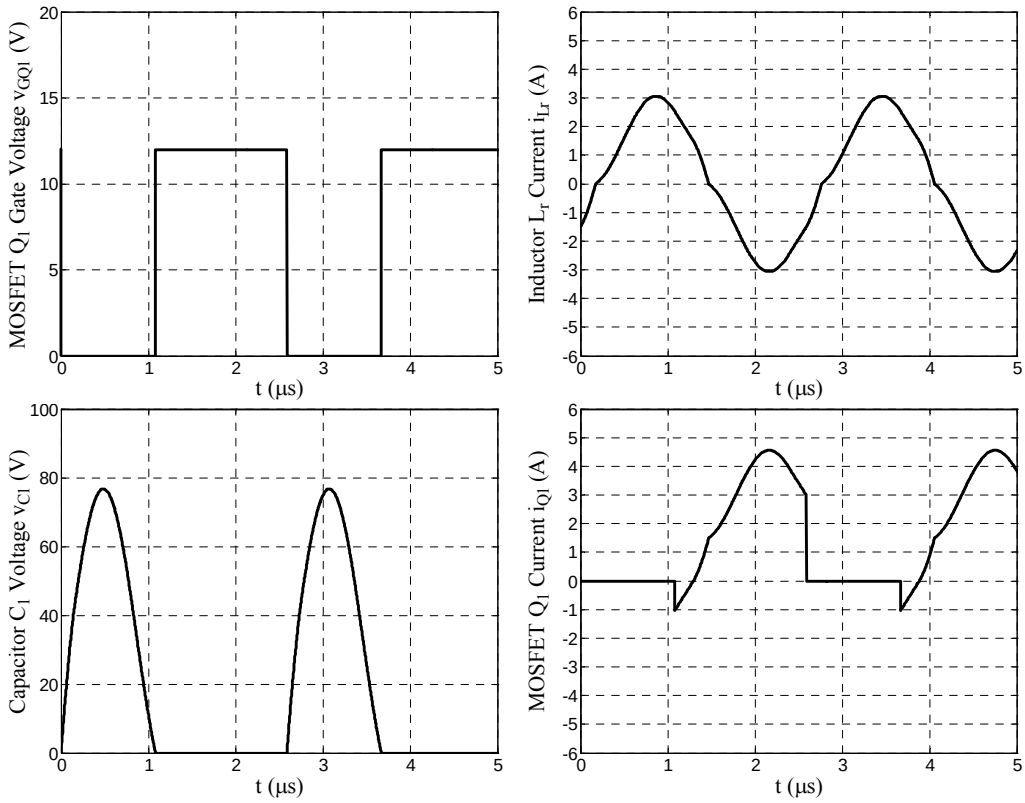

Figure 4.20 Theoretical Waveforms of Point 4

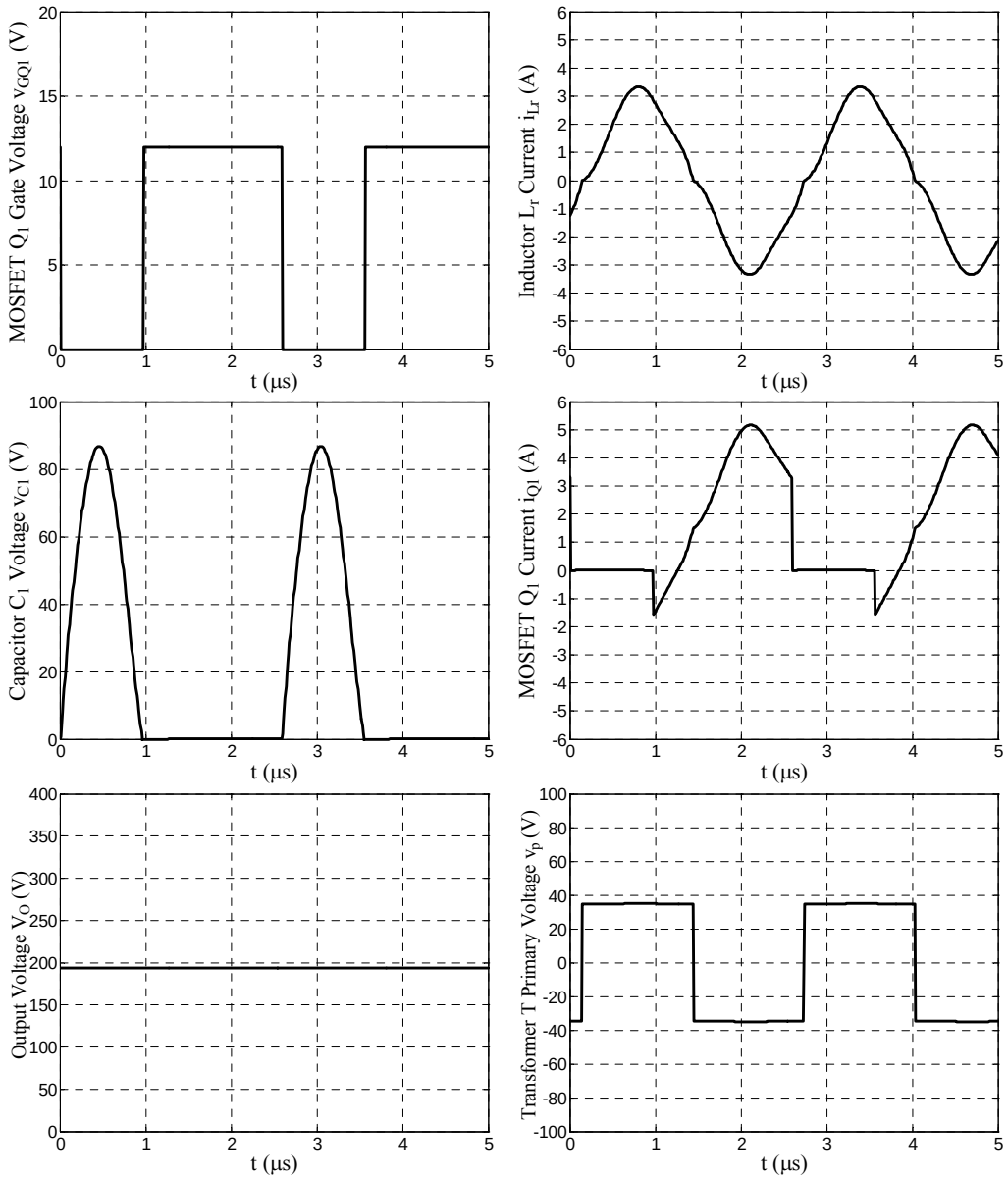

Figure 4.21 Simulation Waveforms of Point 4

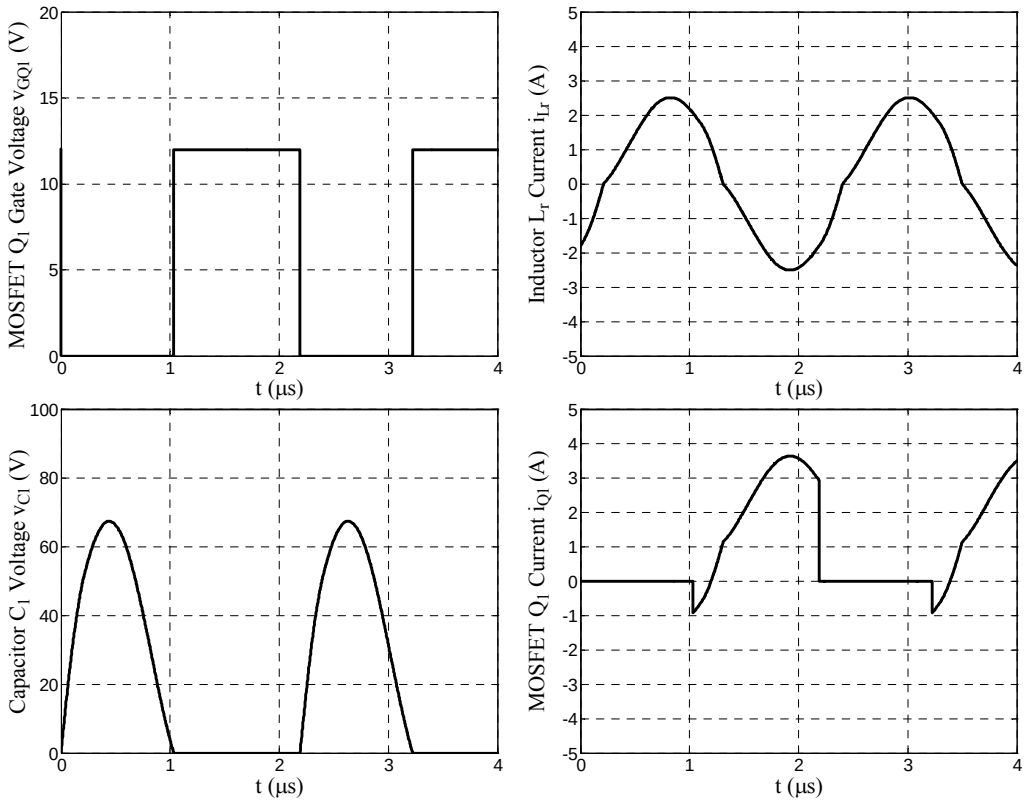

Figure 4.22 Theoretical Waveforms of Point 5

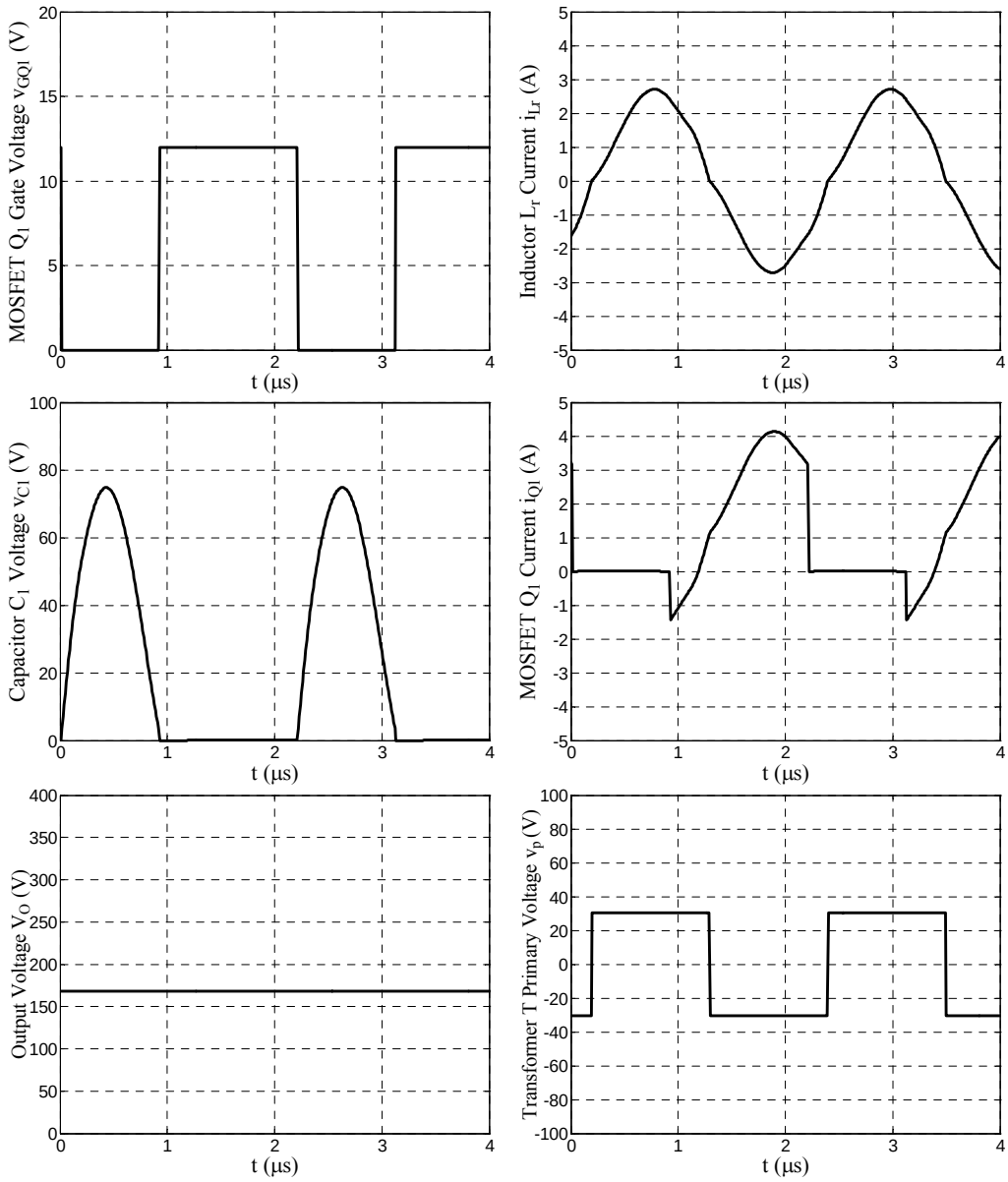

Figure 4.23 Simulation Waveforms of Point 5

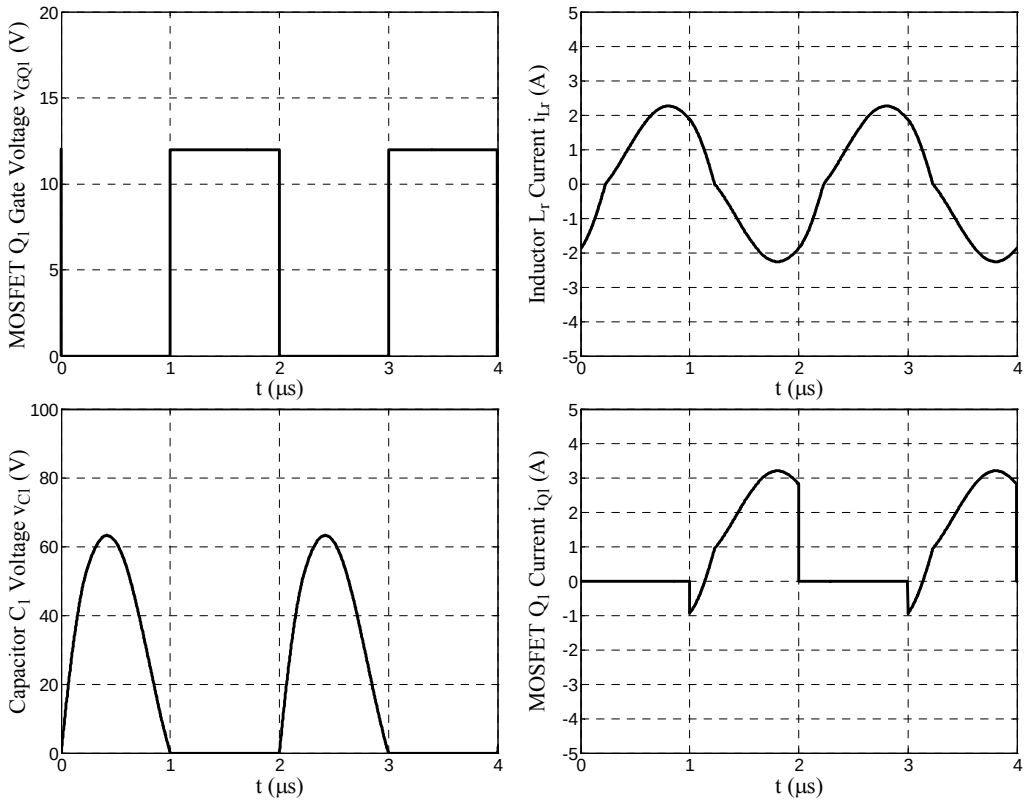

Figure 4.24 Theoretical Waveforms of Point 6

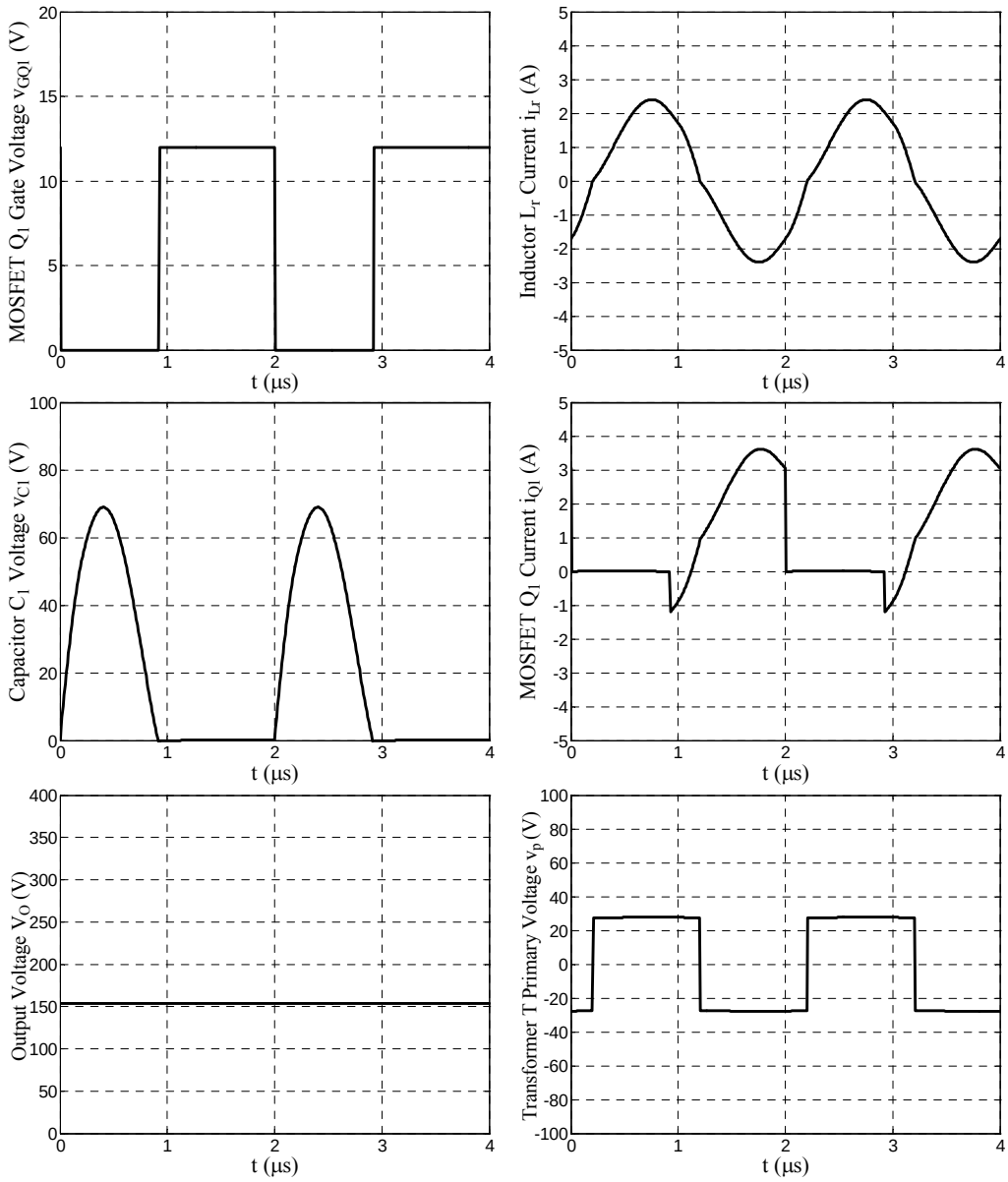

Figure 4.25 Simulation Waveforms of Point 6

4.3.4 Experimental Results

The main components used in the ZVS two-inductor boost converter are listed below:

- Inductors L_1 and L_2 – Core type Siemens RM10 with 0.21-mm air gap in the centre pole, ferrite grade Siemens N48, inductor winding $N_L = 13$ turns.
- Transformer T – Core type Ferroxube ETD29, ferrite grade Ferroxube 3F3, primary and secondary wires: Litz wires respectively made up of 28 and 6 strands of 0.11-mm (0.135-mm overall diameter) wire, primary winding $N_p = 6$ turns, secondary winding $N_s = 34$ turns, leakage inductance reflected to the transformer primary $L_{le} = 0.25\ \mu H$.
- Additional Resonant Inductor – Core type Ferroxube ETD44 with 1.6-mm air gap in the centre core leg, ferrite grade Ferroxube 3F3, Litz wire made up of 34 strands of 0.11-mm (0.135-mm overall diameter) wire, inductor winding $N_{Lr} = 6$ turns, 6.34 μH inductance.
- Additional Resonant Capacitors – Cornell Dubilier surface mount mica capacitor MC22FD102J, 1 nF, $V_{dc} = 500\ V$, 8.5 nF capacitance used.
- MOSFETs Q_1 and Q_2 – ST STB22NS25Z, $V_{DS} = 250\ V$, $I_D = 22\ A$, $R_{DS(on)} = 0.15\ \Omega$, $C_{oss} = 0.34\ nF$.
- Diodes D_1 to D_4 – ST STTA106U, $I_F = 1.0\ A$, $V_{RRM} = 600\ V$, $V_F = 1.5\ V$, $t_{rr} = 20\ ns$.
- Capacitor C_O – Philips MKP capacitor, 1 μF, $V_{dc} = 350\ V$.

The experimental waveforms of the converter operating at different points are respectively shown in Figures 4.26 to 4.30. It is worth mentioning that the converter operation at Point 6 is only theoretically achievable as the switch duty ratio under

this operating point is 50%. This is not practically possible considering the delays over the MOSFET turn-on and turn-off transitions and the experimental waveforms will not be shown for this operating point. Therefore, the lowest output voltage is obtained when the converter operates at Point 5 instead and the practical output voltage range, 160.7 V to 340 V, is slightly narrower than the theoretical one. Figures 4.26 to 4.30 respectively shows the MOSFET Q_1 gate voltage, the resonant capacitor voltage and the resonant inductor current from top to bottom. It can be observed that the experimental waveforms agree reasonably well with the theoretical waveforms except that the peak resonant capacitor voltage or the peak MOSFET drain source voltage in the experimental waveforms is slightly higher than that in the theoretical waveforms.

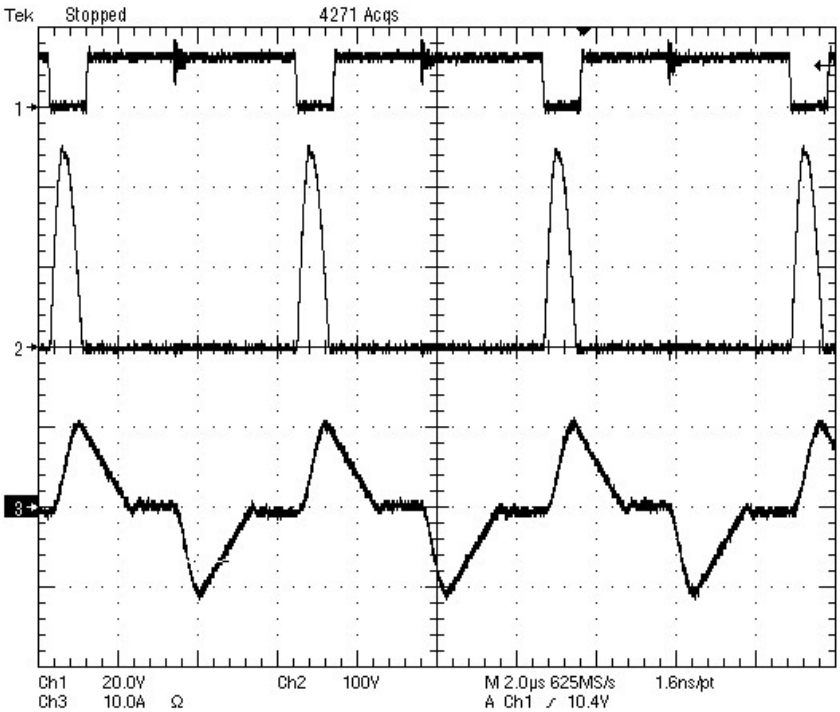

Figure 4.26 Experimental Waveforms of Point 1

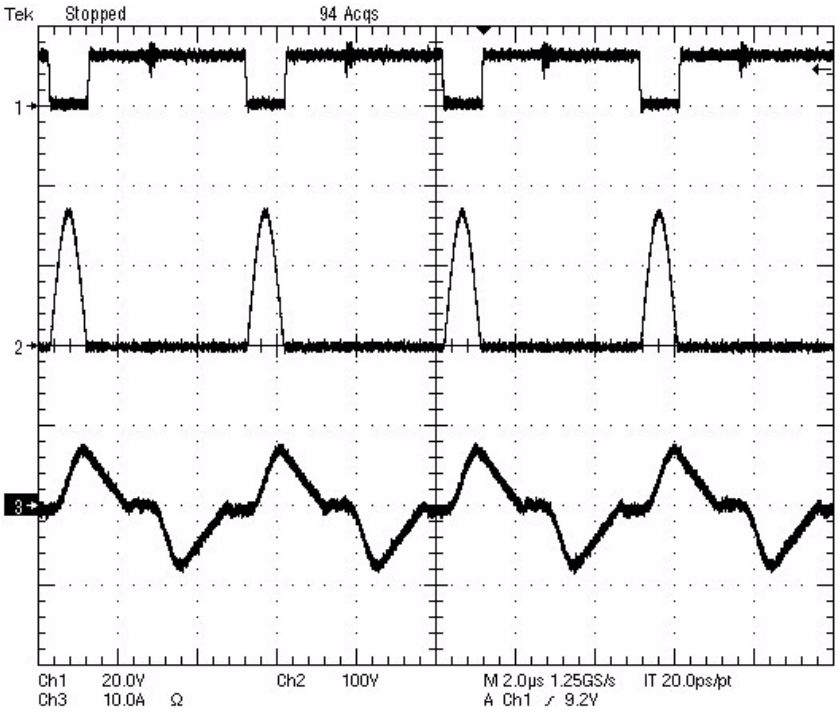

Figure 4.27 Experimental Waveforms of Point 2

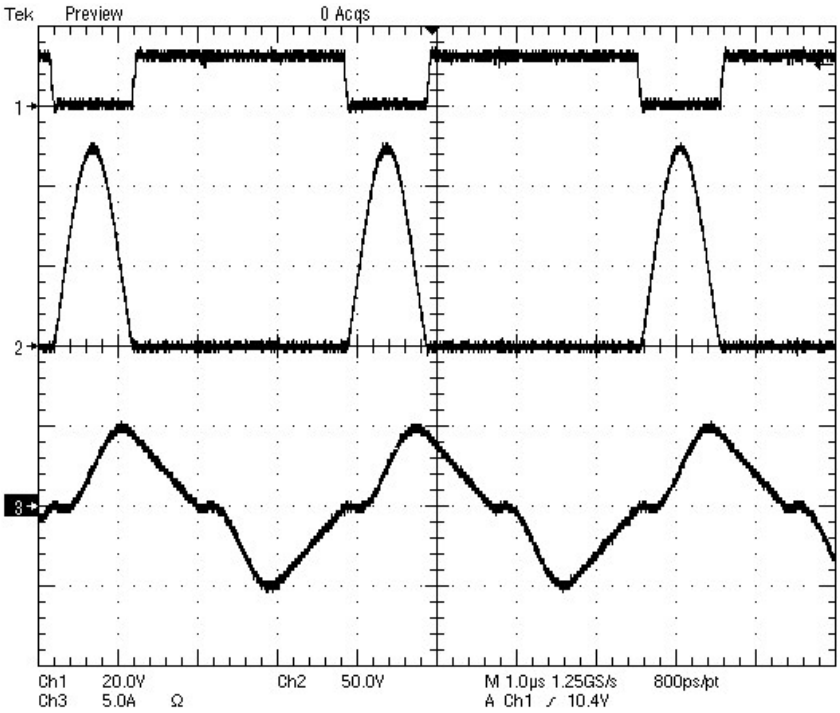

Figure 4.28 Experimental Waveforms of Point 3

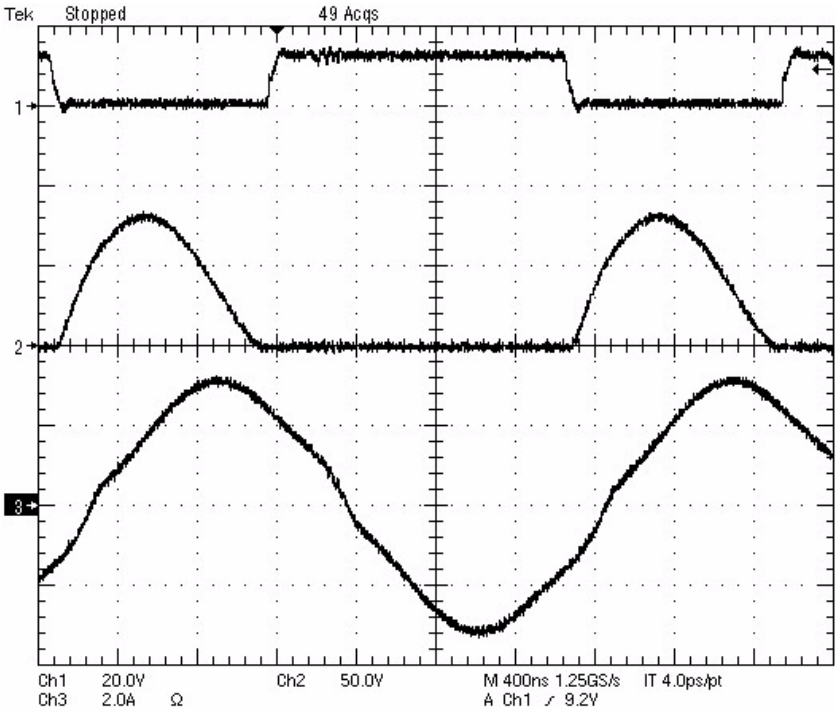

Figure 4.29 Experimental Waveforms of Point 4

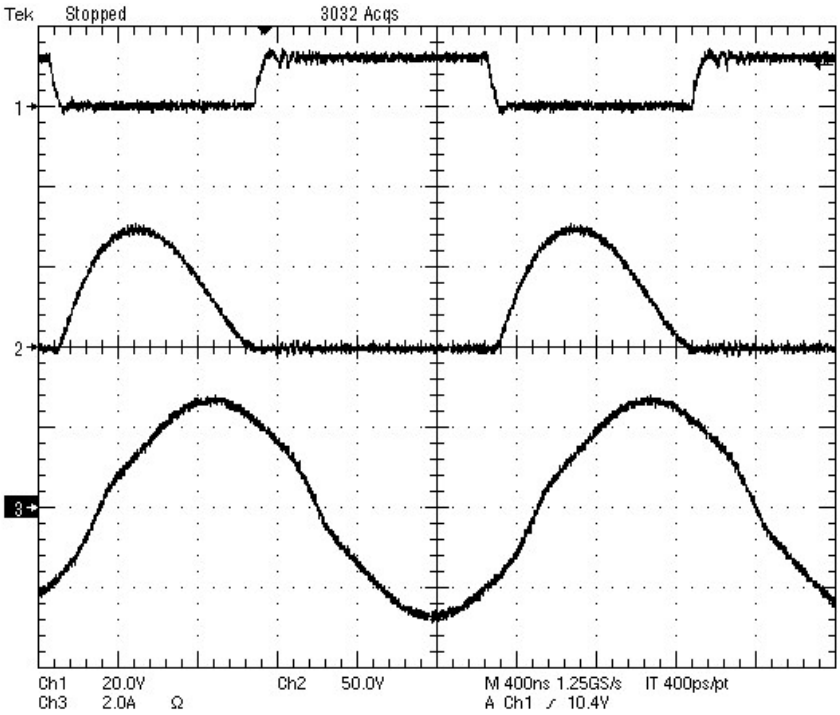

Figure 4.30 Experimental Waveforms of Point 5

The converter output voltages under the individual operating points in the theoretical analysis, the simulation results and the experimental results are listed in Table 4.9 and drawn in Figure 4.31.

Operating Point	Output Voltage V_O (V)		
	Theoretical Analysis	Simulation Result	Experimental Result
1	340.0	347.0	335.0
2	291.1	298.5	278.6
3	234.9	243.1	234.5
4	186.0	193.3	194.4
5	160.7	168.3	174.0
6	147.2	153.2	N/A

Table 4.9 Output Voltage under Each Operating Point

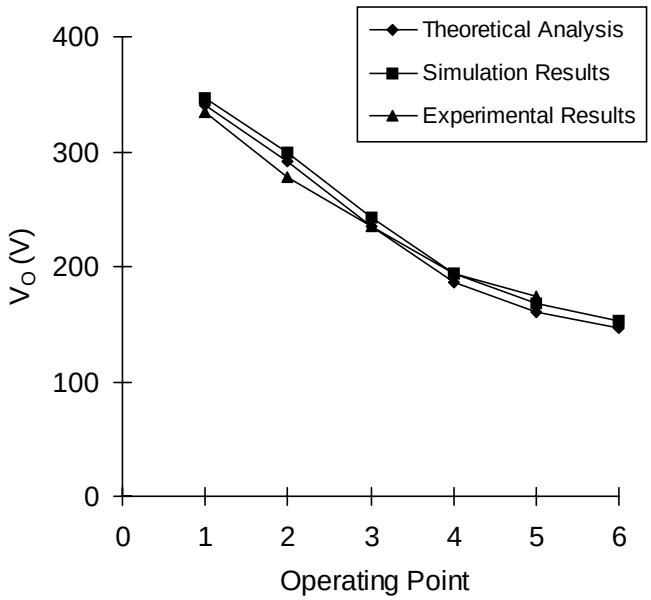

Figure 4.31 Output Voltage under Each Operating Point

4.4 ZVS Two-Inductor Boost Converter with the Voltage Clamp

In the design of the ZVS two-inductor boost converter, the range of the load factor k is required to be less than 2.31 in the selection of the initial set of the circuit parameters in Region 1 to obtain a peak MOSFET voltage of less than 200 V. This constraint inherently results in a very limited output voltage range. However, it can be seen from the surface $V_{Q,peak}$ shown in Figure 4.7 that when k is very large the voltage stress of the MOSFET will become excessively high. This makes it hard to find a MOSFET with a low drain source on resistance to minimise the conduction power loss. In order to operate the converter with a wider output voltage range and without the penalty of the high MOSFET voltage stress, mechanisms which are able to control the MOSFET voltage below a certain level are required. Snubber and voltage clamping circuits are possible solutions and one simple voltage clamping circuit without any active switches will be introduced in this section.

4.4.1 Topology

Figure 4.32 shows the ZVS two-inductor boost converter with the voltage clamp. The voltage clamping circuit is made of two coupled inductors L_{1p}, L_{1s} and L_{2p}, L_{2s} and two additional diodes D_{L1} and D_{L2}. L_{1p} and L_{2p} are the inductances of the inductor main windings. L_{1s} and L_{2s} are the inductances of the inductor clamp windings and are related to the main windings by the square of the turns ratio. The turns ratio of the coupled inductor main winding to the clamp winding is n_L:1. When the voltage across the main winding of each coupled inductor reaches $n_L E$, dot

negative, the diode D_{L1} or D_{L2} will conduct and this clamps the voltage across the MOSFET to V_c, which is defined as:

$$V_c = (1 + n_L)E \tag{4.37}$$

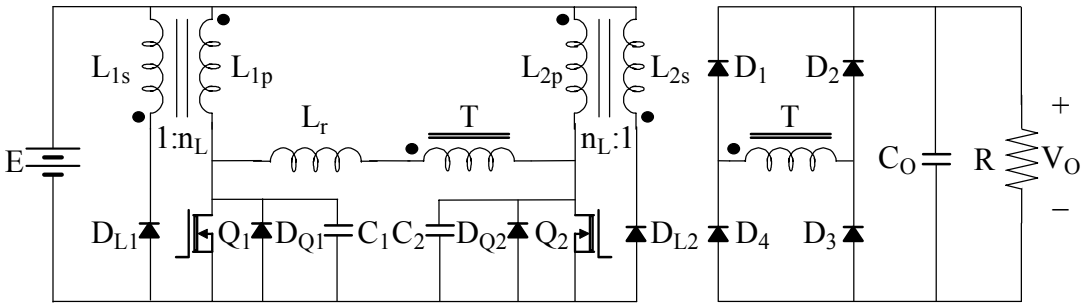

Figure 4.32 ZVS Two-Inductor Boost Converter with the Voltage Clamp

In this analysis, a tight coupling between the two coupled inductor windings is assumed. Although the transfer of the current from one winding to another does not need to be instantaneous in a hard-switched converter, that in a soft-switched converter can be considered instantaneous as small leakage inductances of the coupled inductors have little effect.

4.4.2 State Analysis

This section provides the state analysis of the ZVS two-inductor boost converter with the voltage clamp. Different combinations of the circuit parameters including the load factor k and the timing factor Δ_1 determine different states in Figure 4.4 when the voltage clamping circuit becomes active while the delay angle α_d only

affects the length of the switching period and is irrelevant in the discussion. Before Q_1 turns off, both of Q_1 and Q_2 are on. The number of the possible states after Q_1 turns off and before Q_2 turns off depends on the combinations of the values of Δ_1 and k. According to the specific state in Figure 4.4 when the voltage clamping circuit becomes active, the converter operation can be classified into three operating sets. In each operating set, the values of Δ_1 and k will only be qualitatively discussed as the quantitative analysis requires the exact numerical value of n_L. In Operating Set 1, Δ_1 and k are both small (Δ_1 can be zero) or both medium and the switch voltage does not reach the clamping voltage V_c in the converter operation at all. The converter will move through up to four states as shown in Figure 4.4 and the state analysis has been provided in Section 4.3.1. In Operating Set 2, Δ_1 is small and k is medium or Δ_1 is zero and k is large and the switch voltage reaches the clamping voltage V_c in State (c) in Figure 4.4. The converter will move through up to six states after Q_1 turns off and before Q_2 turns off. In Operating Set 3, Δ_1 is greater than zero and k is large enough and the switch voltage reaches the clamping voltage V_c in State (a) in Figure 4.4. The converter will move through five states after Q_1 turns off and before Q_2 turns off. The above discussion is summarised briefly in Table 4.10.

In Operating Set 2, the voltage clamping circuit becomes active in State (c) shown in Figure 4.4. Six possible states of the converter after Q_1 turns off and before Q_2 turns off are shown in Figure 4.33. If the inductance L_{1p} is large enough, I_0 is the current in the main winding of the coupled inductor when the diode D_{L1} is not conducting

and the voltage clamping circuit is not active. The inductor L_e, the diode D_c and the voltage source V_c form the equivalent circuit of the coupled inductor in State (d) and will be explained in detail in due course. The initial conditions in State (a) are $i_{Lr}(0) = -\Delta_1 I_0$ and $v_{C1}(0) = 0$. The analysis of each state is given below.

Operating Set	Circuit Parameters	Voltage Clamping Circuit Status	Number of States
1	Δ_1 and k are both small or Δ_1 and k are both medium	Inactive	Up to 4
2	Δ_1 is small and k medium or $\Delta_1 = 0$ and k is large	Active	Up to 6
3	$\Delta_1 > 0$ and k is large	Active	5

Table 4.10 Possible Operating Sets

- State (a) ($0 \le t \le t_1$)

This state is similar to State (a) in Section 4.3.1. The capacitor voltage v_{C1} and the inductor current i_{Lr} are respectively given by Equations (4.23) and (4.24).

- State (b) ($t_1 \le t \le t_2$)

This state is similar to State (b) in Section 4.3.1. The capacitor voltage v_{C1} and the inductor current i_{Lr} are respectively given by Equations (4.25) and (4.26).

- State (c) ($t_2 \le t \le t_3$)

This state is similar to State (c) in Section 4.3.1. The capacitor voltage v_{C1} and the inductor current i_{Lr} are respectively given by Equations (4.28) and (4.29).

- State (d) ($t_3 \le t \le t_4$)

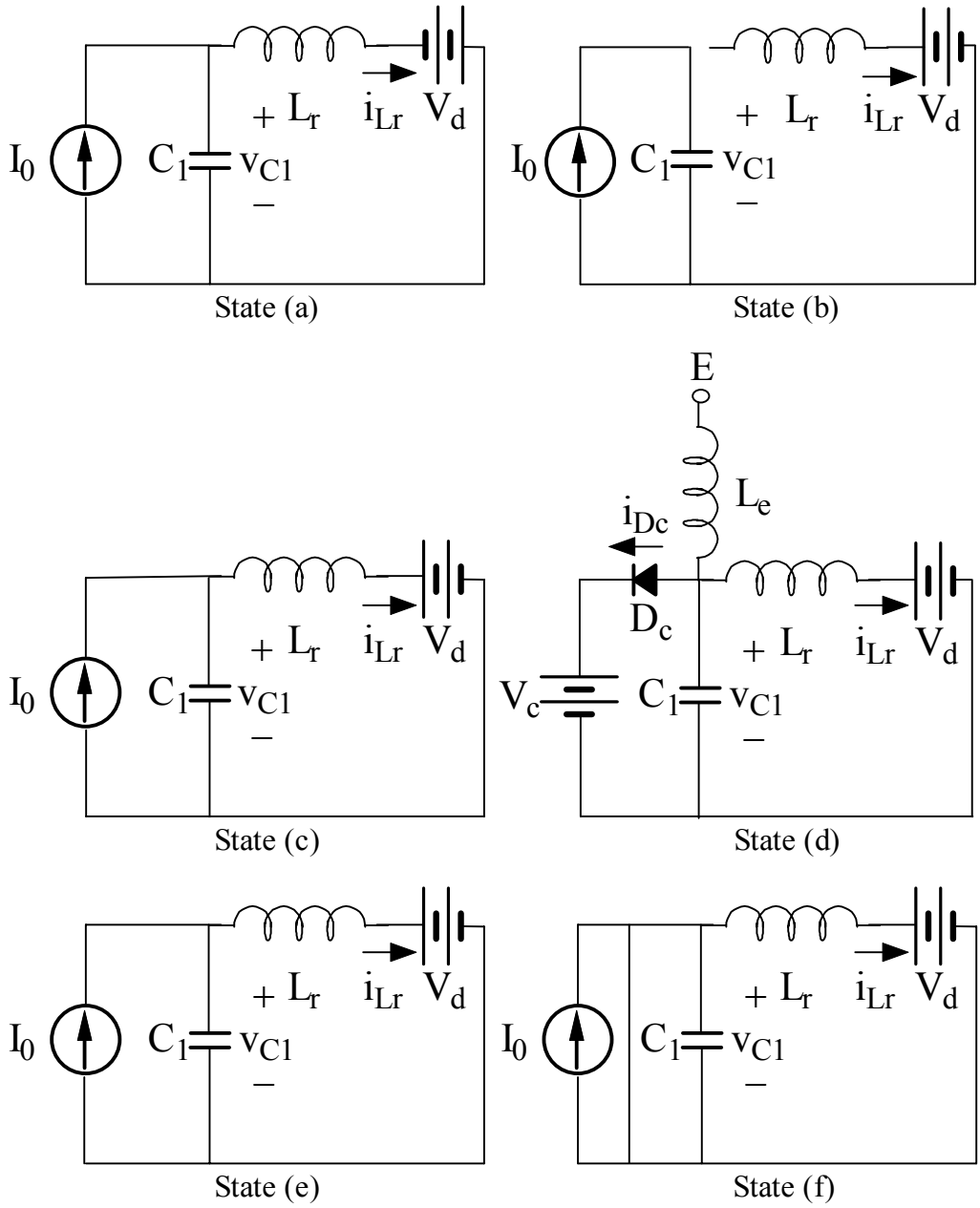

Figure 4.33 Six Possible States in Operating Set 2

This state starts when the diode D_{L1} conducts and the resonant capacitor voltage v_{C1} is clamped. In this state, the coupled inductor can be replaced by an equivalent circuit made up of a single-winding inductor L_e, a diode D_c and a voltage source V_c. The inductor L_e has the same number of turns as L_{1p} therefore the inductor L_e current must be I_0 in order to maintain the flux linkage or the Ampere-turns balance. Part of I_0 feeds the resonant inductor while the rest of I_0 flows through the diode D_c and the voltage source V_c, which represents the clamping voltage. The resonant inductor current i_{Lr} is also the coupled inductor main winding current and the diode D_c current i_{Dc} is the coupled inductor clamp winding current reflected to the main winding. In this state, the resonant inductor current is greater than zero therefore the current i_{Dc} is smaller than I_0. V_c should be greater than or equal to $2V_d$ to maintain the ZVS condition and this will be proved in State (e). The resonant inductor L_r is linearly charged by $V_c - V_d$. The capacitor voltage v_{C1} and the inductor current i_{Lr} are respectively:

$$v_{C1}(t) = V_c \tag{4.38}$$

$$i_{Lr}(t) = i_{Lr}(t_3) + \frac{V_c - V_d}{L_r}(t - t_3) \tag{4.39}$$

Substituting Equation (4.6) to (4.39) yields:

$$i_{Lr}(t) = i_{Lr}(t_3) + \frac{V_c - V_d}{Z_0}\omega_0(t - t_3) \tag{4.40}$$

- State (e) ($t_4 \le t \le t_5$)

This state starts when the resonant inductor current reaches I_0. The diode D_{L1} becomes reverse biased as the coupled inductor main winding current is I_0 and the clamp winding current is zero. Therefore, the capacitor C_1 resonates with the inductor L_r and this state is similar to State (c) in Section 4.3.1. The capacitor voltage v_{C1} and the inductor current i_{Lr} are respectively:

$$v_{C1}(t) = (V_c - V_d)\cos\omega_0(t - t_4) + V_d \tag{4.41}$$

$$i_{Lr}(t) = \frac{V_c - V_d}{Z_0}\sin\omega_0(t - t_4) + I_0 \tag{4.42}$$

According to Equation (4.41), it is required that $V_c \ge 2V_d$ in order to maintain the ZVS condition.

- State (f) ($t_5 \le t \le t_6$)

This state starts when v_{C1} reaches zero and is similar to State (d) in Section 4.3.1. The inductor current i_{Lr} is:

$$i_{Lr}(t) = i_{Lr}(t_5) - \frac{V_d}{L_r}(t - t_5) \tag{4.43}$$

Substituting Equation (4.6) to (4.43) yields:

$$i_{Lr}(t) = i_{Lr}(t_5) - \frac{V_d}{Z_0}\omega_0(t - t_5) \tag{4.44}$$

The capacitor voltage v_{C1} is given by Equation (4.30).

In Operating Set 3, the voltage clamping circuit becomes active in State (a) shown in Figure 4.4. Five states of the converter after Q_1 turns off and before Q_2 turns off are shown in Figure 4.34. The initial conditions in State (a) are $i_{Lr}(t_0) = -\Delta_1 I_0$ and $v_{C1}(t_0) = 0$. The analysis of each state is given below.

- State (a) ($0 \le t \le t_1$)

This state is similar to State (a) in Section 4.3.1. The capacitor voltage v_{C1} and the inductor current i_{Lr} are respectively given by Equations (4.23) and (4.24).

- State (b) ($t_1 \le t \le t_2$)

This state starts when the diode D_{L1} conducts and the resonant capacitor voltage v_{C1} is clamped. In this state, the resonant inductor current is less than zero therefore the current i_{Dc} is greater than I_0. The resonant inductor L_r is linearly charged by $V_c + V_d$. The inductor current i_{Lr} is:

$$i_{Lr}(t) = i_{Lr}(t_1) + \frac{V_c + V_d}{L_r}(t - t_1) \tag{4.45}$$

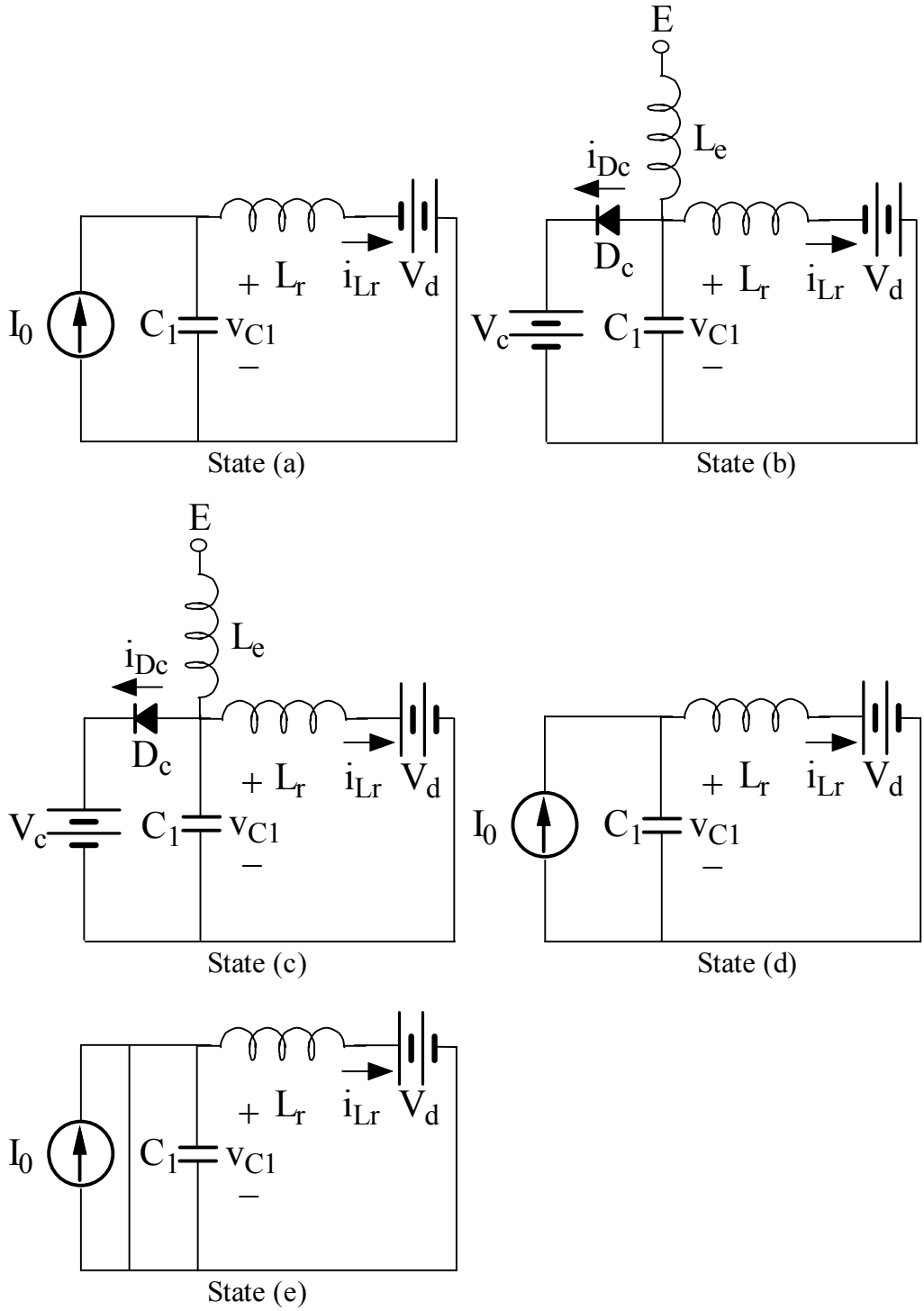

Figure 4.34 Five States in Operating Set 3

Substituting Equation (4.6) to (4.45) yields:

$$i_{Lr}(t) = i_{Lr}(t_1) + \frac{V_c + V_d}{Z_0}\omega_0(t - t_1) \tag{4.46}$$

The capacitor voltage v_{C1} is given by Equation (4.38).

- State (c) ($t_2 \le t \le t_3$)

This state starts when the resonant inductor current reaches zero and V_d reverses. It is similar to State (d) in Operating Set 2. In this state, the resonant inductor current continues to increase linearly but at a slower rate because the voltage across L_r in this stage is $V_c - V_d$ rather than $V_c + V_d$ in the previous state. As the resonant inductor current is greater than zero, the current i_{Dc} is less than I_0. The inductor current i_{Lr} is:

$$i_{Lr}(t) = i_{Lr}(t_2) + \frac{V_c - V_d}{L_r}(t - t_2) \tag{4.47}$$

Substituting Equation (4.6) to (4.47) yields:

$$i_{Lr}(t) = i_{Lr}(t_2) + \frac{V_c - V_d}{Z_0}\omega_0(t - t_2) \tag{4.48}$$

The capacitor voltage v_{C1} is given by Equation (4.38).

- State (d) ($t_3 \le t \le t_4$)

This state starts when the resonant inductor current reaches I_0 and is similar to State (e) in Operating Set 2. The capacitor voltage v_{C1} and the inductor current i_{Lr} are respectively:

$$v_{C1}(t) = (V_c - V_d)\cos\omega_0(t - t_3) + V_d \tag{4.49}$$

$$i_{Lr}(t) = \frac{V_c - V_d}{Z_0}\sin\omega_0(t - t_3) + I_0 \tag{4.50}$$

According to Equation (4.49), it is still required that $V_c \ge 2V_d$ to maintain the ZVS condition.

- State (e) ($t_4 \le t \le t_5$)

This state starts when v_{C1} reaches zero and is similar to State (d) in Section 4.3.1. The inductor current i_{Lr} is:

$$i_{Lr}(t) = i_{Lr}(t_4) - \frac{V_d}{L_r}(t - t_4) \tag{4.51}$$

Substituting Equation (4.6) to (4.51) yields:

$$i_{Lr}(t) = i_{Lr}(t_4) - \frac{V_d}{Z_0}\omega_0(t - t_4) \tag{4.52}$$

The capacitor voltage v_{C1} is given by Equation (4.30).

4.4.3 Design Process

The design process of the ZVS two-inductor boost converter with the voltage clamp is similar to that of the converter without the voltage clamp. However, some design equations listed in Section 4.2 are in different forms due to the introduction of the voltage clamping circuit.

Figure 4.35 shows the equivalent circuit of the primary side of the converter when the MOSFET Q_1 is off and the resonant capacitor C_1 voltage is clamped, where i_{IN} is the input current, i_{L1p} and i_{L1s} are respectively the main and the clamp winding currents of the coupled inductor in the vicinity of Q_1 and i_{L2} is the current of the coupled inductor in the vicinity of Q_2. During this period, part of the energy stored in the resonant tank will be fed back to the voltage source E through L_{1s}. Therefore, the average input power of the converter is not $E \cdot 2I_0$ as given in Equation (4.1).

The calculation of the average input power when the voltage clamping circuit is active is given below. Because the resonant inductor current is half cycle

symmetrical, the average current and power can be calculated over a half switching period. $\hat{T}$ is defined as the half switching period, t_c is defined as the duration when the resonant capacitor voltage is clamped and t_{nc} is defined as the duration when the voltage clamping circuit is not active. Then it is easy to derive:

$$\hat{T} = t_c + t_{nc} \tag{4.53}$$

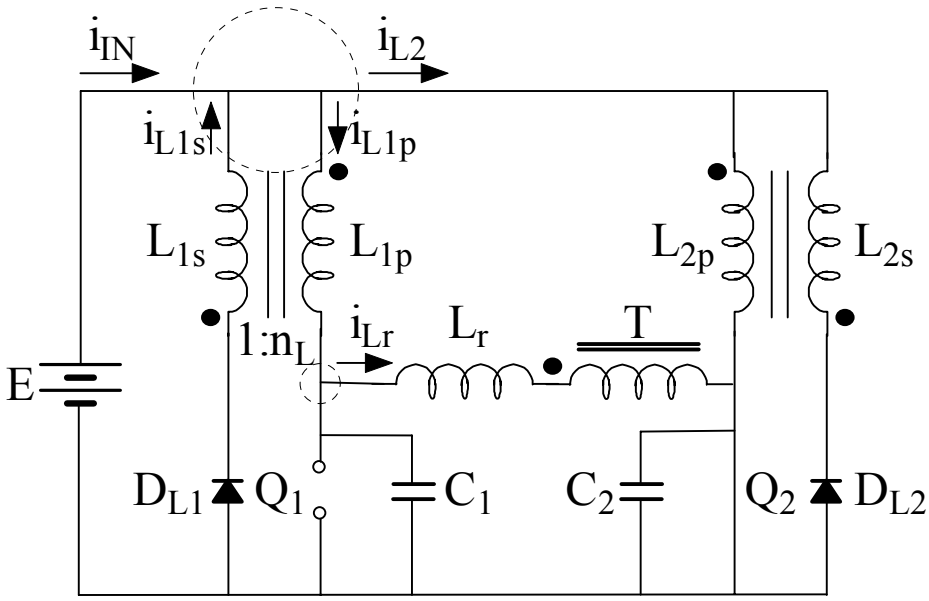

Figure 4.35 Equivalent Primary Circuit with a Voltage Clamped Capacitor

Over the duration when the voltage clamping circuit is not active, the average input current $I_{IN,nc}$ and power $P_{IN,nc}$ are:

$$I_{IN} = 2I_0 \tag{4.54}$$

$$P_{IN,nc} = E \cdot 2I_0 \tag{4.55}$$

Over the duration when the resonant capacitor voltage is clamped, the following equations can be found by applying KCL to the junctions inside the dashed circles shown in Figure 4.35 and the flux linkage or the Ampere-turns balance of the coupled inductor:

$$i_{IN} + i_{L1s} = i_{L1p} + i_{L2} \tag{4.56}$$

$$i_{L1p} = i_{Lr} \tag{4.57}$$

$$i_{L1s} + n_L i_{L1p} = n_L I_0 \tag{4.58}$$

Manipulating Equations (4.56) to (4.58) yields:

$$i_{IN} = I_0 + i_{L2} - (n_L + 1) \cdot (I_0 - i_{Lr}) \tag{4.59}$$

Then it is important to derive the counterparts of Equations (4.1), (4.10) and (4.18) in the ZVS two-inductor boost converter with the voltage clamp and only the derivation process of the equations in Region 2 operation is given here. Other design equations of the converter with the voltage clamp are the same as those of the resonant converter without the voltage clamp.

As the diode D_{L2} is not conducting, i_{L2} is the main winding current of the coupled inductor in the vicinity of Q_2 and I_0 is the average of i_{L2} over the duration when the resonant capacitor C_1 voltage is clamped. If the function $\hat{g}_{\Delta,c}(\Delta_1, k)$ is defined as the ratio of the average resonant inductor current against a specific set of Δ_1 and k

values to I_0 over the duration when the resonant capacitor C_1 voltage is clamped, the average input current $I_{IN,c}$ and power $P_{IN,c}$ during this period can be respectively derived as:

$$I_{IN,c} = 2I_0 - (n_L + 1)I_0[1 - \hat{g}_{\Delta,c}(\Delta_1, k)] \tag{4.60}$$

$$P_{IN,c} = EI_0\{2 - (n_L + 1)[1 - \hat{g}_{\Delta,c}(\Delta_1, k)]\} \tag{4.61}$$

Therefore according to Equation (4.53), the input power P_{IN} of the converter can be calculated as:

$$P_{IN} = \frac{P_{IN,nc}t_{nc} + P_{IN,c}t_c}{\hat{T}} = E \cdot 2I_0 - EI_0 \frac{(n_L + 1)[1 - \hat{g}_{\Delta,c}(\Delta_1, k)]t_c}{\hat{T}} \tag{4.62}$$

If $r_\Delta(\Delta_1, k)$ is defined as:

$$r_\Delta(\Delta_1, k) = \frac{(n_L + 1)[1 - \hat{g}_{\Delta,c}(\Delta_1, k)]t_c}{\hat{T}} \tag{4.63}$$

The counterpart of Equation (4.1) in the resonant converter with the voltage clamp in Region 2 can be derived as:

$$E \cdot 2I_0 - EI_0 r_\Delta(\Delta_1, k) = \frac{V_O^2}{R} \tag{4.64}$$

Using Equation (4.2), Equation (4.64) can be written as:

$$V_d = \frac{[2 - r_\Delta(\Delta_1, k)]E}{\hat{g}_\Delta(\Delta_1, k)} \tag{4.65}$$

Table 4.11 lists Equations (4.1), (4.10) and (4.18) and their counterparts in the resonant converter with the voltage clamp, where $r_\alpha(\alpha_d, k)$ is defined as:

$$r_\alpha(\alpha_d, k) = \frac{(n_L + 1)[1 - \hat{g}_{\alpha,c}(\alpha_d, k)]t_c}{\hat{T}} \tag{4.66}$$

Converter without the Voltage Clamp	Converter with the Voltage Clamp
$E \cdot 2I_0 = \frac{V_O^2}{R}$ (4.1)	$E \cdot 2I_0 - EI_0 r_\Delta(\Delta_1, k) = \frac{V_O^2}{R}$ (4.64)
	$E \cdot 2I_0 - EI_0 r_\alpha(\alpha_d, k) = \frac{V_O^2}{R}$ (4.67)
$V_d = \frac{2E}{\hat{g}_\Delta(\Delta_1, k)}$ (4.10)	$V_d = \frac{[2 - r_\Delta(\Delta_1, k)]E}{\hat{g}_\Delta(\Delta_1, k)}$ (4.65)
$V_d = \frac{2E}{\hat{g}_\alpha(\alpha_d, k)}$ (4.18)	$V_d = \frac{[2 - r_\alpha(\alpha_d, k)]E}{\hat{g}_\alpha(\alpha_d, k)}$ (4.68)

Table 4.11 Design Equations in the Two Converters

The other equations given in Section 4.2 can be used in the design of the resonant converter with the voltage clamp without any change. It is especially worth mentioning that the circuit constraints in Regions 1 and 2 of the resonant converter

with the voltage clamp are respectively the same as those given by Equations (4.19) and (4.11). These can be confirmed by the manipulations of Equations (4.2) to (4.4), (4.15), (4.64) and (4.67).

Because the output voltage of the converter is higher when it operates in Region 1, the maximum output voltage, 340 V, must be designed with a non-zero delay angle α_d. In the design of the converter with the voltage clamp, n_L is selected to be 3.5 and the clamping voltage is therefore 90 V for the 20-V input from the voltage source. In this case, MOSFETs with 100-V drain source voltage ratings can be used in the converter.

From Equations (4.18) and (4.68), the surface V_d can be drawn against α_d and k in Figure 4.36, where $0 \le \alpha_d \le 4$ and $10 \le k \le 25$. Table 4.12 shows the maximum and the minimum values of V_d in Figure 4.36.

Because the maximum peak MOSFET voltage is limited to 90 V, an initial set of the design parameters can be easily selected to be $\alpha_d = 4$ and $k = 25$ without causing an excessive voltage stress across the MOSFETs. The calculation results from Equations (4.3), (4.4), (4.15) and (4.67) and the state analysis are given in Table 4.13.

The key design parameters including the resonant inductance and capacitance will be calculated from Equations (4.5) to (4.7) in due course when the analyses in both

Regions 1 and 2 are conducted and the switching frequency is selected.

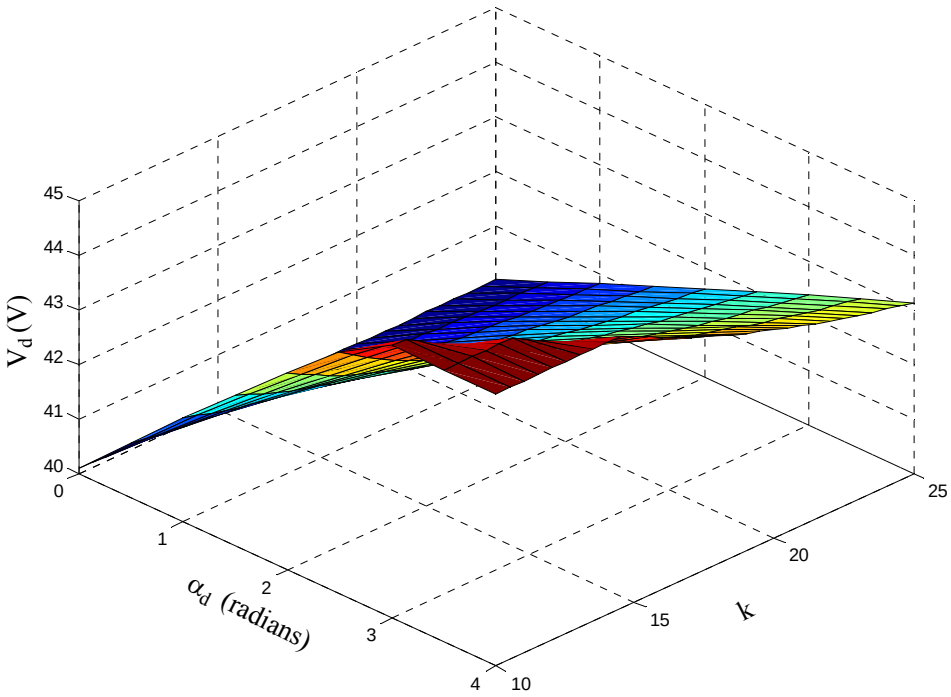

Figure 4.36 Surface V_d in Region 1

V_d (V)	α_d (radians)	k	$\hat{g}_\alpha(\alpha_d, k)$	$r_\alpha(\alpha_d, k)$
45.0	4	10	0.489	0.816
40.0	0	25	0.535	0.929

Table 4.12 Maximum and Minimum Values of V_d

E (V)	I_0 (A)	$\hat{g}_\alpha(\alpha_d, k)$	V_d (V)	$r_\alpha(\alpha_d, k)$	n	Z_0 (Ω)	γ (radians)
20	9.39	0.494	43.1	0.934	7.9	114.75	110.4

Table 4.13 Initial Calculation Results in Region 1

The surfaces $h_{1,\alpha}(\alpha_d, k)$ and $h_{2,\alpha}(\alpha_d, k)$ described in Equations (4.20) and (4.21) are drawn in Figure 4.37. The intersection curve u_α can be found and the corresponding values of α_d and k of the points on the curve u_α are listed in Table 4.14. Under each set of the circuit parameters in Table 4.14, the voltage clamping circuit becomes active in State (c) in Figure 4.4 and the resonant converter with the voltage clamp operates in Operating Set 2.

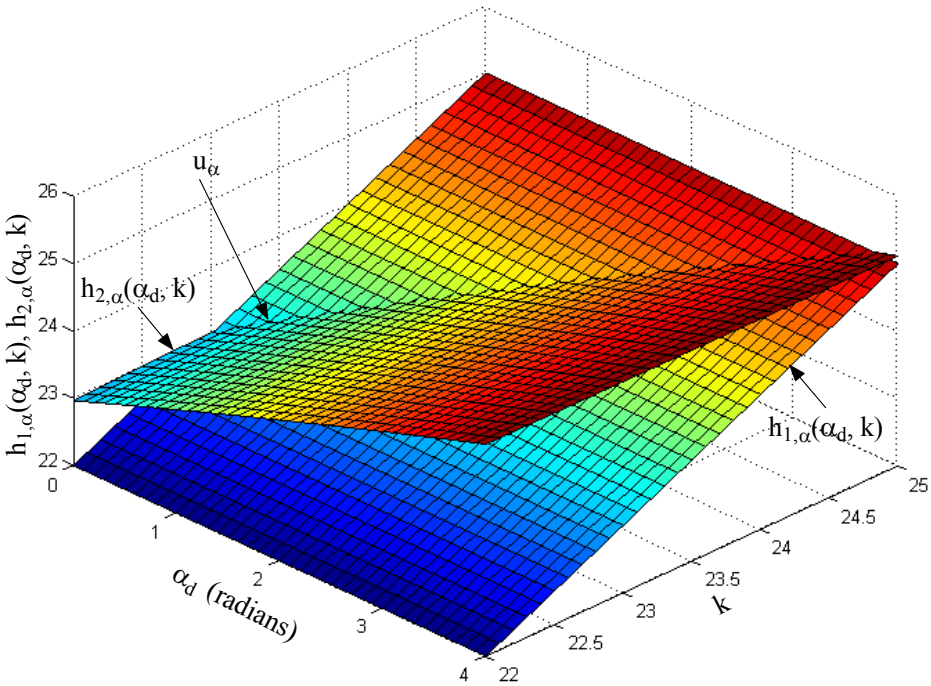

Figure 4.37 Surfaces $h_{1,\alpha}(\alpha_d, k)$ and $h_{2,\alpha}(\alpha_d, k)$ in Region 1

Through the polynomial fitting, the control function $M_\alpha(\alpha_d)$ can be found as:

$$V_d = M_\alpha(\alpha_d) = 0.0024\alpha_d^3 - 0.0413\alpha_d^2 + 0.9032\alpha_d + 40.0161 \qquad (4.69)$$

α_d (radians)	k	V_d (V)	α_d (radians)	k	V_d (V)	α_d (radians)	k	V_d (V)
0.0	23.04	40.0	1.4	23.83	41.2	2.8	24.55	42.3
0.1	23.10	40.1	1.5	23.89	41.3	2.9	24.60	42.3
0.2	23.16	40.2	1.6	23.94	41.4	3.0	24.64	42.4
0.3	23.22	40.3	1.7	23.99	41.4	3.1	24.69	42.5
0.4	23.27	40.4	1.8	24.04	41.5	3.2	24.74	42.6
0.5	23.33	40.5	1.9	24.09	41.6	3.3	24.79	42.6
0.6	23.39	40.5	2.0	24.15	41.7	3.4	24.83	42.7
0.7	23.44	40.6	2.1	24.20	41.8	3.5	24.88	42.8
0.8	23.50	40.7	2.2	24.25	41.8	3.6	24.93	42.8
0.9	23.56	40.8	2.3	24.30	41.9	3.7	24.97	42.9
1.0	23.61	40.9	2.4	24.35	42.0	3.8	25.00	43.0
1.1	23.67	41.0	2.5	24.40	42.1	3.9	25.00	43.1
1.2	23.72	41.0	2.6	24.45	42.1	4.0	25.00	43.1
1.3	23.78	41.1	2.7	24.50	42.2			

Table 4.14 Numerical Relationship of α_d and k

The control function $M_\alpha(\alpha_d)$ can be drawn in Figure 4.38.

When α_d reaches zero, Region 1 operation ends and Region 2 operation starts. At this point, $\alpha_d = 0$, $k = 23.04$ and $V_d = 40.0\ V$.

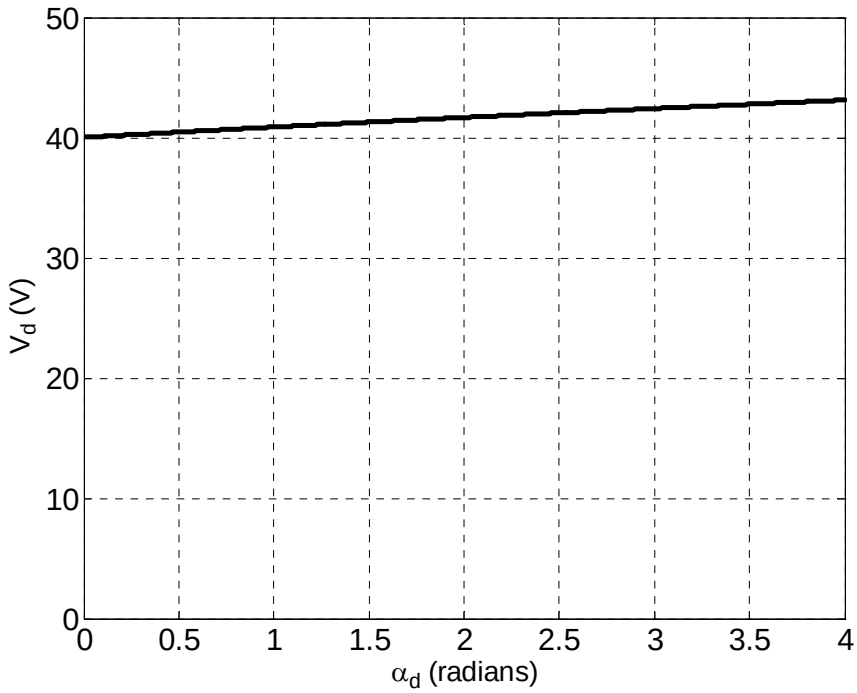

Figure 4.38 Control Function $M_\alpha(\alpha_d)$

In Region 2, k continues to decrease from 23.04. From Equations (4.10) and (4.65), the surface V_d can be drawn against Δ_1 and k as shown in Figure 4.39, where $0 \le \Delta_1 \le 2$ and $1 \le k \le 25$.

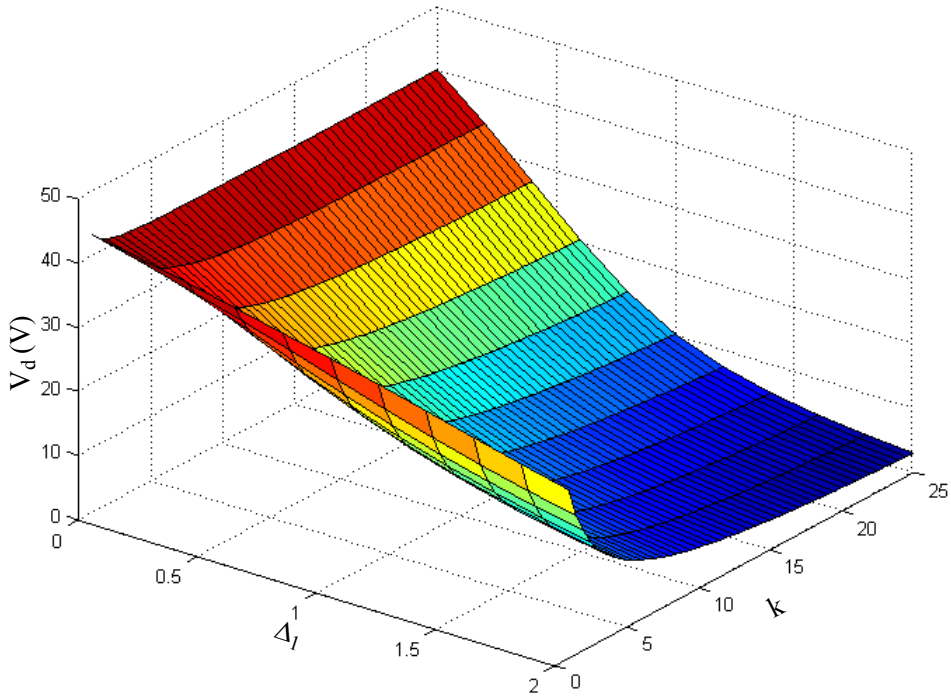

Figure 4.39 Surface V_d in Region 2

The surfaces $h_{1,\Delta}(\Delta_1, k)$ and $h_{2,\Delta}(\Delta_1, k)$ described in Equations (4.12) and (4.13) are drawn in Figure 4.40. The intersection curve u_Δ can be found and the corresponding values of Δ_1 and k of the points on the curve u_Δ are listed in Table 4.15. Under each set of the circuit parameters in Table 4.15, the voltage clamping circuit becomes active in State (a) in Figure 4.4 and the resonant converter with the voltage clamp operates in Operating Set 3 when $\Delta_1 > 0$ while the voltage clamping circuit becomes active in State (c) in Figure 4.4 and the resonant converter with the voltage clamp operates in Operating Set 2 when $\Delta_1 = 0$.

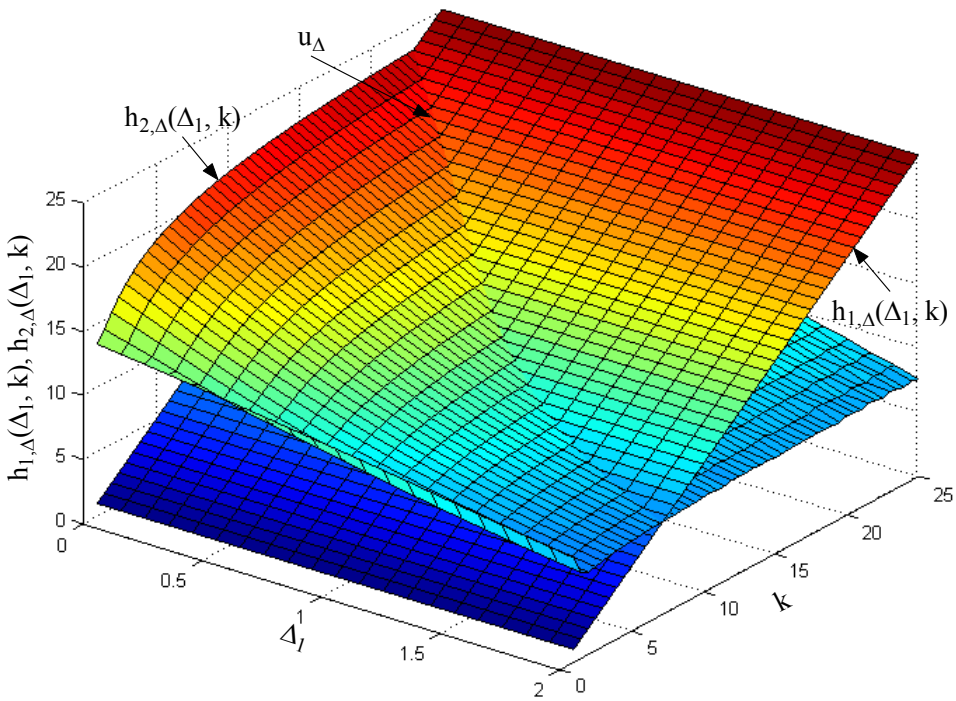

Figure 4.40 Surfaces $h_{1,\Delta}(\Delta_1, k)$ and $h_{2,\Delta}(\Delta_1, k)$ in Region 2

Δ_1	k	V_d (V)	Δ_1	k	V_d (V)	Δ_1	k	V_d (V)
0.0	23.04	40.0	0.7	15.61	19.1	1.4	9.81	10.2
0.1	21.98	37.1	0.8	14.57	16.9	1.5	9.27	9.7
0.2	20.94	34.0	0.9	13.59	15.1	1.6	8.82	9.3
0.3	19.89	30.8	1.0	12.70	13.7	1.7	8.30	8.9
0.4	18.82	27.6	1.1	11.86	12.5	1.8	7.89	8.6
0.5	17.75	24.5	1.2	11.14	11.6	1.9	7.56	8.3
0.6	16.66	21.6	1.3	10.41	10.8	2.0	7.19	8.1

Table 4.15 Numerical Relationship of Δ_1 and k

Through the polynomial fitting, the control function $M_{\Delta}(\Delta_1)$ can be found as:

$$V_d = M_{\Delta}(\Delta_1) = -4.4120\Delta_1^4 + 15.8906\Delta_1^3 - 6.4097\Delta_1^2 - 31.6496\Delta_1 + 40.2458 \quad (4.70)$$

The control function $M_{\Delta}(\Delta_1)$ can be drawn in Figure 4.41.

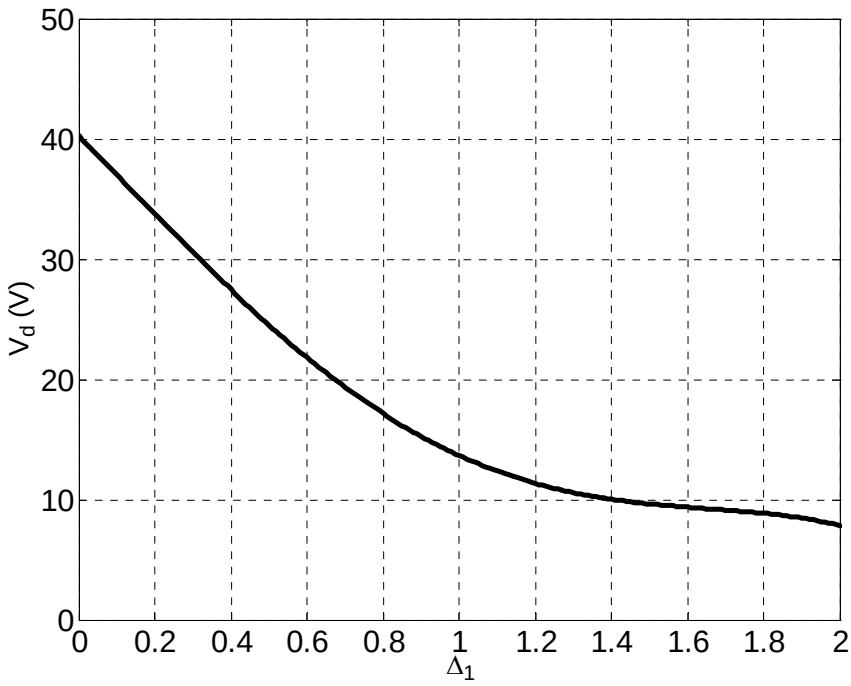

Figure 4.41 Control Function $M_{\Delta}(\Delta_1)$

When Δ_1 reaches 2, k reaches 7.2. At this point, $V_d = 8.1\,V$. It is worth noting that the voltage V_d will further decrease when $\Delta_1 > 2$. However, the change of V_d is very likely to be small according to the tendency shown in Figure 4.41.

It can be summarised that a wider load range can be achieved by the ZVS two-inductor boost converter with the voltage clamp. The maximum and the minimum output voltages are respectively 340 V and 64.0 V, which respectively correspond to 43.1 V to 8.1 V on the transformer primary winding. Therefore, the ratio of the maximum to the minimum voltages is 5.3, which is much higher than that achieved by the resonant converter without the voltage clamp. A higher ratio of the maximum to the minimum voltages can be obtained by a higher initial value of k in the converter design.

In the design of the resonant converter with the voltage clamp, when the converter operates in Region 1 the output voltage range is very limited. Therefore, a relatively wide output voltage range can be achieved simply by operating the converter in Region 2, where $\alpha_d = 0$. Of course, a higher k is required in this case to obtain the same ratio of the maximum to the minimum voltages when the converter operates in both Regions 1 and 2.

A switching frequency of 500 kHz is selected when $\Delta_1 = 2.0$ and $k = 7.19$. Therefore the angular resonance frequency of the resonant tank and the switching frequency when $\alpha_d = 4.0$ and $k = 25$ can be calculated and the results are given in Table 4.16.

According to Equations (4.6) and (4.7), $L_r = 17.19\ \mu H$ and $C_1 = C_2 = 1.31\ nF$.

Δ_1	α_d (radians)	k	γ (radians)	f_s (kHz)	ω_0 (Mrad/s)
2.0	0	7.19	13.4	500	6.676
0	4.0	25.00	110.4	60.5	

Table 4.16 Final Calculation Results in the ZVS Two-Inductor Boost Converter with the Voltage Clamp

4.4.4 Theoretical and Simulation Waveforms

In this section, the theoretical and the simulation waveforms are provided for the selected operating points listed in Table 4.17. These operating points are selected from Tables 4.14 and 4.15. The theoretical waveforms are generated by plotting the device waveforms obtained from Equations (4.23) to (4.29) and (4.38) to (4.52) and the simulation waveforms are generated in SIMULINK. The converter operates in Operating Set 2 under Points 1 to 3 and in Operating Set 3 under Points 4 and 5.

Operating Point	Δ_1	α_d (radians)	k	V_d (V)	Theoretical Waveforms	Simulation Waveforms
1	0	4.0	25.00	43.1	Figure 4.42	Figure 4.43
2	0	2.0	24.15	41.7	Figure 4.44	Figure 4.45
3	0	0	23.04	40.0	Figure 4.46	Figure 4.47
4	1.0	0	12.70	13.7	Figure 4.48	Figure 4.49
5	2.0	0	7.19	8.1	Figure 4.50	Figure 4.51

Table 4.17 Selected Operating Points

Some important parameters used in the theoretical analysis and the simulation circuit are summarised below:

- $E = 20\ V$,
- $L_r = 17.19\ \mu H$,
- $C_1 = C_2 = 1.31\ nF$,
- $n = 7.9$,
- $n_L = 3.5$,
- $R = 576\ \Omega$.

It is worth noting that a 1 μF capacitor is connected in series with the high frequency transformer in the simulation circuit to prevent the dc current from flowing in the transformer. The capacitor reactance is selected to be low enough not to affect the normal circuit operation although this arrangement will affect the transformer primary voltage waveform. When there is an extended period of the zero resonant inductor current and both MOSFETs are on, the dc voltage across this dc balancing capacitor will appear in the transformer primary voltage waveform. However, the power in the transformer during this period is still zero as the transformer current is zero.

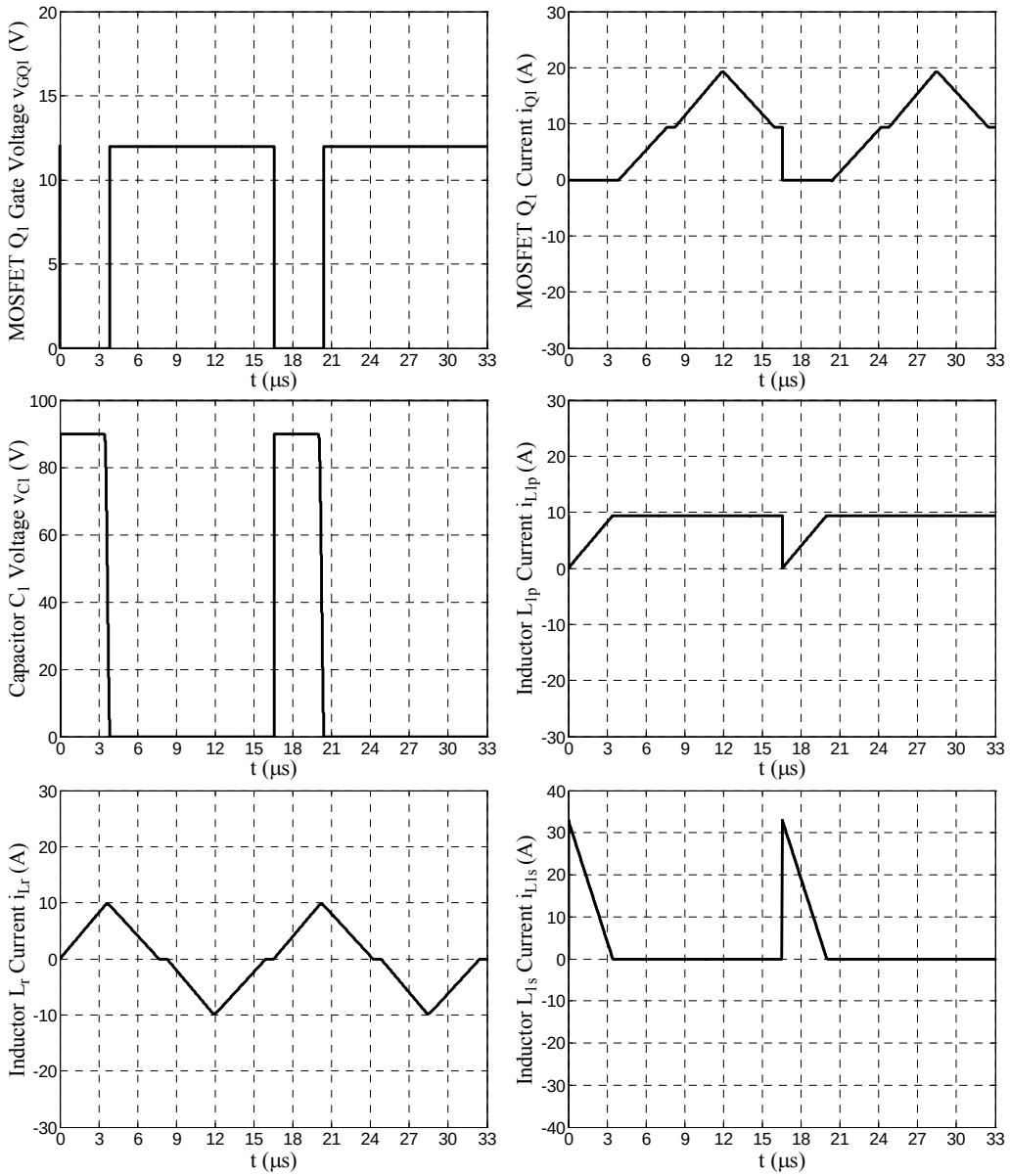

Figure 4.42 Theoretical Waveforms of Operating Point 1

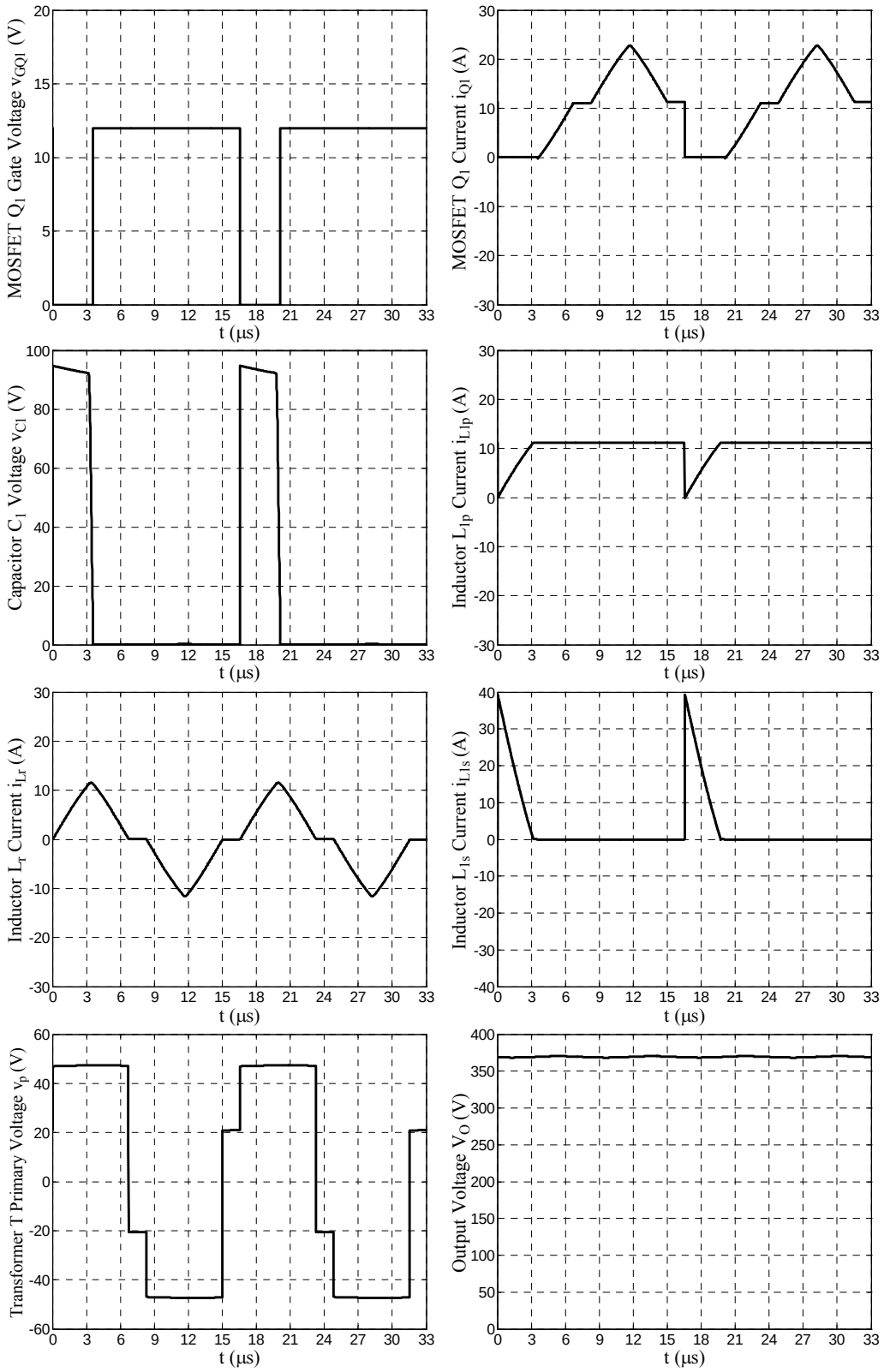

Figure 4.43 Simulation Waveforms of Operating Point 1

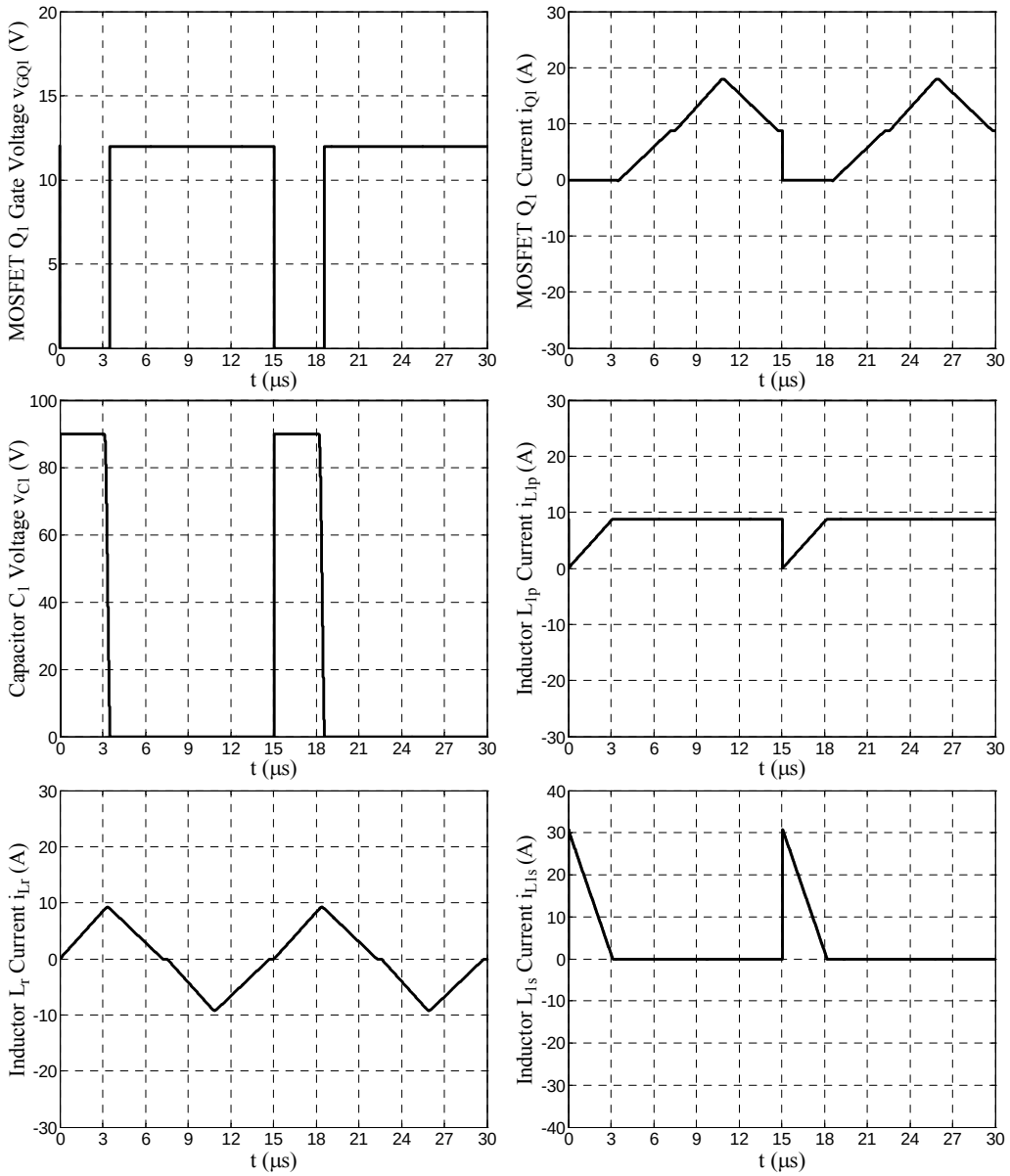

Figure 4.44 Theoretical Waveforms of Operating Point 2

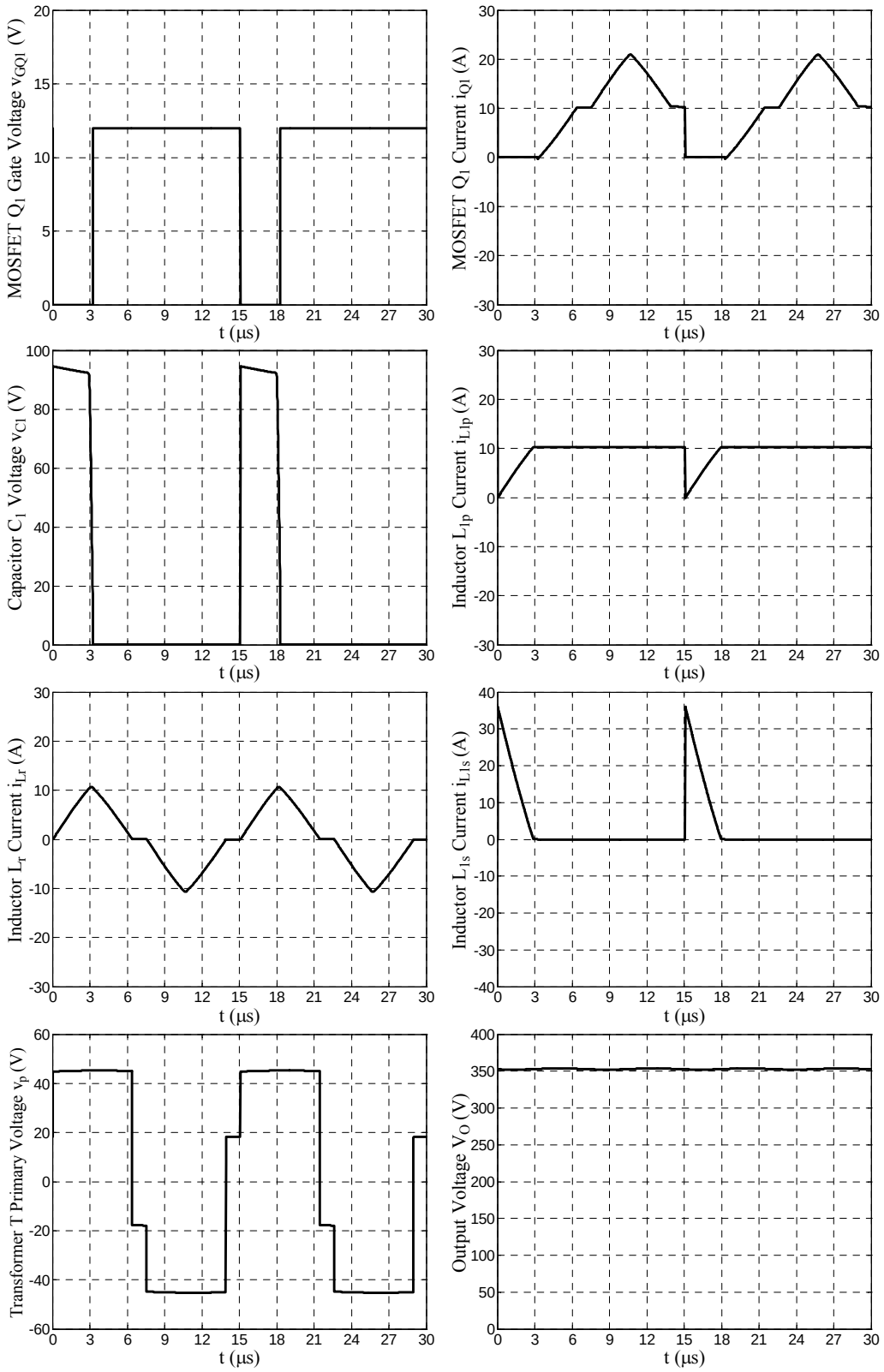

Figure 4.45 Simulation Waveforms of Operating Point 2

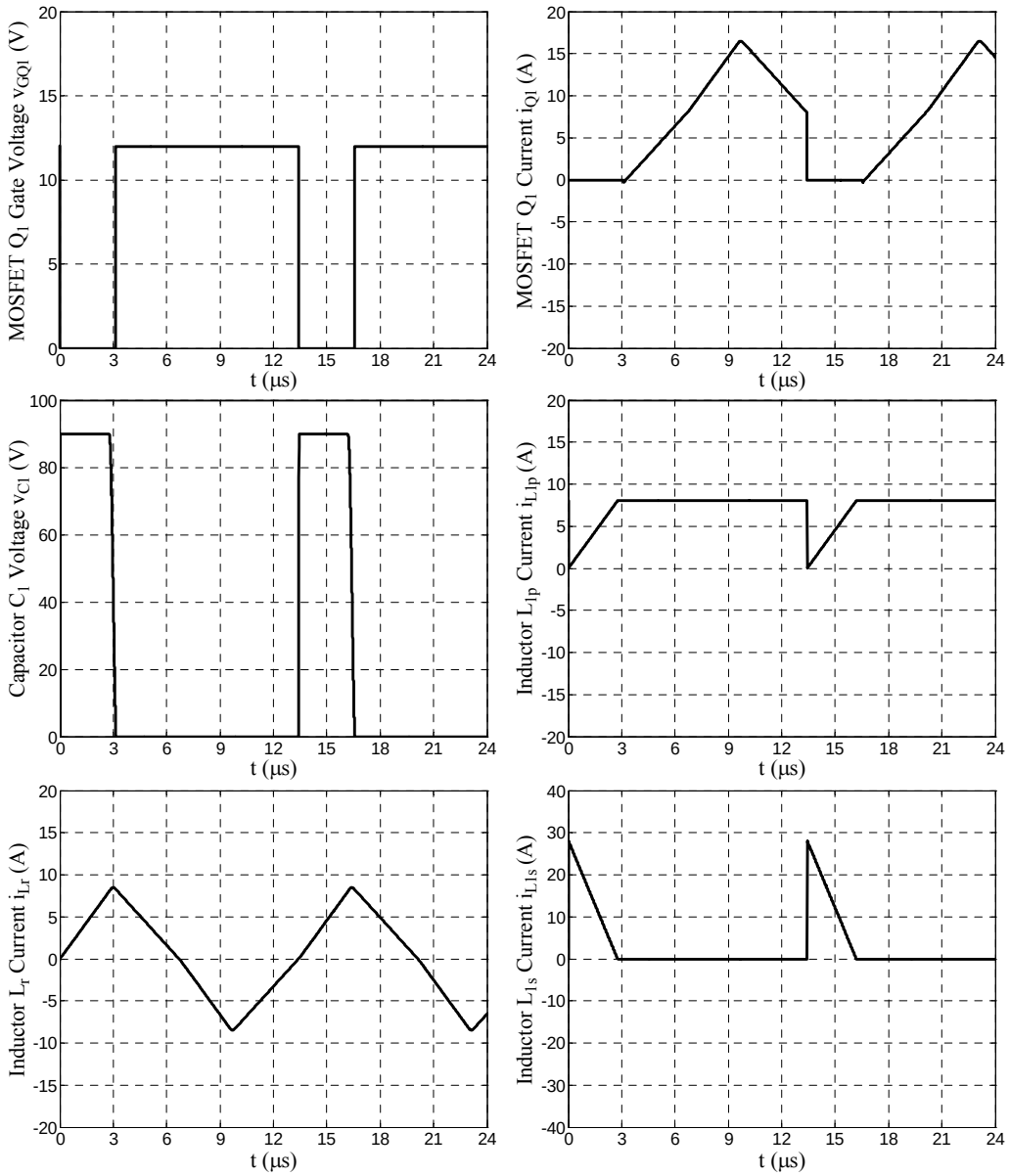

Figure 4.46 Theoretical Waveforms of Operating Point 3

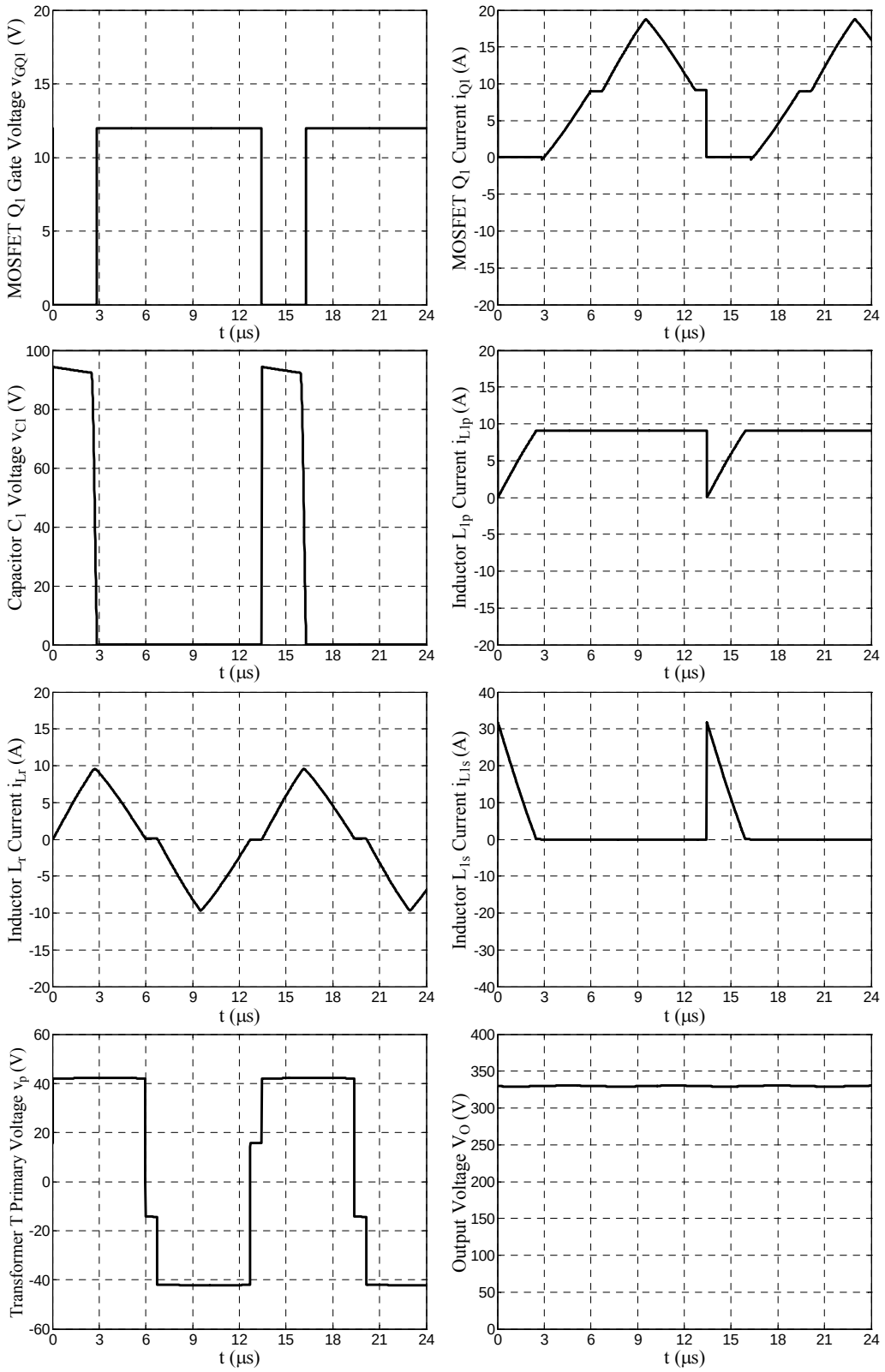

Figure 4.47 Simulation Waveforms of Operating Point 3

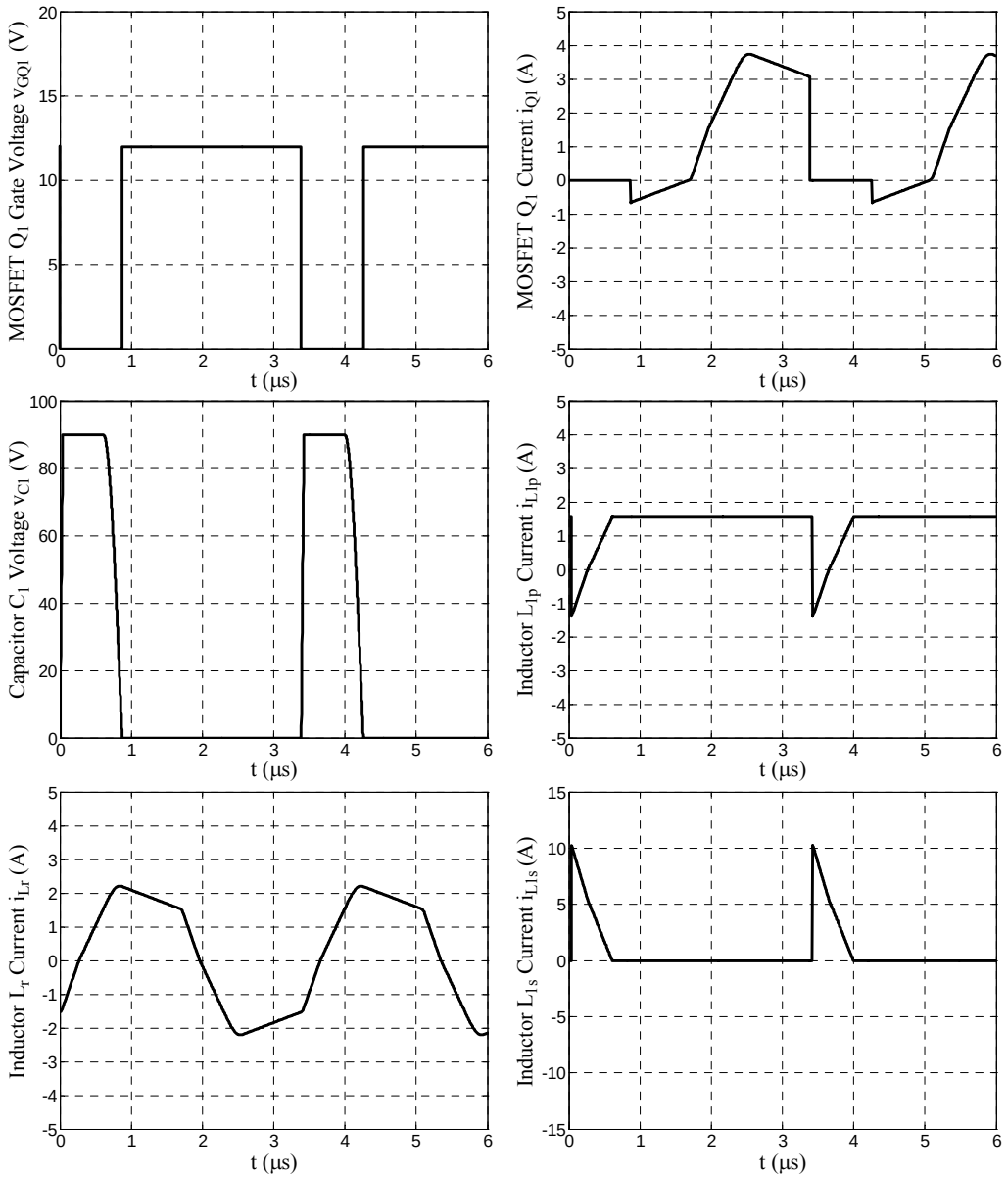

Figure 4.48 Theoretical Waveforms of Operating Point 4

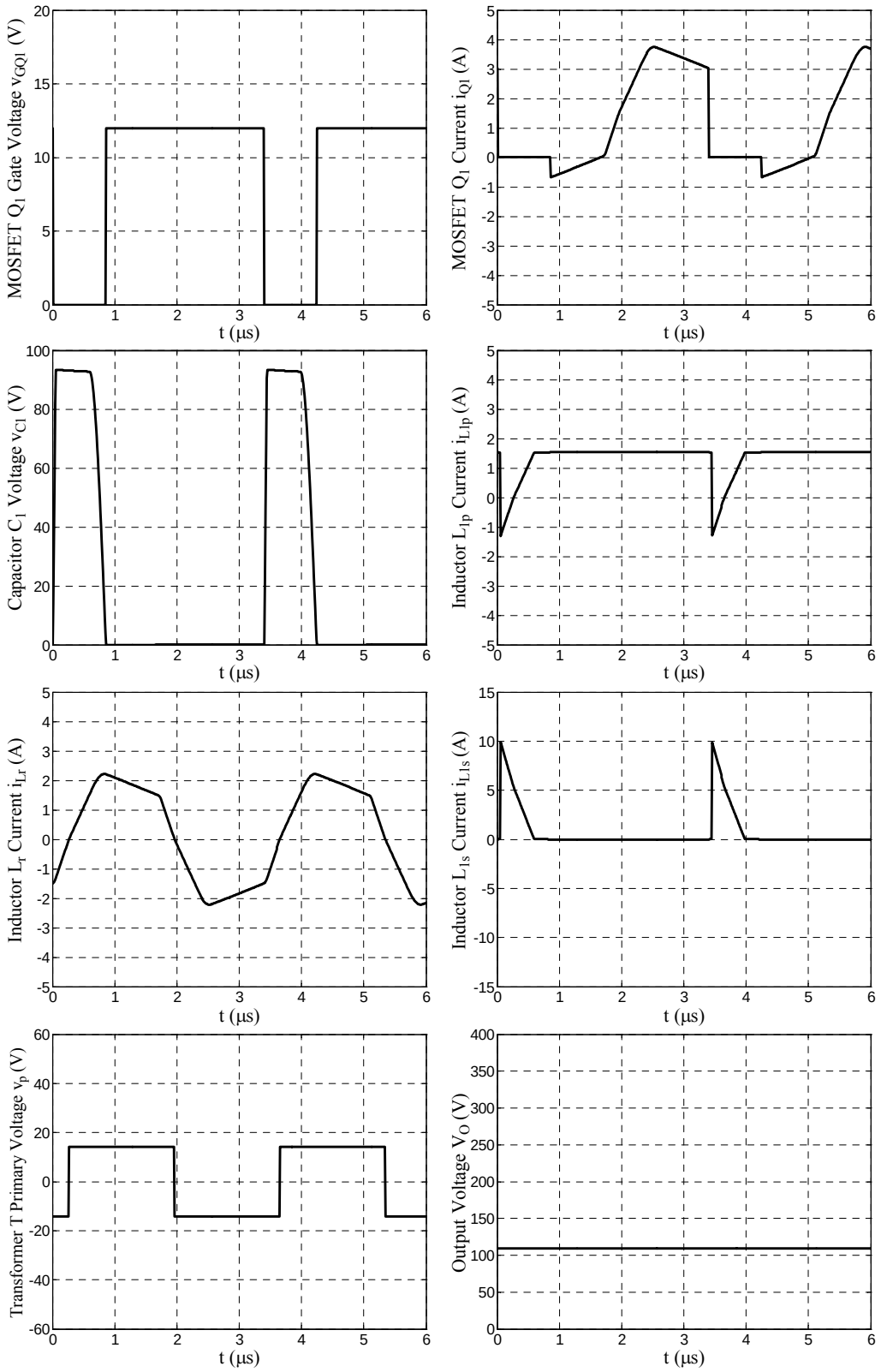

Figure 4.49 Simulation Waveforms of Operating Point 4

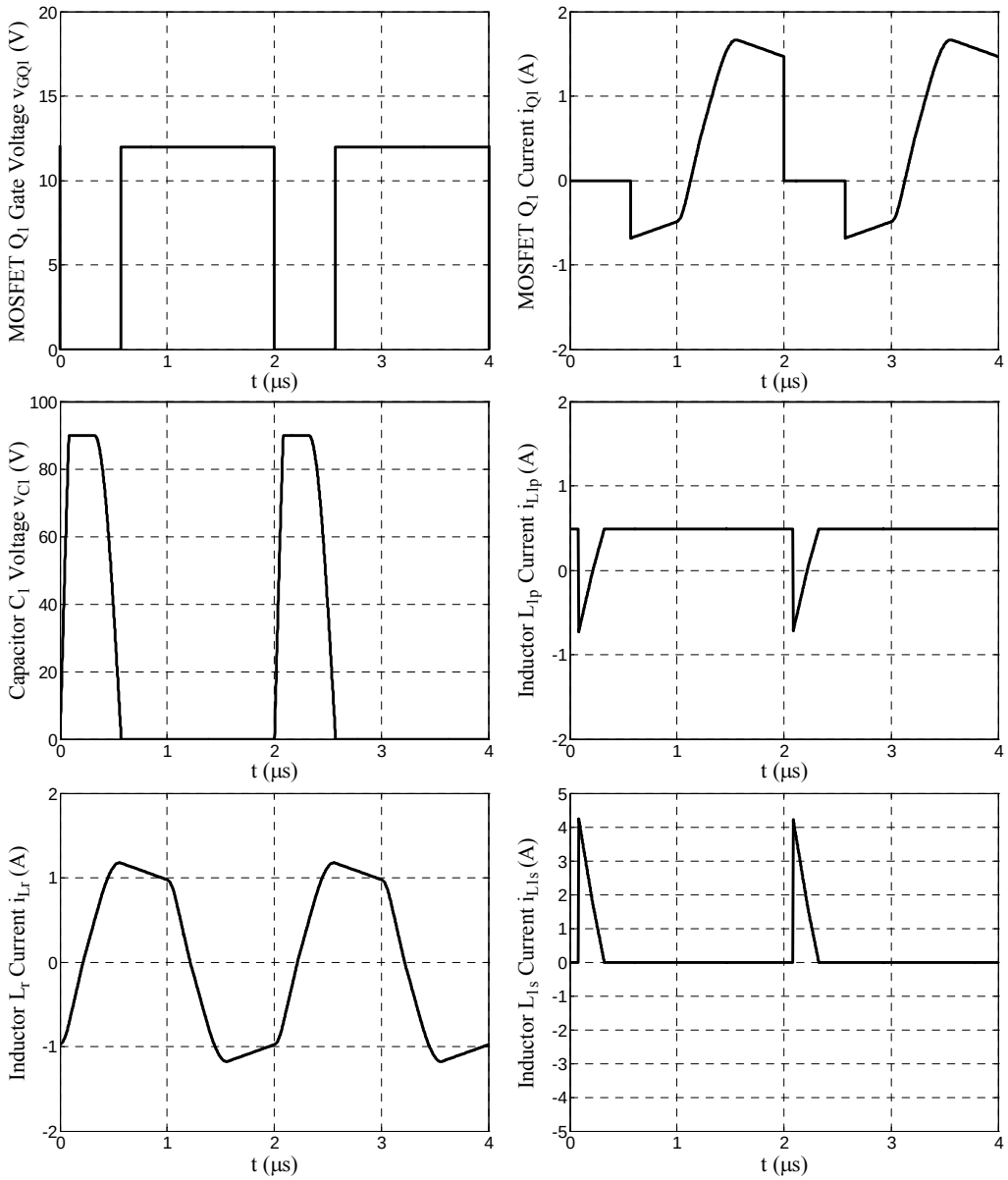

Figure 4.50 Theoretical Waveforms of Operating Point 5

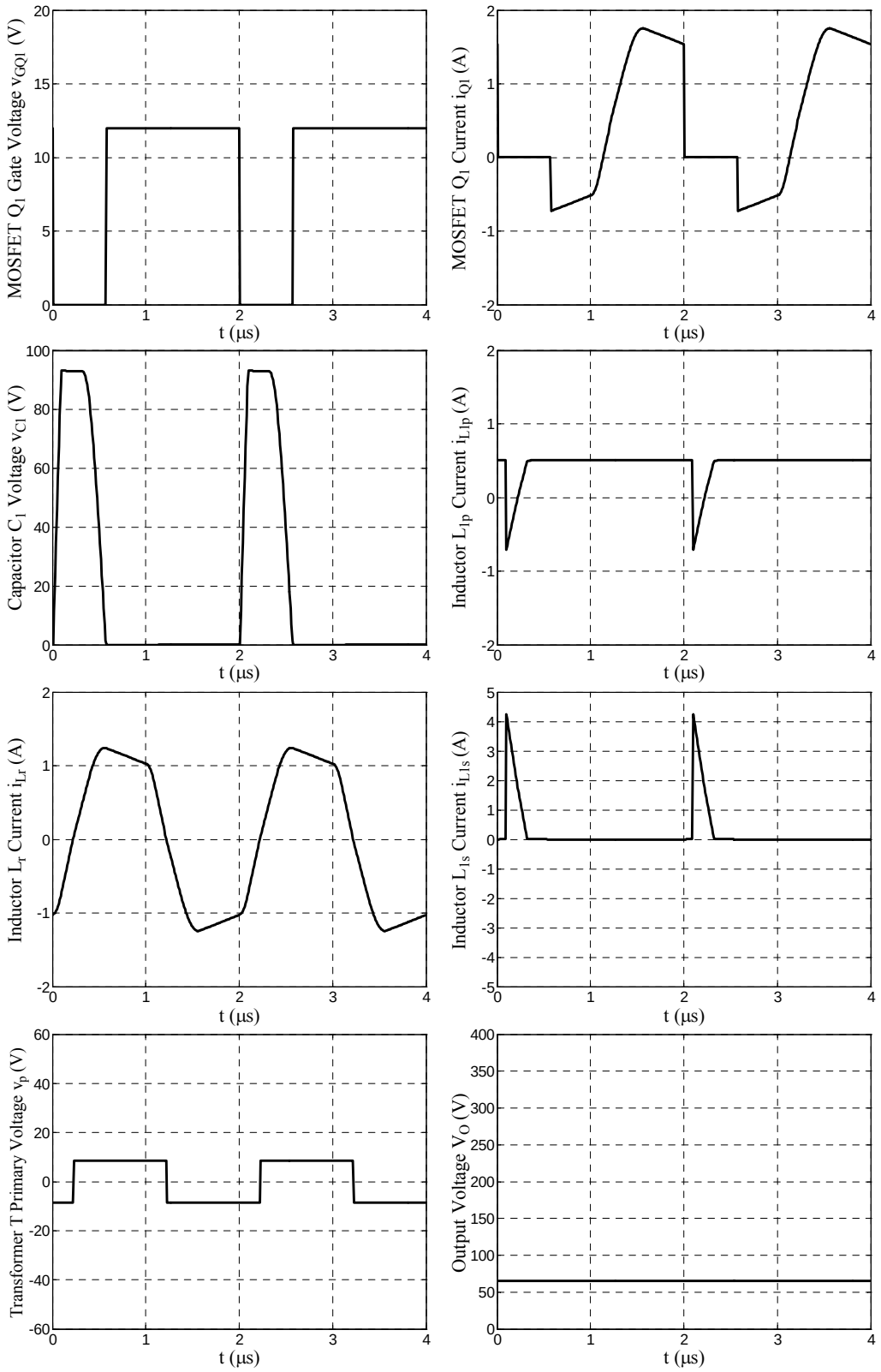

Figure 4.51 Simulation Waveforms of Operating Point 5

The converter output voltages under the individual operating points in the theoretical analysis and the simulation results are listed in Table 4.18 and drawn in Figure 4.52.

Operating Point	Output Voltage V_O (V)	
	Theoretical Analysis	Simulation Results
1	340.0	369.4
2	329.0	352.9
3	315.5	329.7
4	105.7	109.6
5	63.9	65.0

Table 4.18 Output Voltage under Each Operating Point

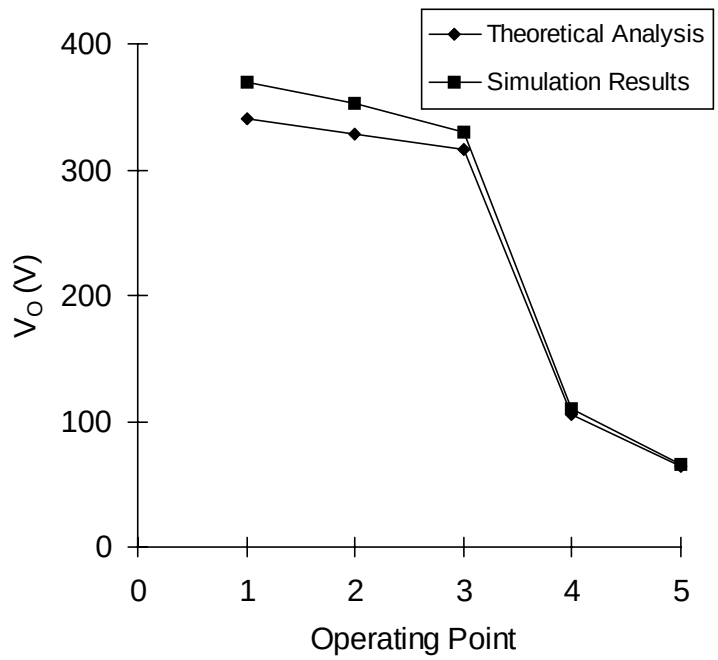

Figure 4.52 Output Voltage under Each Operating Point

4.5 Comparisons of the Two ZVS Two-Inductor Boost Converters

Comparisons on the advantages and disadvantages of the two ZVS two-inductor boost converters are given briefly in the following sections.

4.5.1 Output Voltage Range

The converter without the voltage clamp is able to achieve a theoretical maximum to minimum output voltage ratio of 2.3 while the converter with the voltage clamp is able to achieve a ratio of 5.3. Therefore the maximum to minimum output voltage ratio of the converter with the voltage clamp is significantly higher than that of the converter without the voltage clamp. To further increase the maximum to minimum output voltage ratio is possible with either a higher switch voltage stress in the converter without the voltage clamp or a higher load factor in the converter with the voltage clamp.

4.5.2 Switching Frequency Range

In order to produce a variable output voltage, the switching frequency needs to vary from 163.9 kHz to 500 kHz in the converter without the voltage clamp or from 60.5 kHz to 500 kHz in the converter with the voltage clamp. The wide switching frequency range is a significant disadvantage for the converter operation as this makes it difficult to optimise the design of the magnetic components, the control circuit and the input and the output filters.

4.5.3 Resonant Inductor

The resonant inductor used in the converter with the voltage clamp is 17.19 μH, which is much larger than the resonant inductor of 6.85 μH in the converter without the voltage clamp. The problem with the large inductor is that it has a larger power rating and given a fixed upper limit for the quality factor, it has higher power losses.

4.5.4 Switch Voltage Stress

The above maximum to minimum output voltage ratios are achieved with a maximum switch voltage of 200 V in the converter without the voltage clamp and 90 V in the converter with the voltage clamp. The maximum switch voltage is significantly higher in the converter without the voltage clamp and this requires MOSFETs with higher voltage ratings, which may lead to higher conduction loss or drive power.

4.5.5 Soft-Switching Condition

Theoretically the ZVS condition is maintained for both resonant converters under the variable frequency operation. However, in the ZVS converter with the voltage clamp, the load factor is very large and the soft-switching condition is almost lost as *dv/dt* at the switch turn-on or turn-off is very large. This can be seen from the simulation waveforms of the resonant capacitor voltage in Figures 4.43, 4.45 and

4.47. The voltage waveforms across the resonant capacitor, also the MOSFET, are very similar to those in the hard-switched converters. Only when the output voltage becomes lower, *dv/dt* at the turn-on or the turn-off transitions becomes smaller, offering the ZVS condition as shown in Figures 4.49 and 4.51. Therefore, the resonant converter with the voltage clamp could suffer from high switching losses under medium to high output voltages.

4.5.6 Efficiency

Besides the conduction and the switching losses, the high circulating energy in the two resonant converters could also result in significant power losses. This is especially true in the resonant converter with the voltage clamp, where part of the energy stored in the resonant tank will be returned to the input voltage source when the voltage across the resonant capacitor is clamped. The additional power flow introduced by the voltage clamp causes high current circulating in the converter and contributes to the total power loss in a practical converter with non-ideal components. Therefore, the efficiency of the converter with the voltage clamp is likely to be lower than the converter without the voltage clamp, if no further measures are taken.

4.6 Power Loss Analysis

It has been discussed in the previous sections that for the ZVS two-inductor boost converter with a fixed set of the key design parameters including the resonant

inductance and capacitance and the transformer turns ratio, the variations of the circuit parameters such as the load factor, the timing factor and the delay angle allow the converter to generate a variable output voltage, which results in a variable load condition. However, under a fixed load condition, variations of the three circuit parameters lead to the requirement of different sets of the key design parameters to maintain the ZVS condition. As the circuit parameters determine the resonant condition of the converter, the power loss components in the converter vary.

4.6.1 Variable Power Loss Terms

The major power loss components in the ZVS two-inductor boost converter shown in Figure 4.1 are listed below:

- The conduction loss in the two power MOSFETs Q_1 and Q_2,
- The power loss related to the series dc plus ac resistance of the resonant inductor L_r,
- The power loss related to the Equivalent Series Resistance (ESR) of the resonant capacitors C_1 and C_2,
- The copper and core loss in the two input inductors L_1 and L_2,
- The copper and core loss in the transformer T, and
- The conduction loss in the four diodes D_1 to D_4 in the full-bridge rectifier.

In the physical construction of the ZVS two-inductor boost converter, the

MOSFETs, the additional resonant inductor and the additional resonant capacitors are implemented by the components with the pre-determined electrical characteristics. If the output power is fixed, different resonant inductance and capacitance are required and different resonant voltage and current waveforms are established in the converter under different circuit parameters. Therefore the power losses associated with the MOSFETs, the resonant inductor and capacitors vary. The input inductors and the transformer can be designed after the circuit parameters are selected and the inductor and the transformer windings can be configured in a way to produce a desired total copper and core loss. The power loss in the diodes is only load sensitive once the diodes are selected and will not vary against different circuit parameters. Therefore in order to achieve a minimum total power loss in the ZVS two-inductor boost converter, only the variable power loss components of the MOSFETs, the resonant inductor and capacitors need to be considered. They are respectively discussed below.

- The power loss in the two MOSFETs p_Q:

$$p_Q = 2(I_{Q,rms}^2 R_{DS(on)} + I_{Q,avg} V_F) \tag{4.71}$$

where $I_{Q,rms}$ is the effective forward current in the MOSFET, $R_{DS(on)}$ is the MOSFET drain source on resistance, $I_{Q,avg}$ is the average reverse current in the MOSFET and V_F is the forward voltage drop of the MOSFET body diode. $R_{DS(on)}$ and V_F can be obtained from the component datasheet.

- The power loss in the resonant inductor p_{Lr}:

$$p_{Lr} = I_{Lr,rms}^2 R_{Lr} \tag{4.72}$$

where $I_{Lr,rms}$ is the effective current in the resonant inductor and R_{Lr} is the series dc plus ac resistance of the resonant inductor.

- The power loss in the two resonant capacitors p_{Cr}:

$$p_{Cr} = 2I_{Cr,rms}^2 R_{Cr} \tag{4.73}$$

where $I_{Cr,rms}$ is the effective current in the resonant capacitor and R_{Cr} is the ESR of the resonant capacitors.

The total power loss $p_{total,var}$ which alters with different circuit parameters in the converter is:

$$p_{total,\mathrm{var}} = p_Q + p_{Lr} + p_{Cr} \tag{4.74}$$

In order to calculate the variable power loss components in Equations (4.71) to (4.73), a variety of the current terms and the equivalent series resistances of the resonant inductor and capacitors must be obtained. The current terms can be obtained through the state analysis given in Section 4.3.1 while the series resistance

of the resonant inductor and the ESR of the resonant capacitors must be further derived with two other direct results through the state analysis, the circuit variable γ and the resonant tank characteristic impedance Z_0.

The quality factor of the resonant inductor and the dissipation factor (DF) of the resonant capacitor are respectively defined as:

$$Q = \frac{2\pi f_s L_r}{R_{Lr}} \tag{4.75}$$

$$DF = 2\pi f_s C_r R_{Cr} \tag{4.76}$$

Manipulations of Equations (4.5) to (4.7), (4.75) and (4.76) yield:

$$R_{Lr} = \frac{2\pi Z_0}{Q\gamma} \tag{4.77}$$

$$R_{Cr} = \frac{DF\gamma Z_0}{2\pi} \tag{4.78}$$

An example of the numerical calculation of the variable power loss components in a 200-W ZVS two-inductor boost converter is given below. The converter has an input voltage of 20 V and an output voltage of 340 V and the switching frequency is 500 kHz. The following component parameters of the selected MOSFETs, resonant inductor and capacitors are used [148], [149]:

- $R_{DS(on)} = 0.027\ \Omega$ and $V_F = 1.5\ V$ for STB50NE10 MOSFETs,
- $Q = 96$ at 500 kHz for the air core toroidal inductors,
- $DF = 1/6000$ at 500 kHz for Cornell Dubilier surface mount mica capacitors.

It is worth noting that the selected MOSFET STB50NE10 has a drain source breakdown voltage of 100 V. However a certain set of the circuit parameters may result in a peak MOSFET voltage of more than 100 V and the MOSFET STB50NE10 cannot be used. As a desired peak MOSFET voltage of 100 V is set to limit the drive power and the MOSFETs with higher voltage ratings normally have higher drain source on resistances and similar forward voltage drops of the body diodes, the use of the component parameters of the selected MOSFET over the entire range of the circuit parameters can be justified.

It is also worth mentioning that as the transformer leakage inductance and the MOSFET output capacitance respectively form part of the resonant inductor and capacitors in the ZVS two-inductor boost converter, the actual power losses of these components will be different from the results obtained through Equations (4.72) and (4.73) if the parameters of the selected additional resonant inductor and capacitors are used. However, under the assumption that the values of the parasitic components are relatively small compared with the total required resonant inductance and capacitance values, the errors in the results of Equations (4.72) and (4.73) are unlikely to be large.

When the converter operates in Region 2, the power losses defined in Equations (4.71) to (4.74) are respectively drawn in Figures 4.53 to 4.56, where $0 \le \Delta_1 \le 2$ and $1 \le k \le 4$. In Figures 4.53 to 4.55, the power losses of the MOSFETs, the resonant inductor and capacitors increase along both the Δ_1 and k axes and the lowest power losses are respectively 2.90 W, 1.48 W, 0.04 W when $\Delta_1 = 0$ and $k = 1$. In Figure 4.56, the total variable power loss increases along both the Δ_1 and k axes and the lowest total variable power loss is 4.42 W when $\Delta_1 = 0$ and $k = 1$.

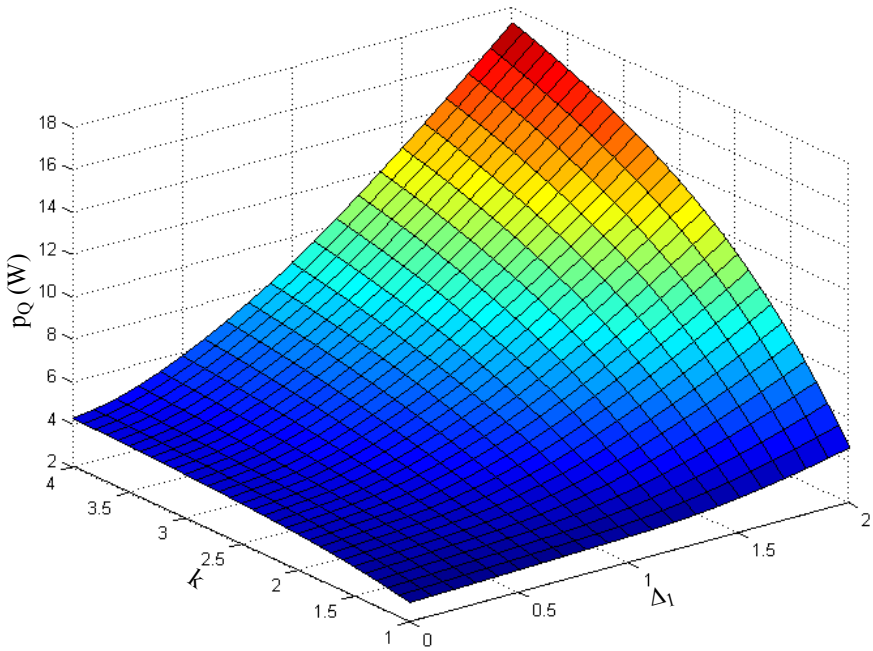

Figure 4.53 Power Loss in the MOSFETs in Region 2

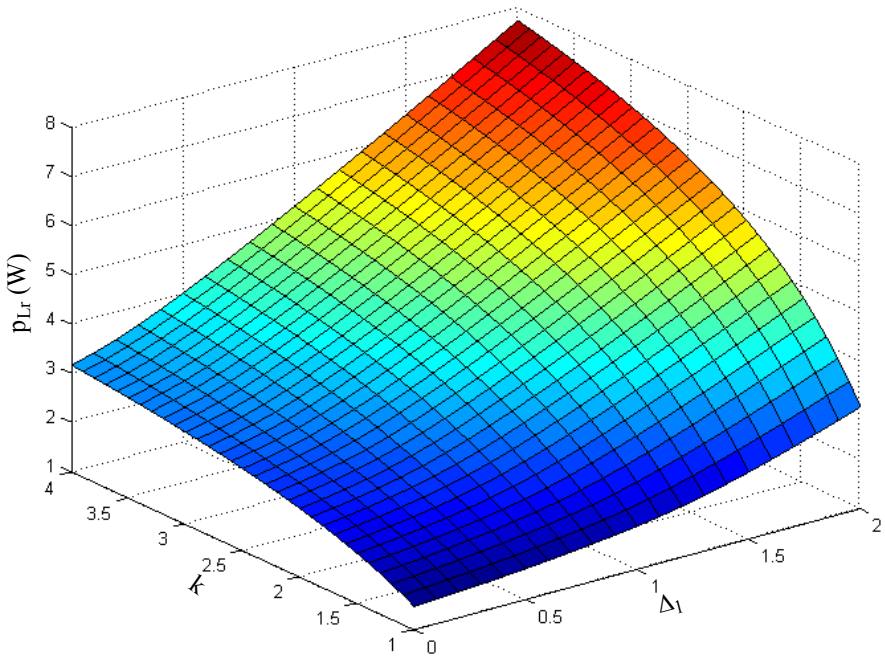

Figure 4.54 Power Loss in the Resonant Inductor in Region 2

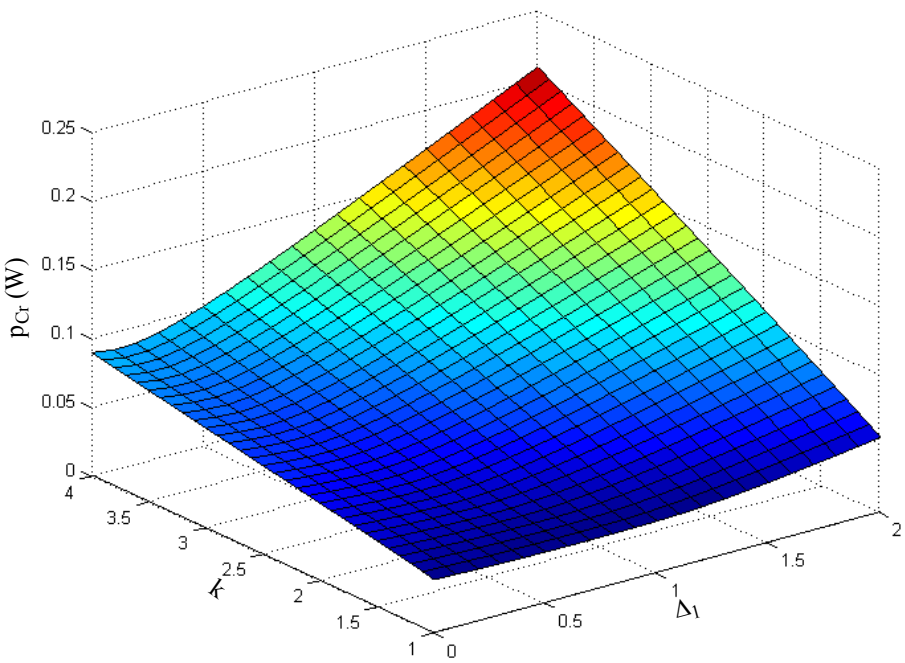

Figure 4.55 Power Loss in the Resonant Capacitors in Region 2

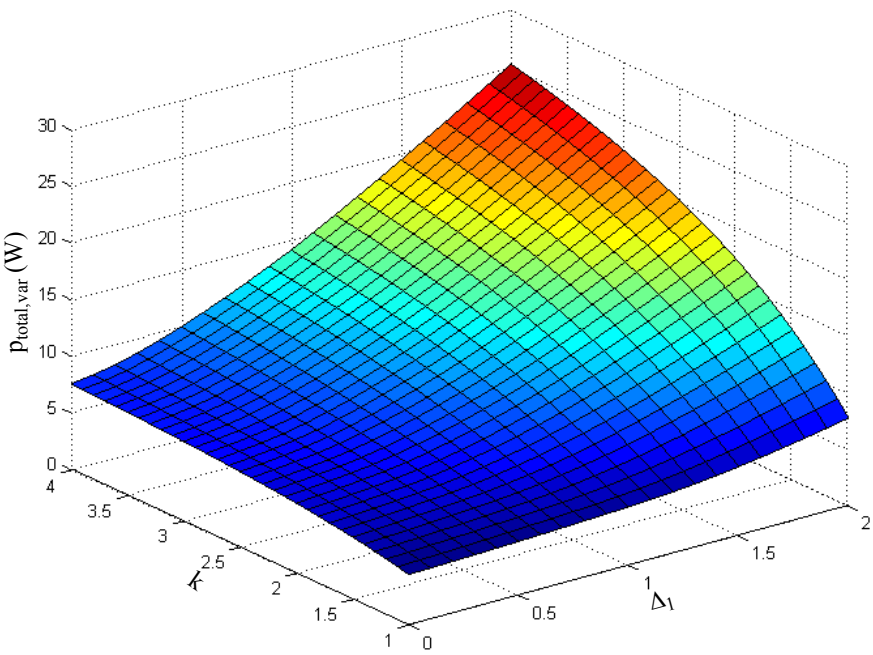

Figure 4.56 Total Variable Power Loss in Region 2

When the converter operates in Region 1, the power losses defined in Equations (4.71) to (4.74) are respectively drawn in Figures 4.57 to 4.60, where $0 \le \alpha_d \le 4$ and $1 \le k \le 4$. In Figures 4.57 and 4.58, the power losses of the MOSFETs and the resonant inductor decrease along the α_d axis and increase along the k axis and the lowest power losses shown are respectively 2.07 W, 0.93 W when $\alpha_d = 4$ and $k = 1$. In Figure 4.59, the power loss of the resonant capacitors increases along both the α_d and k axes. The lowest power loss is 0.04 W when $\alpha_d = 0$ and $k = 1$ and this is the same point in Region 2 where the lowest power loss appears in the resonant capacitors. In Figure 4.60, the total power loss decreases along the α_d axis and increases along the k axis as the power loss in the resonant capacitors is significantly

smaller than the power losses in the MOSFETs and the resonant inductor. The lowest total power loss shown is 3.06 W when $\alpha_d = 4$ and $k = 1$. The theoretical lowest total power loss can be further reduced with a higher value of α_d.

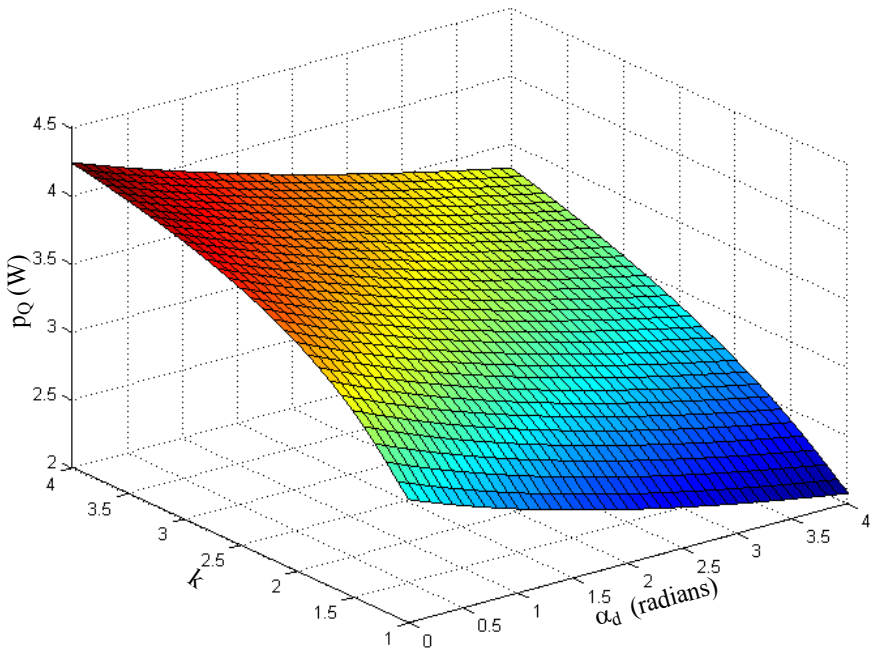

Figure 4.57 Power Loss in the MOSFETs in Region 1

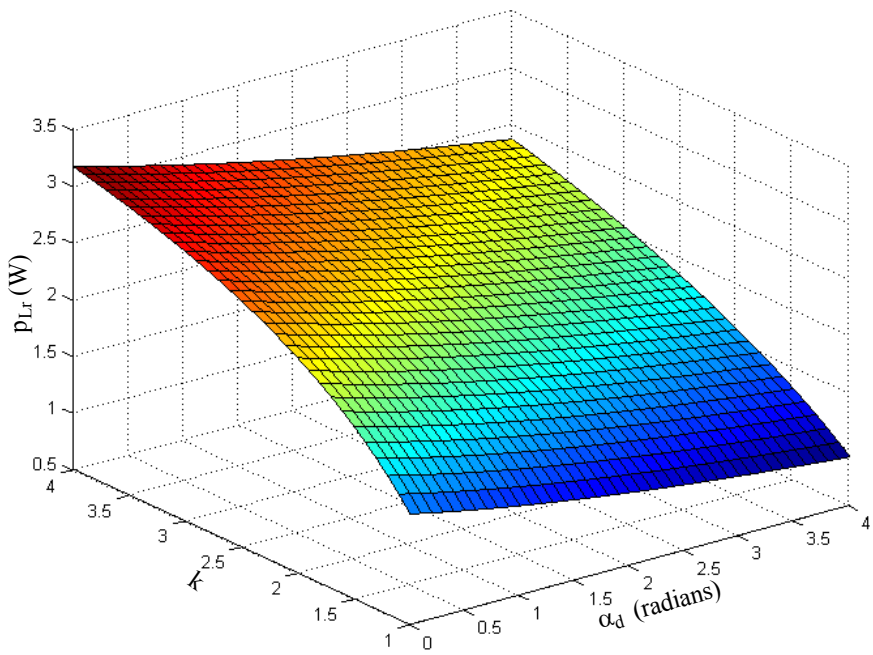

Figure 4.58 Power Loss in the Resonant Inductor in Region 1

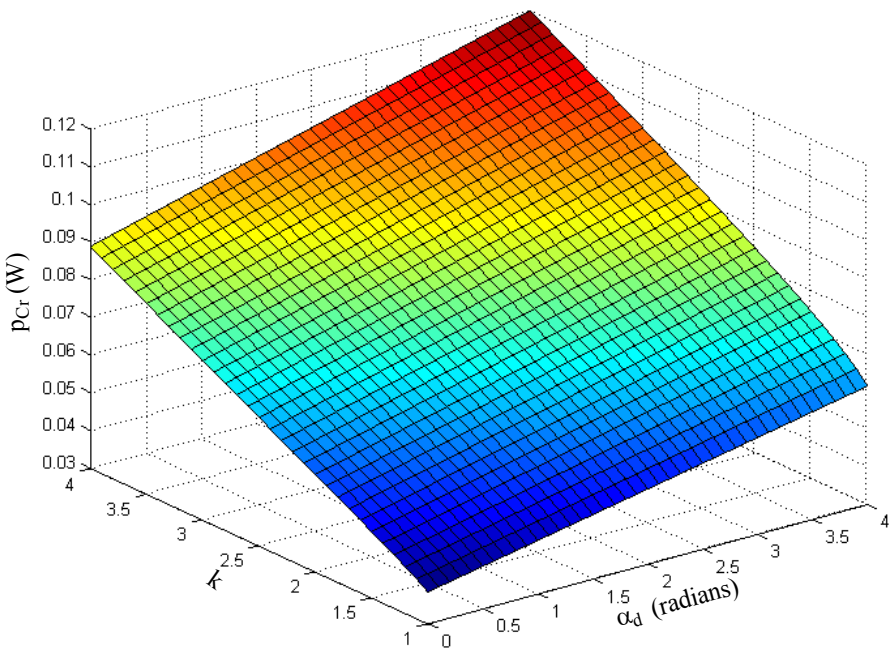

Figure 4.59 Power Loss in the Resonant Capacitors in Region 1

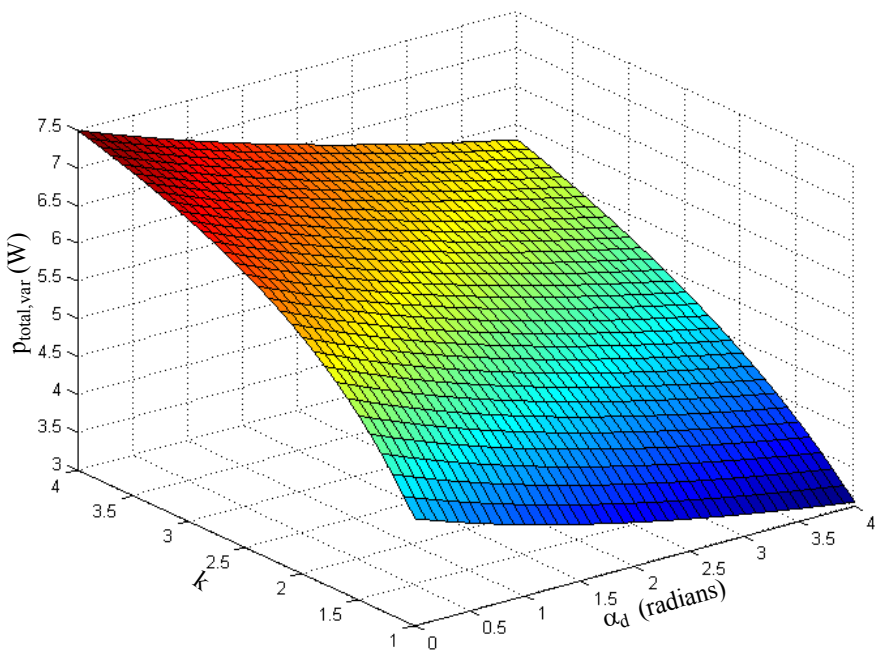

Figure 4.60 Total Variable Power Loss in Region 1

4.6.2 Optimised Operating Point

Considering the converter operations in both Regions 1 and 2, a lower total power loss appears when the converter operates in Region 1. It can be observed from Figure 4.60 that under the same k value, the greater the α_d value, the lower the total variable power loss. However, a higher peak switch voltage appears while α_d increases as shown by the surface $V_{Q,peak}$ in Figure 4.61.

A peak switch voltage of 100 V is set in the converter operation to obtain a low MOSFET drain source on resistance as mentioned before. The MOSFET input capacitance increases for the same value of the drain source on resistance at a higher

voltage rating and this demands a higher power from the drive circuit and lowers the converter overall efficiency. A lower peak switch voltage therefore a lower α_d is preferred. Another reason to choose a lower α_d value is that the gradient of the surface $p_{total,var}$ along the α_d axis is very small. When $k = 1$ and $0 \le \alpha_d \le 4$, the average gradient of the power loss against α_d is -0.34 W/radian, while that of the peak switch voltage against α_d is 12.9 V/radian. Figures 4.60 and 4.61 show that the changes of the total variable power loss and the peak switch voltage along the α_d axis under the same k value are both monotonic. The final circuit parameters for the optimised power loss in the ZVS two-inductor boost converter are $k = 1.1$, $\Delta_1 = 0$ and $\alpha_d = 0$. Under this condition, the total power loss is 4.64 W and the peak switch voltage is 90 V. The safety margin for k to maintain the ZVS condition is justified by the numerical results from MATLAB, which show that the increase of k from 1 to 1.1 when $\Delta_1 = 0$ and $\alpha_d = 0$ only raises the average power loss by an insignificant amount of 0.22 W. Once the circuit parameters are determined, the key design parameters in the converter can be obtained as the following:

- The resonant inductance $L_r = 1.40\ \mu H$,
- The resonant capacitance $C_r = 15.7\ nF$, and
- The transformer turns ratio $n = 7.9$.

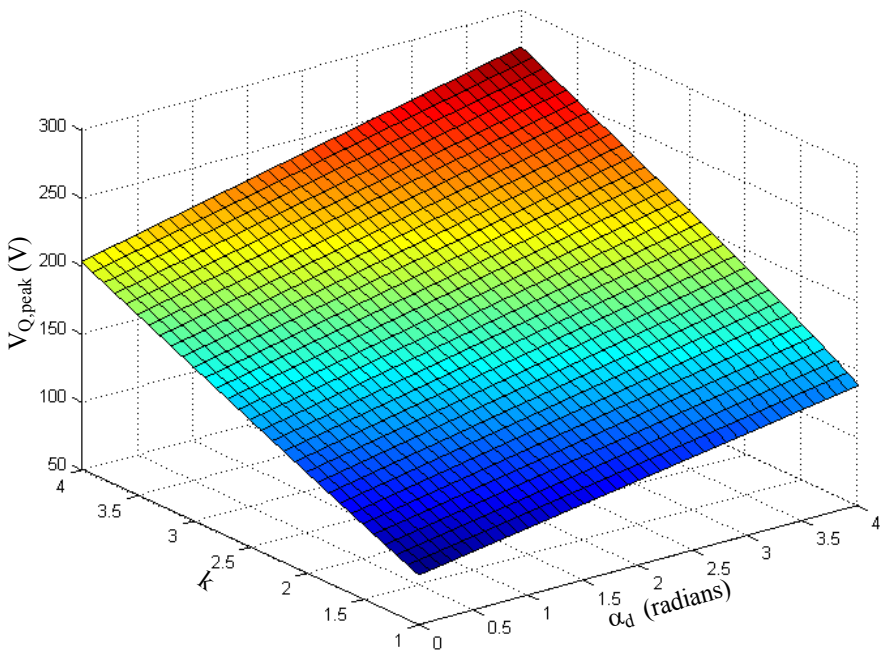

Figure 4.61 Peak Switch Voltage in Region 1

4.7 Summary

This chapter examines the operation of the ZVS two-inductor boost converter in detail. With a fixed set of the key design parameters including the resonant inductance and capacitance and the transformer turns ratio, variations of the circuit parameters such as the load factor, the timing factor and the delay angle result in a variable output to input voltage gain. A set of the explicit control functions is established under the variable frequency control. In order to obtain a wider output voltage range without excessive switch voltage stresses, a voltage clamping circuit can be added to the ZVS two-inductor boost converter. However, the increase of the output voltage range is obtained at the cost of a higher component count and the

potential higher power loss associated with the circulating energy.

If a fixed load condition is desired, the ZVS two-inductor boost converter has the option to operate under any possible combinations of the three circuit parameters in Regions 1 and 2. In this case, the power losses in the MOSFETs, the resonant inductor and capacitors vary against the circuit parameters. An optimised operating point can be selected based on the numerical analysis of the total variable power loss. Resonant cells that have been optimised for loss will form an important part of the current fed MIC solutions presented in the later chapters of this thesis.